

University of Windsor

## Scholarship at UWindor

---

Electronic Theses and Dissertations

Theses, Dissertations, and Major Papers

---

1983

### The interconnection of starred angle compression members.

J. A. Schepers

*University of Windsor*

Follow this and additional works at: <https://scholar.uwindsor.ca/etd>

---

#### Recommended Citation

Schepers, J. A., "The interconnection of starred angle compression members." (1983). *Electronic Theses and Dissertations*. 4071.

<https://scholar.uwindsor.ca/etd/4071>

This online database contains the full-text of PhD dissertations and Masters' theses of University of Windsor students from 1954 forward. These documents are made available for personal study and research purposes only, in accordance with the Canadian Copyright Act and the Creative Commons license—CC BY-NC-ND (Attribution, Non-Commercial, No Derivative Works). Under this license, works must always be attributed to the copyright holder (original author), cannot be used for any commercial purposes, and may not be altered. Any other use would require the permission of the copyright holder. Students may inquire about withdrawing their dissertation and/or thesis from this database. For additional inquiries, please contact the repository administrator via email ([scholarship@uwindsor.ca](mailto:scholarship@uwindsor.ca)) or by telephone at 519-253-3000ext. 3208.

CANADIAN THESES ON MICROFICHE

I.S.B.N.

THESES CANADIENNES SUR MICROFICHE



National Library of Canada  
Collections Development Branch

Canadian Theses on  
Microfiche Service

Ottawa, Canada  
K1A 0N4

Bibliothèque nationale du Canada  
Direction du développement des collections

Service des thèses canadiennes  
sur microfiche

NOTICE

The quality of this microfiche is heavily dependent upon the quality of the original thesis submitted for microfilming. Every effort has been made to ensure the highest quality of reproduction possible.

If pages are missing, contact the university which granted the degree.

Some pages may have indistinct print especially if the original pages were typed with a poor typewriter ribbon or if the university sent us a poor photocopy.

Previously copyrighted materials (journal articles, published tests, etc.) are not filmed.

Reproduction in full or in part of this film is governed by the Canadian Copyright Act, R.S.C. 1970, c. C-30. Please read the authorization forms which accompany this thesis.

THIS DISSERTATION  
HAS BEEN MICROFILMED  
EXACTLY AS RECEIVED

AVIS

La qualité de cette microfiche dépend grandement de la qualité de la thèse soumise au microfilmage. Nous avons tout fait pour assurer une qualité supérieure de reproduction.

S'il manque des pages, veuillez communiquer avec l'université qui a conféré le grade.

La qualité d'impression de certaines pages peut laisser à désirer, surtout si les pages originales ont été dactylographiées à l'aide d'un ruban usé ou si l'université nous a fait parvenir une copie de mauvaise qualité.

Les documents qui font déjà l'objet d'un droit d'auteur (articles de revue, examens publiés, etc.) ne sont pas microfilmés.

La reproduction, même partielle, de ce microfilm est soumise à la Loi canadienne sur le droit d'auteur, SRC 1970, c. C-30. Veuillez prendre connaissance des formules d'autorisation qui accompagnent cette thèse.

LA THÈSE A ÉTÉ  
MICROFILMÉE TELLE QUE  
NOUS L'AVONS REÇUE

The Interconnection of Starred Angle Compression Members

by

J. A. Schepers

A thesis  
presented to the University of Windsor  
in partial fulfillment of the  
requirements for the degree of  
Masters Of Applied Science  
In  
Civil Engineering

Windsor , Ontario, 1983

(c) J. A. Schepers, 1983

---

## ABSTRACT

The interconnection of starred angle compression members and their buckling behaviour has not been clearly understood and hence steel design standards do not show a consistent set of design rules. The consistency with which these members behave, as the number of interconnectors is varied, is developed herein. For any size or shape of equal leg angle that may be used to form starred angle compression members there exists a relationship of the geometric properties and hence the behaviour. This relationship is that the ratio of the radius of gyration for the built-up strut to the radius of gyration for an individual member is 1.96 with a standard deviation of 0.04.

This ratio of the radii of gyration results in the North American steel design standards requiring only one interconnector at mid-height for any pair of equal leg angles forming the starred angle strut. Other steel standards and specifications, British, German, and Australian, which were reviewed, are more conservative than the North American Standards. None of the standards, however, have design requirements which compare precisely with the results of this Thesis.

---

The standards are not consistent with the results of the experiments or the theoretical predictions. Recommendations are made to correct this deficiency. In particular, a recommendation is made that only two interconnectors are required for any pair of equal leg angles. This requirement doubles the number of interconnectors required by the current Canadian Standard.

## ACKNOWLEDGEMENTS

There are countless organizations and individuals who should be acknowledged for their assistance and encouragement in the production of this Thesis. First and foremost the financial support of the Canadian Steel Industries Construction Council (CSICC) is greatly appreciated.

Many individuals must also be thanked for their comments on the drafts of the work that went into the preparation of this Thesis, in particular Mr. M. Gilmore of the CSICC and Mr. D. Stringer of the Dominion Bridge Company Limited. Other individuals, though too countless to name individually, are the correspondents from the governing bodies affecting the standards and specifications.

At the University Dr. M. C. Temple and Dr. D. J. L. Kennedy are thanked for their guidance, persistence and patience. The entire Civil Engineering Faculty and Staff, with whom I had contact, gave encouragement for which I am grateful.

Finally my friends and relations are thanked, particularly Jason and Avril Farlam for their patience and encouragement. My special thanks are for Bonnie my wife and Nathan my son for tolerating me during my struggles to complete this work.

**DEDICATION**

to the memory of  
Gordon Pastorius

CONTENTS

ABSTRACT . . . . . ii  
ACKNOWLEDGEMENTS . . . . . iv  
DEDICATION . . . . . v

PART I

Chapter . . . . . Page

1. INTRODUCTION . . . . . 1  
    Objective . . . . . 3

2. LITERATURE SURVEY . . . . . 4  
    Standards and Specifications . . . . . 4  
        Canadian Standards CSA S16.1-1974 and S16-1969 . . . . . 5  
        American AISC Specification . . . . . 5  
        British Standard BS 449-1970 . . . . . 5  
        German Specification DIN 4114-1972 . . . . . 6  
        Australian Standard AS 1250-1975 . . . . . 6  
        Miscellaneous Standards . . . . . 7  
    Papers . . . . . 7  
    Summary . . . . . 9

3. THEORETICAL DERIVATION . . . . . 10  
    Introduction . . . . . 10  
    Finite Element Model . . . . . 12  
        Analytical Model . . . . . 14  
        Transformation Matrix . . . . . 18  
    Analysis . . . . . 21  
        Eigenvalue Solution Procedure . . . . . 21  
        Linear Iterative-Incremental Solution Procedure . . . . . 22  
    Effect of End Connectors on the Critical Load . . . . . 27  
        Simple Column With End Stiffeners . . . . . 28  
        Spaced Column With End Stiffeners . . . . . 29  
        Critical Length of End Stiffeners . . . . . 31  
    Effect of Number of Interconnectors . . . . . 32  
    Effect of Full Height Interconnection . . . . . 34  
    Forces In The Interconnector . . . . . 36  
    Summary . . . . . 38



4.	EXPERIMENTAL PROCEDURE . . . . .	40
	Introduction . . . . .	40
	Test Set-Up . . . . .	40
	End Conditions and Fixtures . . . . .	40
	Knife Edges . . . . .	41
	Loading Jack . . . . .	43
	Load Cell . . . . .	43
	Testing Frame for 120 inch Specimens . . . . .	43
	Testing Frame for 80 and 40 inch Specimens . . . . .	44
	Instrumentation . . . . .	44
	Test Procedure . . . . .	47
	Test Program . . . . .	48
	Data Reduction . . . . .	50
	Load . . . . .	50
	Displacement . . . . .	50
	Out-of-Straightness . . . . .	53
	Summary . . . . .	54
5.	RESULTS . . . . .	56
	Introduction . . . . .	56
	Properties . . . . .	57
	Geometric Properties . . . . .	57
	Mechanical Properties . . . . .	59
	Requirements of the Standards and Specifications . . . . .	59
	CSA S16, CAN3-S16.1M and AISC . . . . .	59
	British Standard BS 449-1970 . . . . .	60
	German Specification DIN 4114-1972 . . . . .	61
	Theoretical Results . . . . .	62
	Torsional-Flexural Buckling . . . . .	62
	Spaced Columns . . . . .	63
	Battened Columns . . . . .	64
	Eigenvalues . . . . .	65
	Linear Iterative-Incremental Load Deflection Curves . . . . .	65
	Experimental Results . . . . .	67
	Test Summaries . . . . .	67
	Summary . . . . .	68
6.	DISCUSSION . . . . .	70
	Introduction . . . . .	70
	Failure Load . . . . .	70
	120 Inch Specimens . . . . .	70
	Theoretical Predictions . . . . .	70
	Experimental Results . . . . .	73
	Comparison of Theoretical and Experimental Results . . . . .	74
	80 and 40 Inch Specimens . . . . .	75
	Load-Displacement . . . . .	76
	120 Inch Specimens . . . . .	76
	Theoretical Predictions . . . . .	76
	Experimental Results . . . . .	77

Comparison of Theoretical and Experimental Results . . . . .	79
80 and 40 Inch Specimens . . . . .	80
Effect of the Number of Interconnectors . . . . .	81
Effect of the End Connector . . . . .	83
Forces in the Interconnector . . . . .	83
Review of the Requirements of the Design Standards	85
7. CONCLUSIONS AND RECOMMENDATIONS . . . . .	87
Conclusions . . . . .	87
Recommendations . . . . .	88
Further Research . . . . .	89
Appendix . . . . .	page
A. ELASTIC AND GEOMETRIC STIFFNESS MATRICES . . . . .	158
B. COMPUTER PROGRAM FLOW CHART AND LISTING . . . . .	160
C. FORCES IN THE INTERCONNECTORS . . . . .	180
General . . . . .	180
Shear Force in a Column . . . . .	182
Determination of Forces . . . . .	185
Summary . . . . .	190
D. ANCILLARY TESTS . . . . .	192
Calibration . . . . .	192
Mechanical Properties . . . . .	193
Geometric Properties . . . . .	193
End Fixtures . . . . .	194
Summary . . . . .	196
E. NUMBER OF INTERCONNECTORS REQUIRED BY CSA STANDARDS S16 AND S16.1 . . . . .	197
F. EFFECT OF END STIFFENERS ON BUCKLING LOAD . . . . .	199
G. NOTATION . . . . .	202
REFERENCES . . . . .	204

LIST OF FIGURES

<u>Figure</u>	<u>PAGE</u>
1. Arrangements of Double Angles . . . . .	30
2. Starred Angle Geometry . . . . .	31
3. Model of the Starred Angle . . . . .	32
4. Finite Element Models . . . . .	33
5. Knife Edge Assembly . . . . .	99
6. End Fixtures . . . . .	100
7. Set-Up of 120 Inch Specimen . . . . .	102
8. Set-Up of 80 Inch and 40 Inch Specimen . . . . .	103
9. Instrumentation . . . . .	104
10. Effect of Rods on the Measured Displacements . . . . .	108
11. Out-of-Straightness Gauge . . . . .	109
12. 120 Inch Test Specimens . . . . .	110
13. 80 Inch Test Specimens . . . . .	119
14. 40 Inch Test Specimens . . . . .	123
15. Slenderness Ratio versus Effective Length for a Single Angle . . . . .	127
16. Load Deflection Curves for the 120 Inch Test Specimens . . . . .	128
17. Load Deflection Curves for the 80 Inch Test Specimens . . . . .	137
18. Load Deflection Curves for the 40 Inch Test Specimens . . . . .	140
19. Load Versus Number of Interconnectors . . . . .	143

20.	Possible Displaced Shapes of the Angles of the Strut . . . . .	144
21.	Potential Forces in the Interconnector . . . . .	146
22.	Spaced and Battened Column Theories Interconnector Forces . . . . .	147
23.	Shear Force in a Column . . . . .	148
24.	Percent Shear Versus Axial Load for the Starred Angles . . . . .	149
25.	Load Versus Rotation for Test 120A2.1 . . . . .	150
26.	Simple Column With End Stiffeners . . . . .	151

**LIST OF TABLES**

<u>Table</u>	<u>Page</u>
1. Theoretical Results . . . . .	152
2. Geometric Properties . . . . .	153
3. Types of Interconnectors . . . . .	154
4. Experimental Results . . . . .	155
5. Tensile Test Specimen Results . . . . .	157

## Chapter 1

### INTRODUCTION

Initial research was conducted for a report prepared by the Dominion Bridge Company Limited (26) which compares several steel standards with regard to the requirements for the interconnection of starred angle compression members. Indications from the tests conducted for the report led to the conclusion that the number and type of interconnectors has a significant effect on the compressive strength of this built-up section. Comparison of the standards and test results prompted closer scrutiny of the requirements of the Canadian Standard. These requirements are the most liberal of the standards compared and are not in keeping with the experimental results obtained.

Double angles can be used in several configurations, three of which, back-to-back, starred, and box, are shown in Fig. 1. Each of these arrangements has its own advantages and disadvantages which should be carefully considered prior to deciding on the arrangement to be used. Some considerations are:

- 1.. Accessibility to surfaces for maintenance. This is critical in the food and pharmaceutical industry for cleanliness, and in the chemical industry for corrosion protection.

2. The type of end connection, whether bolted or welded. If welded end connections are to be used to fasten the struts to the main members then the starred angle arrangement will permit lighter gusset plates to be used, whereas the back-to-back or boxed double angle arrangements have a higher concentration of shear stresses, tear out failure, on the gusset. When the end connection is to be bolted then the back-to-back arrangement is the most economical as it uses bolts in double shear. For the starred angle the bolts are in single shear, while for the box section bolted connections cannot be used.
3. Consideration of the truss window size is important if the structure is to have services passing through them. The back-to-back arrangement generally has the largest window size. The box section also has a large window size, but the starred angle has the smallest window size.
4. The starred angle and boxed arrangements have a larger minimum radius of gyration than a back-to-back arrangement of the same angles.

### 1.1 OBJECTIVE

Since no published research had been found on starred angle compression members, other than Pauls and Stringer (26) and Temple and Schepers (31), the objective of this thesis is to develop suitable design rules for the interconnection of starred angle compression members.

To carry out this objective the effects of the number and type of interconnector, the length of the end connector, the length of the member, and the forces which the interconnector must resist are examined.

## Chapter 2

### LITERATURE SURVEY

A literature survey, to determine the extent of published research on starred angle compression members, revealed nothing directly related to starred angles except for the steel standards (1,2,4,5,6,12) and the report written by Pauls and Stringer (26).

Several papers on battened columns (19,20,22,27,32,34) and spaced steel columns (17,18,21) were found. They have, however, only limited use in the study of starred angle compression members.

#### 2.1 STANDARDS AND SPECIFICATIONS

The following paragraphs discuss the applicable clauses of the steel standards and specifications with a brief summary of the treatment of the interconnection of starred angle compression members. The word standard shall apply to all standards or specifications referred to in this Thesis.

Section 5.3 contains a more detailed discussion of the requirements of the Canadian, American, British, and German Standards for the interconnection of the starred angle compression members. An example using the nominal geometric properties of the angle section used in the experiments is also given.



### 2.1.1 Canadian Standards CSA S16.1-1974 and S16-1969

These standards (5,6) stipulate that the maximum slenderness ratio of the individual members between points of interconnection must be equal to or less than the maximum slenderness ratio of the built-up member.

There are no specific requirements for the design of the interconnector nor the method of fastening.

### 2.1.2 American AISC Specification

This specification (1) has the same requirements as the Canadian Standards.

### 2.1.3 British Standard BS 449-1970

This standard (4) is presently under review and a draft indicates that there will be changes to the section on the interconnection of starred angle compression members. At the time of this writing BS 449-1970 Standard is applicable.

In this standard the spacing requirements of interconnectors is such that the slenderness ratio for each member between points of interconnection cannot exceed 40 nor 0.6 times the maximum slenderness ratio of the strut as a whole. There shall be not less than two interconnectors, in addition to the end connectors, and they shall be spaced at equal distances along the length of the strut. The interconnectors must be in pairs at points of interconnection so that they form a cruciform.

6

Rivets, bolts or welds used for the fastening of the interconnectors shall be proportioned such that they are sufficient to carry specified shear forces and bending moments.

#### 2.1.4 German Specification DIN 4114-1972

This specification (12) states that the slenderness ratio for each member between points of interconnection shall not exceed 50 and that the built-up member must be connected at least at the third points.

These interconnectors must be fastened using at least two bolts or rivets or an equivalent weld, and must be designed for a specified shear force, and bending moment.

#### 2.1.5 Australian Standard AS 1250-1975

The requirements of this standard (2) are similar to the requirements of the German and British Standards in that the slenderness ratio for each member cannot exceed 50 nor 0.6 times the maximum slenderness ratio of the built-up member.

There are requirements for the design of the interconnector, and its method of fastening to the main members, due to specified shear and bending forces. The interconnectors must be constructed to form a cruciform or be placed in pairs at right angles to each other and be in contact with each other.

11

#### 2.1.6 Miscellaneous Standards

Though translations of the Russian, Yugoslavian and French Standards could not be obtained, discussions with an engineer familiar with these standards indicated that the requirements are similar to, or more conservative than, the British or German Standards already cited.

#### 2.2 PAPERS

Pauls and Stringer's report (26) was the only research found with direct bearing on starred angle compression members. The report did not check mechanical properties or initial imperfections nor did it present any theoretical analysis of the starred angle struts. It was very useful in giving a starting point for this research on the interconnection of starred angle compression members.

Several papers and publications on battened and laced columns (16, 19, 20, 22, 27, 28, 32, 34) have been examined to determine whether or not the theories could be applied to predict the behaviour of slender starred angle struts. Battened and laced columns are built-up members interconnected with horizontal or diagonal interconnectors, respectively. For battened columns the interconnectors are rigidly fastened at regular intervals to the main members. Battened column theory assumes that buckling about one of the principal axes, the U-U axis (see Fig. 2), governs. The capacity of the built-up section about each of the principal axes must be checked using appropriate theories.

Spaced steel column theory (16,17,18) gives an alternate approach to the study of starred angle compression members though it is limited to starred angle struts having zero or one interconnector only. The spaced column is similar to the battened column except that the interconnectors are assumed to be pin-connected to the main members. The rigidity of the interconnectors is assumed not to affect the strength of the built-up member and is not considered in the derivation of the governing equations. The end connectors, however, do affect the capacity of the built-up section, about one axis only, and this effect is included in the governing equations.

Finally, a paper on Vierendeel girders (14) was examined as the standards cited appear to be based, in part, on this theory.

Though the application of these theories cannot be strictly applied to the interconnection of the starred angle compression members, due to the assumptions used in their derivation, they do assist in understanding and explaining the behaviour of the starred angle compression member.

In Chapters 3 and 5 each of these theories is discussed and applied to the starred angle compression member. A numerical example is also given based on the properties of the equal leg angle used in the experiments.

### 2.3 SUMMARY

There is considerable variation among the steel standards examined with respect to the interconnection of the starred angle compression members. No research was found on which to base a consistent design criteria.

Several theories have been investigated, yet they cannot be applied directly due to the inherent limitations in the assumptions used in their derivation, principally that they preclude buckling out of the plane of interconnection.

## Chapter 3

### THEORETICAL DERIVATION

#### 3.1 INTRODUCTION

Starred angle compression members behave consistently in that the first buckling mode changes when two or more interconnectors are used as compared to when zero or one interconnector is used.

Many possible solution procedures were investigated that would predict the behaviour of the strut. These included stability functions and finite element methods using both the eigenvalue and a linear iterative-incremental approaches.

Battēn column and spaced column theories were investigated and are used to assist in explaining the behaviour of the starred angle compression member. They both have limitations in that they assume buckling only occurs in the plane of interconnection so that buckling out of the plane of interconnection must be checked separately. A completely general solution is required and since these theories do not permit buckling about either of the principal axes the finite element method is used.

Stability functions were examined during the preliminary phases of the research and were subsequently abandoned.

They are used to study the effects of varying lengths of end stiffeners on the critical load of a simple column. The finite element method is used in lieu of the stability function method for several reasons. First, the finite element method is easier to set-up and manipulate. Second, the finite element method provides a solution for the critical load directly, whereas the stability function approach requires an iterative procedure. Third, the carry-over stability function tends to infinity in the region of  $P/P_e = 2.046$ ; where  $P$  = the axial load; and  $P_e$  = the Euler buckling load of the section.

The finite element solution procedure used permits buckling about either of the principal axes. It also permits the individual angles to take any flexural displaced shape between points of interconnection. Interconnectors are incorporated into the solution procedure by relating the degrees-of-freedom at the points of interconnection because the interconnectors are small and cannot be input as elements using the beam-column linear finite element. The short length and the small values of the geometric properties of the interconnectors cause the elements of the member stiffness matrix to be large which in turn affects the entire solution by giving erroneous results.

To overcome this problem the interconnector is assumed to be rigid. The method by which the effects of the interconnector are input into the finite element solution proce-

ture, relating the degrees-of-freedom at points of interconnection, is discussed later in this chapter.

### 3.2 FINITE ELEMENT MODEL

Intuitively the placing and fastening of these interconnectors seems insignificant. The steel standards, as indicated earlier, differ in their treatment of how many interconnectors should be used and in the forces they must resist. Due to the close spacing of the angles and the relatively small size of the interconnector the beam-column finite element (Appendix A) cannot be used directly to model the interconnector. Section 3.2.1 describes the method used to model the interconnector within the finite element solution procedure.

At the points of interconnection the geometric properties of the built-up member are altered slightly. This is particularly true of an interconnector which is not symmetric about either of the principal axes of the starred angle section. In Section 3.6 it is shown that the increase in stiffness is insignificant and can be neglected.

When there is zero or one interconnector the starred angle strut behaves essentially as a spaced column. For a strut with zero interconnectors each of the angles is independent of the other except at the end connectors. Because of the independence of each of the angles the behaviour of the strut is dependent on the direction of the initial out-



of-straightness of the individual angles. Varying only the direction of the out-of-straightness of each of the angles can result in larger critical loads. These larger critical loads are associated with alternate modes of buckling.

There are principally two modes of flexural buckling related to the starred angle strut having zero interconnectors. Other buckling modes have no practical significance and are not discussed in this Thesis. Torsional-flexural buckling, discussed in Section 5.4.1, occurs in members that are relatively short and is not considered. The first mode of flexural buckling is when both angles fail by displacing positively, or negatively, in the direction of the V axis. The second mode of flexural buckling is when the angles displace in the opposite direction, one positively and the other negatively in the direction of the V axis.

When the initial out-of-straightnesses of each of the angles are in the same direction, both positive or both negative, then the first mode of buckling is achieved. When the initial out-of-straightnesses of each of the angles are in the opposite direction then the second mode of buckling may be achieved. It can be seen that when there is one interconnector both of the angles are forced to displace together and the second mode of buckling described above cannot occur.

Though there is an increase in the capacity of the strut when it buckles in the second mode, the first mode of

buckling is the only one considered. It is sufficient to state that the alternate mode has no consequence, for practical purposes, on the results and recommendations as it can only occur when there are zero interconnectors joining the angles of the strut.

When there are two or more interconnectors failure is by flexural buckling about the V-V axis. The end connectors give some added stiffness to the ends of the strut which is neglected. It is shown that neglecting the effect of the end stiffeners does not significantly affect the critical load for buckling about the V-V axis.

The above statements are based on experimental observations and preliminary theoretical predictions. They are considered in the following analytical model.

### 3.2.1 Analytical Model

A three-dimensional beam-column linear finite element is used to predict the critical loads and the load-deflection curves. The general solution permits the angles to displace without restriction except at the points of interconnection.

The angles of the strut are forced, at the points of interconnection, to take the same displacements in the plane of interconnection. As the interconnector is assumed to be rigid the displacements of the joints of each of the angles, at the points of interconnection, are assumed to be linearly dependent to account for the effects of interconnection.

Since each angle of the starred angle strut is free to displace in any direction the model has to permit each angle to be independent except at the points of interconnection. At the points of interconnection there are two displacements which each angle can take that are independent of one another, assuming that the difference in the displacements are small. At large displacements the interconnector also forces these two displacements to be dependent. The first of these two displacements is in the direction of the V axis of the individual angles and the second is in the direction of the Z axis of the individual angles, Fig. 3. The differential displacement, the difference between the corresponding displacements of each angle, in the direction of the Z axis can occur when buckling about the U-U axis governs since each angle will shorten by a different amount. This problem of the differential shortening is studied by Johnston (17), as applicable to spaced steel columns, and is also discussed briefly in Section 3.4.2.

The end connectors also restrict the displacements of the individual angles which must be taken into account. This is done by relating the degrees-of-freedom at the ends. Each of the angles must be permitted to displace vertically, in the direction of the Z axis, at both ends. This permits the end connector to rotate about the U-U axis. This is done by assigning vertical degrees-of-freedom to the ends of each member. In so doing there is no vertical restraint

when a column of full height is modelled. To overcome this problem and to save computer time a half column is modelled. Modelling a half column permits buckling modes of single curvature to be studied, however, as was discussed earlier, the buckling mode which is of most significance displaces in single curvature.

The effects of the interconnectors and end connectors are accounted for by using a transformation matrix to relate the degrees-of-freedom. This transformation matrix is described in more detail later in this section.

For a starred angle arrangement the coordinate axes system, the schematic diagram of the model of the starred angle strut with the end conditions is shown in Fig. 3. From this figure it can be seen that at the supported end, the top of the modelled column, there are two lateral restraints and that the strut is prevented from rotating. At the mid-height of the column, the lower end of the modelled column, a vertical restraint and two bending restraints are imposed. These restraints are imposed so that a full-height column can be modelled which has a buckled shape of single curvature, that is, symmetric about its mid-height.

The finite element models used are shown in Figs. 4(a) to 4(f). The member numbers, nodes, and degrees-of-freedom that are used for struts having zero to five interconnectors are shown. The axes used are the Z, V

and U, see Figs. 2 and 3, which is consistent with the CISC Handbook (7). It should be emphasized that the coordinate axes system used is not the system that is conventionally used in finite element problems. All the definitions used in Fig. 4(a) apply to Figs. 4(b) to 4(f). In all cases the end connector is at the top of the figures, at the origin, and the interconnectors are shown as horizontal lines.

It can be seen from the finite element models that the nodes of the left and the right members at points of interconnection and end connection have common degrees-of-freedom. This in itself is not sufficient to define the behaviour at points of interconnection as the degrees-of-freedom are not independent.

At the end connector it has been stated that  $z_l$  can be different from  $z_r$ , where  $z$  represents the displacements in the direction of the Z axis and l and r stand for the left and right members respectively. They are both dependent on  $\lambda$ , which is the rotation about the U axis. The following equation is used to relate the dependent degrees-of-freedom at the end connector:

$$\lambda = \frac{z_r - z_l}{b} \quad (3.1)$$

where  $b$  = the distance between centroids of the angles measured as the perpendicular distance between the  $U^l-U^r$  axes.

At the interconnectors a similar approach is used to derive the following equations:

$$\theta = \frac{u_l - u_r}{b} \quad (3.2)$$

$$\lambda = \frac{z_r - z_l}{b} \quad (3.3)$$

$$\beta_l = \beta_r \quad (3.4)$$

where  $\theta$  and  $\beta$  = the rotation about the Z and V axes respectively; and  $u$  = the displacement in the direction of the U axis. Eq. 3.2 is written such that the difference in the displacements is the reverse of that in Eq. 3.1 and 3.3. This is required to maintain the positive sign convention.

### 3.2.2 Transformation Matrix

The four equations of dependency, Eqs. 3.1 to 3.4, are incorporated into a transformation matrix and used in the solution procedure to account for the effects of interconnection as follows:

$$\{U\} = [T] \{U^*\} \quad (3.5)$$

where  $\{U\}$  = the master displacement vector;  $[T]$  = the transformation matrix; and  $\{U^*\}$  = the reduced master displacement vector, containing all independent degrees-of-freedom. From the potential energy formulation the following equation is used:

$$\Pi_p = \frac{1}{2} \{U\}^T [K_r] \{U\} - \{U\}^T \{P\} \quad (3.6)$$

where  $\Pi_p$  = the potential energy of the system;  $[K_r]$  = the master stiffness matrix; and  $\{P\}$  = the master load vector. Substituting Eq. 3.5 into Eq. 3.6 gives:

$$\Pi_p = \frac{1}{2} \{U^e\}^T [T]^T [K_r] [T] \{U^e\} - \{U^e\}^T [T]^T \{P\} \quad (3.7)$$

This equation can be simplified by using the following equations:

$$[K_r^e] = [T]^T [K_r] [T] \quad (3.8a)$$

$$\{P^e\} = [T]^T \{P\} \quad (3.8b)$$

where  $[K_r^e]$  = the reduced master stiffness matrix; and  $\{P^e\}$  = the reduced master load vector. Substituting Eq. 3.8 into Eq. 3.7 gives:

$$\Pi_p = \frac{1}{2} \{U^e\}^T [K_r^e] \{U^e\} - \{U^e\}^T \{P^e\} \quad (3.9)$$

which is similar to Eq. 3.6. Differentiating Eq. 3.9 with respect to the displacement and setting the resulting function equal to zero to determine the minimum potential energy of the system results in:

$$[K_r^e] \{U^e\} = \{P^e\} \quad (3.10)$$

For large deflection problems the stiffness matrix  $[K_r^e]$  must include the effects of the deformed geometry of the elements in the equilibrium equations. This is done by writing the stiffness matrix in two parts, an elastic and a geometric part.

The element elastic stiffness matrix is available in a number of publications (10,13) and is shown in Appendix A. The geometric stiffness matrix, on the other hand, has been a matter of considerable concern for researchers for some time. The geometric stiffness matrix used was developed by Martin (25) and by Hathout (13). The geometric stiffness matrix is not just a function of the element mechanical and geometric properties, as is the case with the elastic stiffness matrix, but is also a function of the axial force in the members. The element geometric stiffness matrix used is also shown in Appendix A.

For the finite element approach, Eq. 3.10 can be rewritten as:

$$([K_e'] - F[K_g'])\{U'\} = \{P'\} \quad (3.11)$$

where  $[K_e']$  = the reduced master elastic stiffness matrix;  $[K_g']$  = the reduced master geometric stiffness matrix for a unit internal load; and  $F$  = the axial force in the elements which equals half of the total load (Fig. 3). The negative sign is used to indicate that the axial force is compressive.



### 3.3 ANALYSIS

The following two sections describe the solution procedure for the finite element models previously described. Two solution procedures are used. The first being the eigenvalue method which calculates the critical loads only. The second solution procedure is a linear iterative-incremental method which calculates theoretical load-deflection curves.

A computer program of approximately 1000 statements, incorporating both of the solution procedures, was written to run on an IBM 3031 computer. A listing of the computer program is given in Appendix B.

#### 3.3.1 Eigenvalue Solution Procedure

The computer program determines the critical load and corresponding buckled shape based on an approach used by Temple (30) for finding the eigenvalues and eigenvectors. For the eigenvalue approach the determinate of the master stiffness matrix shown in Eq. 3.11 be set equal to zero as follows:

$$|[K_e^*] - F[K_g^*]| = 0 \quad (3.12)$$

Solving Eq. 3.12 determines the force F at which bifurcation buckling occurs. Buckling is defined as the point at which the stiffness tends to go to zero and the lateral displacements become infinite. To solve Eq. 3.12 it must be rewritten as follows:

$$\{\alpha[I] - [K_e']^{-1}[K_g']\} = 0 \quad (3.13)$$

where  $\alpha$  = the inverse of the critical load. This form of the solution, inverting both the force and the elastic stiffness matrix, must be used as the matrix  $[K_g']$  is singular.

The critical load for each angle of the starred angle compression member is the smallest load which satisfies Eq. 3.13. This means that the largest value of  $\alpha$  must be inverted to determine the first critical load of each angle. The critical load of the starred angle strut is twice the critical load determined by solving Eq. 3.13 (Fig. 3). The results of this analysis are discussed in Chapter 5.

### 3.3.2 Linear Iterative-Incremental Solution Procedure

For the linear iterative-incremental method of determining the load-deflection characteristics of the starred angle compression member, the following modification to Eq. 3.11 is required:

$$([K_e'] - F[K_g'])\{\Delta U'\} = \{\Delta P'\} \quad (3.14)$$

where  $\{\Delta U'\}$  = the incremental displacements; and  $\{\Delta P'\}$  = the incremental load.

This solution procedure was selected after a review of several papers on the subject of nonlinear analysis, large deflection theories, and incremental approaches. Each of

the solutions reviewed are shown to work by their respective authors, however, several of the methods described are quite complex and unwieldy. Connor et al. (8) emphasizes the importance of nonlinear analysis and the approach used in this Thesis is fashioned after the method outlined by Connor. A major difference is in the geometric stiffness matrix. Connor presents a matrix in a form which involves the end rotations of each element. He subsequently disregards these rotations stating that in most practical problems the rotations can be considered to be small and the final form of his matrix is that for a truss element. The truss form of the geometric stiffness matrix is not sufficient for the beam-column element as has been clearly demonstrated by Martin (25) and Hathout (13).

Other methods of solving the large deflection problem were reviewed (23,29) but were not used. However, these papers emphasized that, in the case of a linear incremental method, the matrices become increasingly ill-conditioned when the critical load is approached. Thus the critical load should be determined by some other method, such as the eigenvalue method, then used as the upper limit of the load in the linear iterative-incremental computer model.

As the matrices become increasingly ill-conditioned near the critical load (23) post buckling behaviour, in general, cannot be predicted, however, Mallet and Marcal state that the linear incremental method is applicable in the presence of large rotations.

The drawback to the method used by Mallet and Marcal is that three matrices are used to define the master stiffness matrix. Though the matrices include extra terms not found in the geometric stiffness matrix developed by Martin (25), the manipulation of the matrices is more cumbersome. These matrices consist of the conventional elastic stiffness matrix and two geometric stiffness matrices. The first geometric stiffness matrix is a linear function of the displacements, and the second is a quadratic function of the displacements.

Since the problem being studied is slender columns up to the elastic buckling limit, and since Martin's beam-column element geometric stiffness matrix has been verified by the use of Hermite Interpolation Polynomials (13), the matrices of Mallet and Marcal are not used.

To determine the load-deflection curve a process of load increments and iterations is used. The procedure is similar to that used by Wong (35). To describe the procedure Eq. 3.14 is written as follows:

$$([K_e^i]_j - F_j [K_g^i]_j) \{\Delta U^i\}_j = \{\Delta P^i\}_j \quad (3.15)$$

where  $i$  = the number of the iteration cycle; and  $j$  = the number of the incremental loading step.

The value of the load increment  $\{\Delta P^i\}_j$  was set at 1/20 of the critical load determined by the eigenvalue method. This load increment was kept constant for the calculation of the

load-deflection curve. As the buckling of a double angle built-up strut is being considered the load increment for each of the members is one-half of the total load increment.

The axial force,  $F$ , in each member was found by the summation of the incremental loads up to and including the load increment for which deflections were calculated. When the next increment was to be calculated the force  $F$  was increased by the addition of the amount of the next load increment. At each load increment Eq. 3.14 was solved by an iterative procedure. This iterative procedure involved the recalculation of the stiffness matrices based on the revised geometry of the strut which in turn was based on the displacements  $\{\Delta U^i\}$  calculated by Eq. 3.14.

For each increment,  $j$ , the master stiffness matrices were calculated using the geometry of the strut at the start of the iteration cycle. The first iteration,  $i=1$ , used the initial out-of-straightness for the geometry of the strut.

The incremental displacements that were calculated,  $\{\Delta U^i\}$ , were added to the displaced shape of the strut. This revised displaced shape was then used to calculate the master stiffness matrices for the next iteration cycle,  $i=i+1$ . The procedure is self evident from Eq. 3.15. For each increment,  $j$ , the stiffness matrices,  $[K_e^i]_j$  and  $[K_g^i]_j$ , and the axial load,  $F_j$ , are determined. The displacements,  $\{\Delta U^i\}_j$ , are then calculated which are used to determine a revised geometry of the strut which are used to

recalculate the master stiffness matrices. The stiffness matrices are always based on a displaced shape of the strut which are then used to calculate the next displaced shape. The difference between the displacements at the end of successive iterations was checked to determine if they converged, within acceptable limits, or diverged.

Once the difference in the displacements between successive iterations was less than one percent the displacements were considered to have converged and the displaced shape was reset using the displacements obtained from the final iteration. New stiffness matrices were calculated,  $[K_e']_{j+1}$  and  $[K_g']_{j+1}$ , using the new displaced shape, the load increment,  $\Delta P$ , was added to the axial force,  $F_j$ , to get the next axial force,  $F_{j+1}$ , and then the iterative procedure was started again for the next load increment,  $j+1$ . This process was repeated for twenty increments as the incremental load was 1/20 of the critical load.

The one percent criteria for convergence was selected after results using five percent, one percent, and one-tenth of one percent convergence criteria were compared. It was found that the refinement achieved when using one-tenth of one percent compared to one percent did not warrant the additional expense in computer time and the five percent criteria did not give precise enough results.

To determine when the strut had buckled it became a simple matter of checking the displacements at the end of

each iteration, for each load increment, to see if the displacements were diverging. Divergence indicates an ill-conditioned state of the matrices, hence the critical load had been exceeded. Prior to the displacements diverging the load-displacement curve flattens out. At the critical load the displacements should, under ideal conditions, neither converge or diverge. This condition is impossible to achieve hence the final output data for load and displacement were plotted to determine the shape of the load-displacement curve and the critical load.

A flow chart of the linear iterative-incremental solution procedure is given in Appendix B.

#### 3.4 EFFECT OF END CONNECTORS ON THE CRITICAL LOAD

The following three sections demonstrate the effect that the end connector has on the strength of the strut.

There are two separate conditions that have to be considered when assessing the effect of the end connectors. The first of these is when the starred angles buckle about the V-V axis, which is Euler buckling of a simple column with stiffened ends. The second effect is when failure occurs about the U-U axis in which case buckling is similar to that of spaced or battened columns.

The approach used is to calculate the critical loads about each of the principal axes separately then to compare the results to determine the effect of the end stiffeners on

the critical load. Stability functions were used when considering buckling about the V-V axis and spaced steel column theory was used when considering buckling about the U-U axis.

Solving each of these parts results in two equations for critical loads, one equation for buckling about each of the principal axis. These equations are then equated to calculate a length of end connector that forces the starred angle compression member to have the same buckling load about both of the principal axes. The length of end connector at which the buckling load of the starred angle compression member is the same about both of the principal axes is called the critical length of the end stiffener.

#### 3.4.1 Simple Column With End Stiffeners

Stability functions (15) are used to study the effect of end stiffeners on the buckling of the starred angle compression member about the V-V axis. The analysis is explained in detail in Appendix F. The results indicate an insignificant increase in strength as the end stiffener length is increased.

An assumption made in generating the stability functions is that the end stiffener is rigid. This permitted a much simpler development and is valid as the calculated effect on the overall strength of the strut, with relatively short end stiffeners, is negligible. As a real end stiffen-




er has some flexibility, that is, it is not rigid, the actual effect will be less than that calculated. Since the calculated effect is small the actual effect will be even smaller.

Thus when considering buckling about the V-V axis, the added stiffness provided by the end connector, normally a Tee section, will be neglected. In neglecting the effect of end stiffeners the critical load about the V-V axis of the starred angle compression member equals the Euler buckling load of a simple column having a constant moment of inertia, Eq. F.8.

### 3.4.2 Spaced Column With End Stiffeners

The examination of the second condition, buckling about the U-U axis, is based on Johnston (17). Johnston formulates the effects of end tie plates on the buckling strength of spaced steel columns which are used to closely approximate the starred angle strut.

Spaced column theory is applicable to starred angle struts only when there is zero or one interconnector in the strut. When there are two or more interconnectors the buckling behaviour of the strut can be approximated using the battened column theory. The battened column theory is used later in this chapter to determine the effect of the number of interconnectors on the buckling strength, about the U-U axis, of the starred angle compression member.



The effect of the end stiffeners restricting the bending of the individual angles is an important factor in the spaced column theory. When buckling occurs about the U-U axis of the starred angle compression member the rotation of the end stiffener, about the U-U axis, forces the individual angles to shorten by different amounts. The effect of the bending restriction imposed by the end stiffeners is similar to the Vierendeel girder (14). If the interior verticals of the Vierendeel girder are pin connected to the main members then additional strength comes from the end stiffeners only.

Johnston (17) discusses four modes of buckling which can occur when end stiffeners are present. Two of these modes have fixed end conditions and are not considered. The other two modes have pin end conditions, double curvature (Mode A) and single curvature (Mode B) (Fig. 3 of Ref. 17), and are the only buckling modes that are considered. Johnston also demonstrates that when a tie plate, rigidly fastened to the individual angles at mid height, is used then the spaced column must assume the Mode B shape when it buckles.

The critical load, based on the spaced column theory, is calculated using the following equation:

$$P_{cr} = \frac{2\pi^2 EI_U}{(KL)^2} \quad (3.16)$$

where  $K = \pi\sqrt{2/C}$ ; and  $C =$  a function of the length of the end stiffener and the ratio of  $I_U/I_U'$ . Values for  $C$  are plotted in Fig. 8 of Ref. 17.

From Eq. 3.16 it can be shown that as the length of the end stiffener is increased the buckling load about the U-U axis increases.

### 3.4.3 Critical Length of End Stiffeners

In the previous two sections the critical load was calculated for the starred angle compression member about both of the principal axes, V-V and U-U. It was found that the end stiffeners have a significant effect on the critical load only when buckling occurs about the U-U axis. The critical length of the end stiffener is defined as the length of end stiffener which forces the strut to have the same buckling load about the V-V axis and the U-U axis. A longer or shorter length of end stiffener will force the starred angle strut to buckle about either the V-V axis or the U-U axis respectively.

Equating the Euler load for buckling about the V-V axis, Eq. F.3, to Eq. 3.16 for buckling about the U-U axis gives:

$$\frac{\pi^2 EI_V}{L^2} = \frac{2\pi^2 EI_U'}{(KL)^2} \quad (3.17)$$

which can be reduced to:

$$K = \sqrt{\frac{2I_U'}{I_V}} \quad (3.18)$$

Substituting  $I = Ar^2$  into Eq. 3.18 gives:

$$K = \sqrt{2 \left( \frac{r_{u'}}{r_v} \right)^2 \left( \frac{A_0}{A} \right)} = \frac{r_{u'}}{r_v} \quad (3.19)$$

where  $r_{u'}$  = the radius of gyration for an individual angle;  
 $r_v$  = the radius of gyration for the strut;  $A_0$  = the area of  
 an individual angle; and  $A$  = the area of the built-up  
 section =  $2A_0$ .

Because  $r_{u'}/r_v = 1/1.96$  for equal legged starred angles  
 (see Appendix E for details) and since  $K = \pi \sqrt{2/C}$ , Eq. 3.19  
 gives  $C = 75.83$ .

For two 2-1/2 x 2-1/2 x 1/4 in. starred angles, used in  
 the experiments,  $I_u/I_{u'} = 15.99$ . From Fig. 8 of Johnson  
 (17) the critical length of the end stiffener required to  
 force the starred angle compression member with one inter-  
 connector to have the same buckling load about the V-V axis  
 and the U-U axis is 8.0 in. For a length of end stiffener  
 less than 8.0 in. the strut will buckle about the U-U axis  
 and if the length of the end stiffener is greater than  
 8.0 in. the strut will buckle about the V-V axis.

### 3.5 EFFECT OF NUMBER OF INTERCONNECTORS

The battened column theory as presented by Timoshenko  
 and Gere (33) is used to predict the effect of the number of  
 interconnectors on the buckling load. Though this theory  
 gives results that are generally greater than those obtained  
 experimentally (20) the results are sufficiently accurate to

assist in explaining the buckling behaviour about the U-U axis of starred angle compression members. Battened column theory applies only to the critical load about the U-U axis of the starred angle compression member. This theory is applicable to built-up columns which have interconnectors that are rigidly fastened to the individual angles of the strut as opposed to the pin connection of the interconnector to the individual angles assumed in the spaced column theory.

The following equation (Eq. 2.63 in Ref. 33) is used:

$$P_{cr} = \frac{\pi^2 EI_U}{L^2} \left\{ \frac{1}{1 + \frac{\pi^2 EI_U}{L^2} \left( \frac{db}{24EI_{iU}} + \frac{d^2}{24EI_{U'}} \right)} \right\} \quad (3.20)$$

where  $d$  = the spacing between interconnectors;  $b$  = the centroidal distance between individual angles; and  $I_{iU}$  = the second moment of area, in the Z-U plane, for the interconnector.

From Eq. 3.20 it is obvious that as the number of interconnectors is increased, i.e. the spacing between points of interconnection,  $d$ , is decreased, the critical load increases. It should be emphasized that when the battened column theory, at some number of interconnectors, predicts a larger buckling load about the U-U axis than the Euler load about the V-V axis then the Euler load about the V-V axis governs. A numerical example is given in Chapter 5.

### 3.6 EFFECT OF FULL HEIGHT INTERCONNECTION

This section shows that the effect of inserting a continuous interconnector for the full height, in lieu of a few, equally spaced, short pieces of interconnectors, is to increase the critical load of the strut by only a small amount. The significance of this is that the increase in the stiffness of the strut, at the points of interconnection, due to the short length of the interconnector, need not be considered.

As was stated earlier, in Section 3.2, the geometric properties of the starred angle are altered at points of interconnection. Extending the interconnector for the full height of the column, instead of over the short length required for interconnection results in an increased stiffness of the strut. The moments of inertia of the section,  $I_u$  and  $I_v$ , are increased when the interconnector is installed for the full height. The minimum and maximum moments of inertia of the starred angle compression member are also rotated slightly from the V-V and U-U axes when a nonsymmetrical interconnector, with respect to the U-U and V-V axes, is used.

The following equations, taken from Ref. 32, are used to determine the rotation of the principal axes and the value of the maximum and minimum moments of inertia of the built-up strut:

$$\tan 2\phi = \frac{2I_{uv}}{I_u - I_v} \quad (3.22)$$

$$I_{\max/\min} = \frac{I_u + I_v}{2} \pm \sqrt{\frac{(I_u - I_v)^2}{4} + I_{uv}^2} \quad (3.23)$$

where  $\phi$  = the angle of rotation of the principal axes;  
 $I_{\max/\min}$  = the maximum and minimum moments of inertia; and  
 $I_{uv}$  = the product of inertia.

A 2 x 3/8 in. bar is used as the interconnector and its moments of inertia about the U-U and V-V axes are added to those of the angles. The only element that contributes to the product of inertia,  $I_{uv}$ , is the 2 x 3/8 in. bar as the starred angle strut is symmetrical about both the U-U and V-V axes.

For the bar  $I_u = I_v = 0.129 \text{ in.}^4$  and  $I_{uv} = 0.121 \text{ in.}^4$ . Adding these values to the nominal geometric properties of the starred angles (see Table 2) and substituting the values into Eqs. 3.22 and 3.23 results in  $\phi = 3.08$ ;  $I_{\min} = 2.37 \text{ in.}^4$ ; and  $I_{\max} = 4.63 \text{ in.}^4$ .

The ratio of  $I_{\min}$ , calculated above, to the nominal value of  $I_v$  tabulated in Table 2, is 1.053 or an increase of 5.3 percent. Therefore the critical load is 5.3 percent higher for a strut having a continuous 2 x 3/8 in. bar running full height between end connectors in lieu of short pieces of interconnectors since the critical load is directly proportional to the moment of inertia.

### 3.7 FORCES IN THE INTERCONNECTOR

To determine the forces in the interconnector several assumptions are made as follows:

- a) two interconnectors are used,
- b) batten column theory is used to determine the shear and bending forces, which results in a condition of plane stress, and
- c) the stresses are calculated for the interconnector, a  $2 \times 3/8 \times 2$  in. plate, and the related weld,  $3/16$  in. all around, used in the experiments.

The first assumption is made as one interconnector at mid-height transfers no shear or bending as there is zero curvature at mid-height when the column buckles in single curvature. Also two interconnectors were found to be the minimum required to force the starred angle strut to buckle about the V-V axis.

The third assumption was used to determine the stresses in the specimen interconnectors used experimentally.

From Appendix C the shear and bending are determined to be the contributing factors to the stresses in the interconnectors. The forces acting on the interconnector are small due mainly to the fact that when two interconnectors are rigidly fastened to the individual angles, buckling occurs about the V-V axis. At present the Canadian Standard (5) has no requirements for these forces.



The battened column theory predicts higher critical loads for the starred angle compression member as the number of interconnectors is increased, as shown in Table 1. With one interconnector the critical load predicted by the battened column theory agrees with the critical load predicted by the spaced column theory. With two or more interconnectors the critical load is greater than the Euler load about the V-V axis and thus cannot be reached.

The critical load predicted by the spaced column theory is independent of the number of interconnectors and the predicted critical load is less than the Euler load about the V-V axis. For two interconnectors to increase the strength of the strut they must be rigidly fastened to the individual angles of the starred angle strut. If the interconnectors are pin-connected to the individual angles, unable to transfer shear or bending, failure then occurs about the U-U axis. The forces, that must be resisted by the interconnector, calculated in Appendix C, are based on the battened column theory and take into account the fact that the curvature about the U-U axis will be less for the starred angle compression member with two interconnectors which buckles about the V-V axis.

### 3.8 SUMMARY

This chapter deals mainly with the finite element solution procedure for calculating the critical loads and load-deflection curves for starred angle compression struts. These are determined using the eigenvalue method to predict the critical load and a linear iterative-incremental method to determine the load-deflection curve. Spaced steel column and battened column theories are also used. These theories have limited application although they are useful in explaining the behaviour of the starred angle compression members.

It is shown that the end stiffener affects the critical load of the starred angle compression member when buckling about the U-U axis governs. The battened column theory demonstrates that the critical load about the U-U axis increases as the number of interconnectors is increased. With a continuous interconnector extending over the full height of the strut, in lieu of the short lengths of interconnection, the total increase in the capacity is small.

The effects of the end stiffener are not included in the finite element solution. These have been neglected as it affects the critical load only when there are less than two interconnectors. The experimental results, Chapter 5, confirm that the effect predicted theoretically is negligible for actual specimens.

The forces developed in the interconnector are small but must be considered in the design of the starred angle strut. If the interconnector cannot resist any forces, that is, they are pin-connected to the individual angles, failure is predicted about the U-U axis with a lower critical load. The present Canadian Standard (5) does not specify forces. Recommendations for calculating the shear and bending are given in Chapter 7.

## Chapter 4

### EXPERIMENTAL PROCEDURE

#### 4.1 INTRODUCTION

The first experiments were designed to duplicate the results of the tests conducted by Pauls and Stringer (26). The results from these tests and other preliminary tests were used to decide what ancillary tests were required, discern areas of potential error, confirm that the instrumentation of specimens functioned properly, and form a foundation for the test program.

All ancillary tests are reported in Appendix D. These tests were conducted to calibrate the equipment and to verify that the knife edge assemblies, loading frame and loading method all functioned as planned. The results obtained from the calibration tests were used to reduce the data obtained from the testing of the starred angle struts.

#### 4.2 TEST SET-UP

##### 4.2.1 End Conditions and Fixtures

The test specimens were pin ended through the use of the knife edges. Twisting of the ends, rotation about the Z-Z axis, was prevented by the use of specially constructed end fixtures.

This section describes the pieces of equipment necessary to apply and record the load; the loading jack, knife edges, load cell and the testing frame.

#### 4.2.1.1 Knife Edges

The knife edges were attached to the top and the bottom of the test specimens. An assembled set and a disassembled set of knife edges are shown in Fig. 5. The knife edges consist of three plates with machined and hardened grooves and two square bars placed on edge in the grooves. The center plate has two grooves, each having a included angle of 135 degrees, one on each side of the plate and at right angles to one another. The edge of the bars rotate about the vertex of each of the grooves in the center plate. The assembled plates and bars were not fastened together but were held in place by the compressive load applied to the strut. This ensured a minimum of resistance to rotation. Two locking bolts, which held the knife edges together when they were not in use, were removed after the specimen was set up and prior to the commencement of any test.

A possible source of error, due to the use of these knife edges, is that the rotation of the edge of the square bars about the vertices of the grooves in the center plate of the knife edge assembly are not in the same U-V plane. The vertices of the grooves in the center plate of the knife edge assembly are 1/2 in. apart. This 1/2 in. separation

could result in a total change in the height of 1/2 in. as the length of the specimen is taken to the center of the middle plate of the knife edge assembly. The worst condition is on a column having a length of 40 in. and when the knife edges are oriented in such a fashion that the axis about which the specimen fails is parallel to the grooves nearest the specimen, in the middle plate of the knife edge assemblies, at both the top and the bottom of the specimen. This orientation results in a maximum difference in length between parallel axes of rotation of 2.5 percent. For longer columns the difference is substantially reduced. For columns having a length of 120 in. the difference is less than 1 percent.

To overcome this problem the knife edges were oriented such that the groove nearest the specimen in the center plate of the top knife edge assembly was perpendicular to the groove nearest the specimen in the center plate of the bottom knife edge assembly. The principal axes of the specimen, U-U and V-V, were also oriented at 45 degrees to the axes of rotation of the knife edges. Assuming that the specimen fails about one of the principal axes, the knife edges will rotate about both of its axes of rotation making the center-to-center distance of the knife edge assemblies equal to the design length of the strut.

#### 4.2.1.2 Loading Jack

At the base, the load was applied through a mechanical jack having a capacity of 60 kips. Directly on top of the jack was an 8 x 1 x 12 in. plate to which the bottom knife edge assembly was bolted, Fig. 6(a). A frame was used to guide the bottom plate, and hence the knife edge assembly, in the vertical direction while preventing any rotation about the Z axis. The sides of the frame in contact with the plate were thoroughly lubricated to make certain that the restraint to vertical movement was minimized.

#### 4.2.1.3 Load Cell

A bracket at the top of the column was fabricated for this experiment, to which a flat load cell of 50 kip capacity was attached. This bracket and the load cell were fastened to an existing frame, in the University of Windsor's Structures Laboratory, at a height to suit the length of the specimen. A second plate, similar to the lower plate on the jack, was attached to the load cell and the upper knife edge assembly was attached to the upper plate, Fig. 6(b).

#### 4.2.1.4 Testing Frame for 120 inch Specimens

The specimens to be tested were placed between the upper and lower knife edge assemblies for testing. Fig. 7 shows the complete set-up of mechanical jack, lower knife

edge, specimen, upper knife edge, and load cell. This set-up was used, only for the test specimens having a length of 120 in.

#### 4.2.1.5 Testing Frame for 80 and 40 inch Specimens

A Gilmore testing machine in the Structures Laboratory, with a 100 kip capacity, was used for the testing of the specimens having lengths of 80 and 40 in. as the test set-up described previously did not have sufficient capacity to fail the 40 in. specimens. Fig. 8 shows a specimen set up between the platens of the Gilmore testing machine. The same knife edge assemblies previously described were used to ensure that the end conditions were kept the same. The hydraulic jack, electronic control circuits and load cell, built-in as part of the Gilmore testing machine, were used to apply, control and record the load.

#### 4.2.2 Instrumentation

The most critical aspect of the experiment was to acquire enough data so that the behaviour of the starred angle compression member could be accurately studied and experimental results compared to the theoretical predictions. Since the starred angle strut is free to buckle about either of the principal axes the following arrangement of dial indicators was used to measure the displacements in both directions.



Figs. 9(a) and 9(b) show the arrangement of the dial indicators at an interconnector in a plane perpendicular to the longitudinal axis of the specimen. Two dial indicators, 6 in. apart, were used so that each was three inches from, and parallel to, the V-V axis to measure displacements in the direction of the V axis. A third dial indicator was placed to measure the displacements in the direction of the U axis.

At points between interconnectors a double arrangement, similar to that described above, as shown in Figs. 9(c) and 9(d), was used. The displacements in the direction of the U' axis of each of the angles were measured instead of the displacements in the direction of the U axis of the entire cross-section. The measurements of displacements in the direction of the V axis were made using the two dial indicator arrangements.

All the dial indicators were separated from the specimens by an 1/8 in. outside diameter, hollow, aluminum rod 18 in. long to minimize the effect that displacements in one direction had on the dial indicator readings in the perpendicular direction. The effect of the perpendicular displacements was to give a reading which is either less than or greater than the actual displacement as shown in Fig. 10. Though the effect is minimal at small displacements, at large displacements it can produce readings which vary as much as 10 percent calculated from the actual measured displacements.

As the buckling load was approached the lateral displacements increased and hence the effect on the displacement reading in the perpendicular direction was greatest at the higher loads. These effects were taken into account in the reduced data. From Fig. 10 it is seen that the measured displacements,  $\Delta_i$  and  $\Delta_j$ , are less than the actual displacements,  $\Delta_{ir}$  and  $\Delta_{jr}$ , when displacements are in the direction drawn. When either of the displacements is in the negative direction it will cause the readings in the perpendicular direction to be greater than the actual displacements.

To keep the aluminum rods in place one of the ends was restrained by a bead of hardened epoxy on the specimen and the other end was restrained by the conical end of the dial indicator. This system permitted the rods to rotate freely thus the dial indicator readings were unaffected. The bead of epoxy was placed on a bar  $1/2 \times 1/4 \times 7$  in. long which was clamped directly to the specimen or to a small, light gauge, steel angle cemented to the specimen. Figs. 9(b) and 9(d) show the aluminum rods, the bar and light gauge angle on the specimen, and the dial indicators.

#### 4.3 TEST PROCEDURE

The test procedure used is based, in part, on the procedures outlined in the "Guide to Stability Design Criteria For Metal Structures" (16).

Specimens were first measured to determine the initial out-of-straightness. These measurements were made using a theodolite to sight, to the nearest 0.01 in., a specially constructed scale (Fig. 11) placed against each angle of the built-up strut at the top, upper quarter point, mid-height, lower quarter point, and the bottom. The out-of-straightness results were used in the linear iterative-incremental procedure to predict theoretical load-deflection curves.

After recording the imperfections, the specimen was slowly preloaded to 1,000 lb. then released to 40 lb. to ensure that initial settling in would not affect any of the dial indicator readings. The 40 lb. load was maintained while zeroing all the dial indicators and to preserve the alignment of the specimen and the knife edges.

Dial gauges were then installed at mid-height and other selected locations. These other locations varied from specimen to specimen and were used primarily as a check on the behaviour of the column. The mid-height deflections of the tests were plotted and compared to the theoretical results.

The loading of the specimens was applied slowly in increments of two kips. When the lateral displacements

increased beyond 0.1 in. the load increment was reduced to one kip. As the deflections increased further the load increment was reduced to 500 lb. and finally to 250 lb. In all cases the system was allowed to reach equilibrium, the point at which lateral displacements had, for all practical purposes, stopped increasing at a given load, prior to reading the dial indicators. At higher loads the load at equilibrium was also recorded since it had fallen off from the initially applied load.

All specimens were tested while in the vertical position and the test frame was checked periodically during this work for plumbness and alignment. The precision of the alignment reduced the eccentricity at the ends hence reducing the moments.

#### 4.3.1 Test Program

This section describes the test program which was limited to starred angle specimens having lengths of 120, 80, and 40 in. only.

To reduce the number of variables, the individual angles used throughout were 2-1/2 x 2-1/2 x 1/4 in. angles. Where variations of the specimens, such as base and cap plates in lieu of structural Tees as end connectors, or different types of interconnectors, were studied the same size angles were used.

To study the effect of the number and type of interconnector on the capacity of the starred angle strut, a series of tests was prepared with the number and type of interconnector as the only variables.

All of the test specimens constructed for this research are detailed in Figs 12, 13 and 14 which show the length, type of interconnector, end connector, and type of fastener. The test number contains all the test information. For example, for test number 120A2.1, the 120 indicates that the specimen is 120 in. long with a type A interconnector (see Table 3) and that a total of two interconnectors were used. The last figure (.1) indicates that the specimen was the first 120 in. specimen to be tested with two type A interconnectors.

The results from the specimens having a length of 120 in., Figs. 12(a) to 12(i), were used to devise the test program for specimens having lengths of 80 and 40 in. These are shown in Figs. 13 and 14, respectively.

For the specimens with a length of 120 in., two series of tests were run on the same specimens increasing the number of interconnectors on the specimen from one test to the next. These were 120A0.1, 120A1.3 and 120A3.1, Figs. 12(b), 12(c), and 12(e), as the first series and 120A0.2, 120A2.1 and 120A5.1 (Figs. 12(b), 12(d), and 12(g)) as the second series. Precautions such as measuring the out-of-straightness, before and after each test, and check-

ing the dial indicator readings obtained at the end of each test, were taken to ensure that the specimens had not yielded during testing.

#### 4.4 DATA REDUCTION

The data collected was reduced to a usable form for the preparation of graphs and tables. All of the reduced data is discussed in Chapter 5. Described below are the methods used to reduce the load, displacement, and out-of-straightness data.

##### 4.4.1 Load

Calibration results for the Strainert flat load cell and Gilmore load cell were used to convert the microstrains and voltage readings, respectively, to pounds. The Strainert, flat load cell was calibrated periodically and the data was reduced using the most recent calibration factor. The variation in the calibration factor was less than one percent.

##### 4.4.2 Displacement

From the instrumentation used, both deflections and rotations can be calculated for the individual angles of the specimen and for the specimen as a whole. Deflections in the direction of the V axis were calculated as the average of the two dial indicator readings, in Fig. 9(a) dial indi-

cators 1 and 2 and in Fig. 9(c) dial indicators 1 and 2, and 3 and 4. At points of interconnection deflections were calculated for the specimen as a whole, Fig. 9(a). Between points of interconnection the deflections were calculated for each of the members, Fig. 9(c). Deflection in the direction of the U or U' axis was read directly from the dial indicator on that axis, in Fig. 9(a) dial indicator 3 and in Fig 9(c) dial indicators 5 and 6.

The displacement data had to be corrected since the readings were not independent (Fig. 10). The effects were accounted for using:

$$\Delta_{ir} = \Delta_i + 18 \left\{ 1 - \left( \cos \left( \sin^{-1} \left( \frac{\Delta_j}{18} \right) \right) \right) \right\} \quad (4.1a)$$

$$\Delta_{jr} = \Delta_j + 18 \left\{ 1 - \left( \cos \left( \sin^{-1} \left( \frac{\Delta_{ir}}{18} \right) \right) \right) \right\} \quad (4.1b)$$

where  $\Delta_i$  and  $\Delta_j$  = the dial indicator readings; and  $\Delta_{ir}$  and  $\Delta_{jr}$  = the corrected displacements.

To calculate the corrected displacement  $\Delta_{ir}$ , the smallest dial indicator reading in the direction of either the U or V axis was substituted into Eq. 4.1a as  $\Delta_i$ . The larger dial indicator reading, in the direction perpendicular to the dial indicator reading used for  $\Delta_i$ , was substituted into Eq. 4.1a as  $\Delta_j$ . The corrected displacement  $\Delta_{jr}$  was then calculated by substituting the corrected displacement  $\Delta_{ir}$  calculated in Eq. 4.1a into Eq. 4.1b.

Eq. 4.1a was not recalculated substituting  $\Delta_{jr}$ , calculated in Eq. 4.1b, into Eq. 4.1a as  $\Delta_j$ , as it was found that the increase in the smallest deflection (when the perpendicular displacements were large) was a maximum of 10 percent after only one calculation and less than one percent after a second calculation. Also, the change in the large displacement (when the perpendicular deflections were small) is less than one percent after only one calculation. Additional calculation would result in more precise values for the displacements; however, the displacement data was only accurate to about one percent. The percentages quoted above were calculated based on the actual displacements, near the critical load, collected from the tests.

As the rotations were calculated using the difference of the dial indicator readings in the direction of the V axis, the corrections of Eq. 4.1 were not included since they applied equally to each of the dial indicators. The equation for calculating the rotation is:

$$\tan \theta = \frac{\Delta_1 - \Delta_2}{6} \quad (4.2)$$

where  $\theta$  = the angle of rotation about the Z axis; and  $\Delta_1$  and  $\Delta_2$  = the dial indicator readings for dial indicators 1 and 2 (Fig. 9a). The readings from dial indicators 3 and 4 (Fig. 9c) were substituted when calculating the rotation of the second angle at points between interconnectors. The number 6 in the denominator of Eq. 4.2 is the six inch spac-



ing of the dial indicators which measure the displacements in the direction of the V axis (see Section 4.2.2).

#### 4.4.3 Out-of-Straightness

From the data obtained using the theodolite it was a simple task to calculate the initial out-of-straightness at points along the length of the specimen.

This was done by assuming a straight line relationship between the points at which readings were taken at the top and the bottom of the specimen. The readings at the top and the bottom of the specimen were then reduced to zero and all the readings along the length were reduced accordingly. The detail of the procedure is as follows:

- a) subtract the bottom reading from all the readings.  
This reduces the bottom reading to zero,
- b) the ratio of the height of the point being reduced to the total height of the specimen was multiplied by the reduced top reading, the top reading less the bottom reading, then
- c) the value calculated in the second step is added to the respective readings reduced in the first step. This results in the top reading being reduced to zero and all the points in between are then the actual out-of-straightnesses.

In the computer program the strut was assumed to be straight between nodes. The maximum out-of-straightness calculated for the actual specimen was applied at the mid-height of the corresponding model and the remainder of the out-of-straightnesses for the nodes were assumed to have a sinusoidal relationship. This assumption is reasonable as the maximum out-of-straightness occurred near the mid-height of the specimens. The sinusoidal displaced shape is normally used theoretically to represent the out-of-straightness of a column when the buckling load is being calculated for an axially loaded specimen. For the computer program, as only half a column is modeled, this is the most efficient relationship.

#### 4.5 SUMMARY

The methods and materials used for testing and data acquisition for the twenty nine tests conducted are described herein. Once the behaviour of the slender starred angle compression members was determined tests on shorter columns, having lengths of 80 and 40 in., were conducted to verify if the shorter struts behaved in a similar manner.

The methods used to reduce the data for load, displacement, and out-of-straightness are also presented. Use of the reduced data in the computer program is also outlined. Notably the out-of-straightness is input as a sine curve with the maximum measured out-of-straightness of the speci-

mens applied to the theoretical column at mid-height as the amplitude of the sine curve.

The results from the experiments are discussed in Chapter 5.

## Chapter 5

### RESULTS

#### 5.1 INTRODUCTION

Critical loads for starred angle compression members are calculated using the spaced column theory; battened column theory, and the eigenvalue method. Experimental and theoretical load-displacement curves are plotted. The theoretical curves are calculated using the linear iterative-incremental method described in Chapter 3. The experimental curves are plotted using the reduced data obtained from the tests as described in Chapter 4.

The geometric and mechanical properties are determined for the test specimens and a comparison is made with the tabulated values in the CISC Handbook (7).

Finally, the requirements of the design standards are calculated to show the differences in the standards with respect to design capacities of the strut and the design of the interconnector.

## 5.2 PROPERTIES

### 5.2.1 Geometric Properties

As all specimens were constructed from equal leg angles, arranged in the form of a cruciform, the geometric properties can be easily calculated using values that are already tabulated, for the individual angles, in the CISC Handbook (7). The geometric properties of starred angles are:

$$A = 2A_0 \quad (5.1a)$$

$$I_x = A(r_x'^2 + (\bar{y} + a/2)^2) \quad (5.1b)$$

$$I_y = I_x \quad (5.1c)$$

$$r_x = \sqrt{I_x/A} \quad (5.1d)$$

$$r_y = r_x \quad (5.1e)$$

$$I_u = A(r_u'^2 + 2(\bar{y} + a/2)^2) \quad (5.1f)$$

$$r_u = \sqrt{I_u/A} \quad (5.1g)$$

$$I_v = I_x' + I_y' - I_u' \quad (5.1h)$$

$$I_v = 2I_v' \quad (5.1i)$$

$$r_v = \sqrt{I_v/A} \quad (5.1j)$$

$$J = (At^2)/3 \quad (5.1k)$$

$$r_t = \sqrt{0.039JL^2/I_p} \quad (5.1l)$$

$$I_p = I_u + I_v \quad (5.1m)$$

where  $A$  = the total area;  $A_0$  = the area of an individual angle;  $I$  = the moment of inertia;  $r$  = the radius of gyration;  $J$  = the torsional constant;  $r_t$  = the torsional radius of gyration; and  $I_p$  = the polar moment of inertia. The

torsional radius of gyration, Eq. 5.11, is taken from Eq. 260 of Ref. 3 and assumes that the warping constant is zero which is reasonable as it is small for angle sections. The subscripts  $u$ ,  $v$ ,  $x$  and  $y$  = the respective axes of the starred angle and these subscripts primed indicate the axes of the individual angle.

For 2-1/2 x 2-1/2 x 1/4 in. angles the properties taken from the CISC Handbook (7) are substituted into Eqs. 5.1a to 5.1m to calculate the nominal values of the starred angle geometric properties. The results are tabulated in Table 2.

The angles of the test specimens were carefully measured to determine the actual geometric properties. The same procedure that is outlined in the CISC Handbook (7) was used to calculate the properties from the data measured in the laboratory, that is, the rounds and fillets were neglected. Table 2 contains tabulated values of the actual geometric properties averaged from four specimens.

The variation between the actual and nominal values of the geometric properties, tabulated in Table 2, are not consistent with the standard mill practice tolerances (7). The actual area is 4.8 percent higher than the tabulated value and the permitted variation is only 2.5 percent.

The geometric properties used in calculating the theoretical results are the actual values as listed in Table 2. In calculating the requirements of the design standards the nominal values listed in Table 2 are used.

### 5.2.2 Mechanical Properties

Four tensile test specimens were prepared from the material of the test specimens. Two strain gauges were attached to each. The average value of the modulus of elasticity,  $E$ , was found to be 29,700 ksi and the average yield stress was 52.7 ksi, Table 5, and were used throughout. The actual test procedure is discussed in detail in Appendix D.

### 5.3 REQUIREMENTS OF THE STANDARDS AND SPECIFICATIONS

#### 5.3.1 CSA S16, CAN3-S16.1M and AISC

All of these standards have the same criteria for determining the maximum spacing of interconnectors which is:

$$d/r_{U'} \leq KL/r_v \quad (5.2)$$

where  $KL/r_v$  = the design slenderness ratio of the strut;  
 $r_{U'}$  = the minimum radius of gyration for a member; and  
 $d$  = the maximum spacing between interconnectors.

Substituting the actual values of the geometric properties from Table 2 and a length of 120 in. into Eq. 5.2, a value for the spacing,  $d$ , of 60.6 in. is calculated. Therefore only one interconnector is required for this specimen.

No requirements for the forces to be resisted by the interconnectors are specified though the present practice is to use an interconnector which is of a size to be manageable and to fasten the interconnector to the individual angles using a fillet weld all around the interconnector.

### 5.3.2 British Standard BS 449-1970

As stated earlier this standard is under review. The present standard, however, will be used to determine the interconnection requirements.

This standard has two requirements for the spacing of the interconnectors which are:

$$d/r_{U1} \leq 40 \quad (5.3a)$$

or

$$d/r_{U1} \leq 0.6(KL/r_v) \quad (5.3b)$$

Eq. 5.3a governs as it results in a spacing,  $d$ , of 19.6 in.

The forces which the interconnector must resist and the maximum permissible load for the column come from Clauses 30, 36 and 37 of BS 449-1970 and are:

$$P = 20.4 \text{ kips} \quad (5.4a)$$

$$F_{qr} = 0.025 * P = 0.510 \text{ kips} \quad (5.4b)$$

$$F_l = F_{qr} * d/b = 3.97 \text{ kips} \quad (5.4c)$$

$$M = F_{qr} * d/2 = 5.10 \text{ kip-feet} \quad (5.4d)$$

where  $F_{qr}$  = the transverse shear;  $F_l$  = the longitudinal shear;  $M$  = the moment; and  $P$  = the maximum permissible load.

This standard also requires that the interconnectors be placed in pairs at right angles to one another.

Specimens were tested which had five interconnectors as required by the British Standard. The requirements not met were the design capacity of the interconnector, as per



Eqs. 5.4b to 5.4d, and the requirement for the interconnectors to be in pairs. Results from the test program indicate that testing of a specimen to meet all of the BS 449 requirements was not necessary.

### 5.3.3 German Specification DIN 4114-1972

There are two criteria used in this specification to determine the spacing of interconnectors. They are:

$$d/r_u \leq 50 \quad (5.5)$$

or a minimum of two interconnectors at the third points, whichever gives the smallest spacing. In this case, Eq. 5.5 governs and gives a spacing  $d$  of 24.5 in.

The forces which must be resisted by the interconnectors and the maximum permissible load are based on Clauses 8.213, 8.22 and 8.36 of DIN 4114-1972 and are:

$$P = 20.4 \text{ kips} \quad (5.6a)$$

$$F_{qr} = P*\psi/80 = 0.992 \text{ kips} \quad (5.6b)$$

$$F_l = F_{qr} *d/b = 9.26 \text{ kips} \quad (5.6c)$$

where  $\psi = 3.89$ , a buckling constant depending on the slenderness ratio and the type of steel.

Specimens were tested which had four interconnectors as required by the German Standard. The requirement not met was the design capacity of the interconnector, as per Eqs. 5.6b and 5.6c. The results from the test program indi-

cate that the testing of a specimen to meet the DIN 4114 requirements was not necessary.

## 5.4 THEORETICAL RESULTS

### 5.4.1 Torsional-Flexural Buckling

A graph of the slenderness ratio to the effective length has been plotted on Fig. 15 based on the properties of a single 2-1/2 x 2-1/2 x 1/4 in. angle. Fig. 15 is used to determine the effective length required to initiate torsional-flexural buckling. The nominal properties from Table 2 and the following equation, Eq. 4-17 of Ref. 11, are used to calculate the values plotted in Fig. 15:

$$\frac{1}{r_e^2} = \frac{1}{2r_v^2} + \frac{1}{2r_t^2} + \sqrt{\left(\frac{1}{2r_t^2} - \frac{1}{2r_v^2}\right)^2 + \frac{A y_o^2}{I_p} * \frac{1}{r_v^2 r_t^2}} \quad (5.7)$$

where  $r_e$  = the equivalent torsional bending radius of gyration; and  $y_o$  = the distance from the centroid of the angle to its shear center. Eq. 5.7 has been programmed into a programmable calculator to increment the length,  $L$ , to determine the intersection point on the graph Fig. 15. Torsional-flexural buckling governs to the left of the point of intersection, while flexural buckling governs to the right of this point of intersection.

Based on the results of these calculations, a member which has an effective length less than 20.0 in. will fail by torsional-flexural buckling. This information was required to ensure that torsional-flexural buckling would

not occur for the individual angles of the starred angle section being tested.

#### 5.4.2 Spaced Columns

Spaced column theory (17) applies to starred angle compression members only if there is zero or one interconnector. In either case the starred angle compression member will buckle in either the Mode A or Mode B configuration, which is double or single curvature about the U-U axis, respectively. The following equation:

$$P_{cr} = \frac{2\pi^2 EI_U}{(KL)^2} \quad (5.8)$$

predicts either mode of buckling. The difference between the buckling modes is incorporated in the value of K, the effective length factor. The value of K is taken from Table 1 of Ref. 17 for flexural buckling in double curvature (Mode A) and from Fig. 8 of Ref. 17 for flexural buckling in single curvature (Mode B).

Eq. 5.8 was derived by assuming that the individual elements of the built-up member are forced to take the same displaced shape, that the strut is pin-ended and has rigid end stiffeners. The interconnectors are assumed to be pin-connected to each of the individual angles of the strut. The theory also assumes that buckling about the U-U axis governs.

For Mode A buckling, if the end stiffener has a length of zero then  $K = 0.5$  and  $P_{cr} = 51.66$  kips. When the length of the end stiffener is 6 in.  $K = 0.498$  and  $P_{cr} = 52.08$  kips. For the Mode B buckling for end stiffener lengths of 0 and 6 in. the effective length,  $K$ , is 0.567 and 0.521 respectively and the critical load,  $P_{cr}$ , is 40.18 and 47.52 kips respectively. As the Mode B critical loads are less than the Mode A critical loads the Mode B, single curvature buckling about the U-U axis, governs.

The critical load for the Mode B buckling with end stiffeners having lengths of zero inches is tabulated in Table 1 for comparison with the battened column theory and the eigenvalue procedure critical loads.

#### 5.4.3 Battened Columns

This theory is limited to buckling about the U-U axis. It is similar to the spaced column theory except that the interconnectors are assumed to be rigidly fastened to the individual angles.

Koenigsberger and Mohsin (20) compare several different theories on battened struts and point out that Bleich's equation, Eq. 3.20, predicts higher critical loads than experimental buckling loads. Bearing this in mind the critical load can be calculated for the starred angle compression member with one or more interconnectors. Substituting the actual properties from Table 2 into Eq. 3.20 and select-

ing values for the spacing of the interconnectors,  $d$ , the critical load can be calculated. When there is one interconnector,  $d = 60$  in.  $P_{cr} = 42.90$  kips, and for two interconnectors  $d = 40$  in.  $P_{cr} = 61.25$  kips. These values are tabulated in Table 1.

#### 5.4.4 Eigenvalues

These results come directly from the computer program described previously and are tabulated for zero to five interconnectors in Table 1. The eigenvalue procedure permits the starred angle compression member to buckle about either of its principal axes, U-U or V-V.

There are fluctuations in the critical loads from two to five interconnectors, particularly between four and five, which is attributed to truncation and round-off error. This type of error is inherent in large matrices of the order used in this theoretical solution.

#### 5.4.5 Linear Iterative-Incremental Load Deflection Curves

Results of the computer analysis of load versus deflection are plotted in Figs. 16(a), 16(b), 16(d), 16(e) and 16(f) for the starred angle compression members having lengths of 120 in. The theoretical and experimental load-deflection results are shown in the same figures. The theoretical load-deflection curves were checked using the following equation:

$$y = y_0 / (1 - P/P_e) \quad (5.9)$$

where  $y$  = the required displacement;  $y_0$  = the initial out-of-straightness in the plane of the displacements;  $P$  = the axial load; and  $P_e$  = the critical load in the plane of the displacements. The term  $1/(1-P/P_e)$  is known as the amplification factor.

The theoretical curves plotted in conjunction with several of the experimental curves in Fig. 16 show reasonable agreement. Differences between the theoretical and the experimental curves may be a result of:

a) Experimental

- i) the actual physical and mechanical properties may differ slightly from the average values used, and
- ii) inaccuracies in the measurement of the initial out-of-straightness.

b) Theoretical

- i) assuming that the length of the end stiffener is zero,
- ii) the assumption that the interconnector is rigid,
- iii) the finite element procedure is based on the assumption that the shear center and the centroid coincide which for the angle section is not the case, and
- iv) that the load is applied centrically.

## 5.5 EXPERIMENTAL RESULTS

### 5.5.1 Test Summaries

The failure load and principal axis of failure are listed in Table 4 for all tests conducted. Table 4 also shows the largest initial imperfection measured in each specimen. It is also seen that the initial out-of-straightness varied from  $L/1000$  to  $L/10000$  for the specimens tested.

All of the experimental data was reduced and is plotted in Figs. 16, 17 and 18, for specimens having lengths of 120, 80 and 40 in., respectively. These figures show the load displacement behaviour of the specimens as well as the failure load and test designation.

Superimposed on Figs. 16(a), 16(b), 16(d), 16(e), and 16(f) are theoretical load-deflection curves generated by the linear iterative-incremental approach. It can be seen that the theoretical curves are in reasonable agreement with the experimental results at low loads. At higher loads the agreement is not as good. The variance may be due to the reasons listed at the end of the previous section and because the stiffness matrices become increasingly ill-conditioned as the failure load is approached.

In all the tests conducted there is generally a difference in the failure mode between the struts with zero and one interconnector and the struts with two or more interconnectors. The change in the failure mode is the principal

axis about which failure occurs. For the struts having zero and one interconnector failure occurred about the U-U axis and for the struts with two or more interconnectors failure occurred about the V-V axis.

Graphs of load versus displacement for tests on specimens of shorter lengths, 80 in. and 40 in., are plotted in Figs. 17 and 18, respectively. These tests were conducted as an experimental investigation only to determine the failure loads and failure modes of the struts. From these graphs it is seen that failure occurs about the U-U axis for specimens with zero and one interconnector. For specimens having two interconnectors the failure mode switches to bending about the V-V axis. There are displacements in both of the principal axes which may be caused by the initial imperfections, residual stresses, and the rigidity of the end connectors.

## 5.6 SUMMARY

Geometric properties are calculated for the  $2\frac{1}{2} \times 2\frac{1}{2} \times \frac{1}{4}$  in. angle and the actual properties are found to be greater than the nominal properties listed in the CISC Handbook (7) by an amount greater than the standard mill practice tolerance. The actual values for the geometric properties were used in the theoretical calculations and in reducing the experimental results. For the purpose of design and review of the requirements of the standards



nominal values of the geometric properties are used. Canadian and American, British, and German Standards are used to calculate interconnection requirements.

The critical loads are calculated using three theories; the eigenvalue procedure, spaced column theory, and the battened column theory. The eigenvalue procedure is the only procedure which could be used to predict the critical loads for the starred angle struts with zero to five interconnectors. The other two theories are limited to starred angle struts with zero or one interconnector only.

The linear iterative-incremental approach, the theoretical analysis procedure used to calculate the theoretical load-deflection curves, yields results which agree favourably with the experimental results for specimens with a length of 120 in. (Fig. 16). These results also show that there is a change in failure mode between struts with zero and one interconnector when compared to struts with two interconnectors. Experimentally the results of the tests of specimens having lengths of 80 in. and 40 in. are plotted on graphs in Figs. 17 and 18. The same behaviour of the change in the buckling mode is seen in these graphs.

## Chapter 6

### DISCUSSION

#### 6.1 INTRODUCTION

The theoretical and experimental results described in the preceding chapters are broken down and discussed under the following headings: failure load, load-deflection curves, number of interconnectors, effect of end connectors, and forces in the interconnectors. The implications to the present design standards are discussed.

#### 6.2 FAILURE LOAD

##### 6.2.1 120 Inch Specimens

##### 6.2.1.1 Theoretical Predictions

The 120 in. specimens are slender starred angle compression members and hence elastic theories are used to predict critical loads. In Table 1 the predicted critical loads for the starred angle compression member, constructed from two  $2\frac{1}{2} \times 2\frac{1}{2} \times \frac{1}{4}$  in. angles, using each of the respective theories, spaced column, battened column, and eigenvalue, are tabulated against the number of interconnectors.

Spaced column theory predicts only the critical loads for starred angle compression members having zero or one

interconnector. Battened column theory predicts the critical loads for a starred angle compression member having one or more interconnectors. Two critical loads are calculated, using the battened column theory, for starred angle struts having one and two interconnectors. It is not necessary to calculate critical loads having three or more interconnectors using the battened column theory as the predicted load becomes larger with the addition of more interconnectors and, as can be seen in Table 1, the predicted critical load for a specimen having two interconnectors is higher by the battened column theory than the Euler load about the V-V axis.

The eigenvalue procedure is used to predict the buckling load for starred angle struts having zero to five interconnectors. This procedure also predicts the buckling mode of the strut.

Both the battened column and spaced column theories predict critical loads when failure occurs about the U-U axis. The eigenvalue procedure, on the other hand, predicts the lowest critical load that occurs about either the U-U or V-V axis.

Comparing the predicted critical loads for starred angle struts having zero or one interconnector shows good agreement between the eigenvalue procedure and the spaced column theory. Battened column theory gives slightly higher results for a starred angle strut having one interconnector

which is not unexpected as the equation used is reported to generally give higher results (20).

Examining the results of a starred angle strut having two interconnectors shows that there is a considerable discrepancy between the battened column and eigenvalue procedure predictions. This is attributed to the fact that when two or more interconnectors are installed in the starred angle strut the buckling mode changes. With zero and one interconnector the starred angle strut buckles about the U-U axis and with two or more interconnectors it buckles about the V-V axis. The eigenvalue procedure predicts this change in buckled shape.

The non-dimensional graph, Fig. 19, a plot of the failure load versus the number of interconnectors clearly shows the change in critical load between starred angle struts having one and two interconnectors.

The eigenvalue procedure was used with the geometric properties of other pairs of equal leg angles to verify that the theoretically predicted behaviour is more general than for just the pair of 2-1/2 x 2-1/2 x 1/4 in. angles. The same behaviour of the change in the buckled shape and load between specimens having zero and one interconnector and specimens having two or more interconnectors is predicted.

The critical load is calculated for a starred angle compression member having a continuous interconnector running the full height. The results of using a 2 x 3/8 in.

bar full height increases the critical load by five percent. This increase is small and for all practical purposes insignificant. It does point out, however, that any localized increase in stiffness at the point of interconnection by the interconnector can be neglected.

The effect of the length of end connector is calculated and found to be insignificant particularly when the starred angle buckles about the V-V axis. As the starred angle compression member with two interconnectors failed about the V-V axis the effect of the end connectors is neglected.

#### 6.2.1.2 Experimental Results

Table 4 tabulates the buckling load and principal axis of failure for all tests conducted. From this table it can be seen that for specimens having zero and one interconnector the principal axis of failure, for the starred angle struts, occurred about the U-U axis. For specimens with two or more interconnectors failure of the starred angle strut occurred principally about the V-V axis.

The size or type of interconnector had no apparent effect on the buckling mode or strength, however, the method of fastening the interconnector did have an effect. For specimens having types A, B, C, D and E interconnectors (see Table 3 for types of interconnectors) there is no apparent change in buckling shape or load at a given number of interconnectors. All of these five types of interconnectors were rigidly connected, by welding, to the individual angles.

Specimens with type F and G interconnectors, tests 120F2.1 and 120G2.1, indicate that the failure mode changes when a pin connector was used. Both of these types of interconnectors were pin-connected to the individual angles and both specimens tended to fail about a combined axis.

Test 120 AF, a test with an interconnector installed full height, resulted in a buckling load less than predicted. The results were no different than those for tests with two or more interconnectors. The buckling load should have been five percent higher, however the large amount of welding may have caused unfavourable residual stresses.

These experimental buckling loads and buckled shapes agree favourably with the theoretically predicted critical loads and buckling modes and are compared in the following section.

#### 6.2.1.3 Comparison of Theoretical and Experimental Results

Fig. 19 shows both the experimental and theoretically predicted results for the 120 in. starred angle specimens. The ordinates are plotted as the ratio of failure load to the Euler buckling load versus the number of interconnectors. Only the theoretical predictions obtained using the eigenvalue procedure and only the test results for specimens having type A interconnectors were used.

The variations in the experimental buckling load are principally a result of the differences in the initial out-

of-straightness. Test 120AO.2 is substantially different from test 120AO.1 as they had different buckled shapes as a result of the difference in the direction of the initial out-of-straightnesses of each of the angles. In general the experimental failure loads agreed with the theoretical predictions.

#### 6.2.2 80 and 40 Inch Specimens

The test results from 80 in. and 40 in. specimens are discussed together as only an experimental program was carried out on these specimens. The purpose of these tests was to determine if the behaviour of the shorter, 80 in. and 40 in., specimens, which failed inelastically, were similar to that of the 120 in. specimen.

All of the failure loads and principal axes of failure are tabulated in Table 4. It is evident from this data that there is no significant difference in the capacity of the specimens with zero and one interconnector to those specimens having two interconnectors.

There is, however, a definite difference in the failure mode between the specimens having zero and one interconnector to the specimens with two interconnectors in that the specimens failed about different axes. In this regard the behaviour of the 80 in. and 40 in. specimens was similar to that of the 120 in. specimen. Specimens with zero or one interconnector failed, for practical purposes, about the U-U

axis, whereas specimens with two interconnectors failed about the V-V axis.

### 6.3 . LOAD-DISPLACEMENT

#### 6.3.1 . 120 Inch Specimens

##### 6.3.1.1 Theoretical Predictions

The analytical procedure used to predict the load-deflection curves for the specimen is a linear iterative-incremental method as discussed earlier.

Fig. 16(a) and 16(b) show the theoretical and experimental curves for the tests 120A0.1 and 120A0.2. Examination of only the theoretical curves, of the two graphs Fig. 16(a) and 16(b), indicates that they represent different buckling modes of the respective specimens. Test 120A0.1, buckles about the U-U axis, and, test 120A0.2, buckles about the V-V axis. This is a result of the difference in the direction of the initial out-of-straightnesses of each of the individual angles for each of the two specimens. The initial out-of-straightness is shown as the initial deflection at zero load.

Figs. 16(d) and 16(e) show the theoretical and experimental curves for tests 120A1.3 and 120A1.5. In both cases the theory predicts failure to occur about the U-U axis. Only one curve is plotted for each of the axes as the specimens had one interconnector, fastening the individual angles at mid-height, which in turn forced the individual angles to



take the same displaced shape. The theoretical curves are based on the assumption that the interconnector forces the angles to deflect the same. This assumption is confirmed experimentally.

Fig. 16(f) shows the theoretical and experimental curves for test 120A2.1. The theoretical curve clearly predicts that buckling occurs about the V-V axis. It is interesting to note that even though the individual angles have initial out-of-straightness in opposite directions they are forced to take the same displaced shape. When compared to the behaviour of specimens with zero interconnectors (Fig. 16(a) and 16(b)) it demonstrates the necessity of interconnection.

No theoretical curves were plotted for specimens having three or more interconnectors as two interconnectors are optimum. The effect of the number of interconnectors is discussed later in this section.

#### 6.3.1.2 Experimental Results

The test results are plotted in Figs. 16(a) to 16(i). On several of the figures the theoretical predictions, which agree favourably with the actual results, are superimposed.

By comparing Figs. 16(a) and 16(b) the reason that the failure load was higher for test 120A0.2 than test 120A0.1 can be seen. The load-deflection curves for test 120A0.2, in the direction of the V axis,  $V_1$  and  $V_2$ , are in opposite

directions and the load to sustain this displaced shape is greater than the failure load in the perpendicular direction. This condition was somewhat dangerous as either angle could have snapped-through to buckle about the U axis. The snap-through load was predicted, from Fig. 16(b), to be 36 kips. At about this load there is a change in the theoretical predictions for the deflection  $V_2$ .

Figs. 16(c), 16(d) and 16(e) show the deflection for tests 120A1.2, 120A1.3, and 120A1.4, all of which had only one interconnector at mid-height. All these curves indicate that the specimen failed principally about the U-U axis which is similar to that for specimens with zero interconnectors. The experimental deflections in the direction of the V axis agree favourably with the theoretical predictions.

Fig. 16(f), for test 120A2.1, a specimen with two interconnectors, shows that the individual angles take the same displaced shape even though the initial imperfections start in the opposite directions. Failure of this specimen occurs about the V-V axis. Displacements in the direction of the U axis occur because of initial out-of-straightness in this direction though failure did not occur in this direction. This is in contrast to the specimens with zero and one interconnector where failure occurs principally about the U-U axis.

Figs. 16(g), 16(h), and 16(i) for tests 120A3.1, 120A3.2 and 120A5.1, specimens having three to five interconnectors, clearly show that failure is about the V-V axis. All these specimens demonstrate that there is no advantage to installing more than two interconnectors.

#### 6.3.1.3 Comparison of Theoretical and Experimental Results

For the 120 in. long specimens the agreement between the theoretical predictions and the experimental results is good. For all tests the failure mode was determined simply by the number of interconnectors. This was shown experimentally by conducting two series of tests on the same specimens by simply increasing the number of interconnectors from one test to the next. The first series of tests were tests 120A1.3 and 120A3.1, where two interconnectors were added to test specimen 120A1.3 to obtain specimen 120A3.1. The second series of tests were tests 120A0.2, and 120A2.1, where two interconnectors were added to the test specimen 120A0.2 to obtain specimen 120A2.1.

Precautions were taken to ensure that the specimens remained elastic during the first loading of each specimen. The initial out-of-straightness both before and after testing were determined and the dial indicators were monitored to ensure that they returned to zero upon the completion of each test. No changes in the initial out-of-straightness were recorded. The dial indicator readings returned to within 0.005 in. of the initial zero.

These two series of tests indicate that there is a definite change in the buckled shape between specimens having zero or one interconnector and specimens having two or three interconnectors.

In general the theoretical predictions for the load-deflection curves agree with the experimental results. However, the theoretical curves for displacements in the direction of the , U axis do not agree with the experimental results for tests 120A1.3 and 120A1.5 where the experimental deflections are greater than the theoretical predictions. The reasons for the difference are listed in Section 5.4.5.

#### 6.3.2 80 and 40 Inch Specimens

Figs. 17(a), 17(b), and 17(c) show the experimental load-deflection curves for tests 80A1.2, 80A2.2, and 80A2.3 respectively. No theoretical analysis was performed on specimens of 80 in. and 40 in. lengths.

These curves show that there is a definite change in the deflected shape as the number of interconnectors is increased from one to two. Specimen 80A1.2 had about equal displacements in the direction of the U and the V axes, while specimens 80A2.2 and 80A2.3 deflect primarily in the direction of the U axis.

Figs. 18(a), 18(b), and 18(c) show the experimental load-deflection curves for tests 40A0.1, 40A1.2, and 40A2.2 which indicate the same tendency to bend about the U-U axis.

for specimens with zero or one interconnector and to bend about the V-V axis for specimens with two interconnectors. Again with one interconnector the 40 in. long specimen had about equal displacements in the direction of both axes, however, with two interconnectors there is no doubt that failure occur about the V-V axis.

#### 6.4 EFFECT OF THE NUMBER OF INTERCONNECTORS

Simple theory would suggest that if interconnectors are provided to make the slenderness ratio of the individual angles about the U'-U' axis equal to the slenderness ratio of the entire cross section, the V-V axis, then both the individual angle and the built-up strut would have the same buckling load. For the equal leg angles this situation should always exist as the slenderness ratio of the individual angles is  $1/2$  of the slenderness ratio of the entire cross section. This suggests that only one interconnector at mid-height would be sufficient for the starred angle arrangement.

Both theory and test show that this is not the case and that with one interconnector failure is always about the U-U axis. This is considered to be due to the increased flexibility of the starred angle member about the U-U axis as compared to that of a member with a continuous interconnection and the same geometric properties.

Once the number of interconnectors is increased to two the member is made sufficiently rigid that the starred angle compression member has an effective slenderness ratio for the buckling about the V-V axis that is less than that for buckling about the U-U axis. Thus for two or more interconnectors buckling takes place about the V-V axis, as demonstrated both experimentally and theoretically.

The required number of interconnectors is therefore two to ensure that buckling about the V-V axis occurs. Fewer interconnectors are unsatisfactory and more interconnectors are unnecessary. The interconnector should be designed as discussed in Section 6.5.

#### 6.5 EFFECT OF THE END CONNECTOR

Theoretically the end connectors should contribute to the stiffness of the strut. The end connector should provide some end restraint when the strut bends about the U-U axis and negligible restraint when the strut bends about the V-V axis. Both effects have been previously described in detail.

Experimentally no significant change in the buckling load was found when different end conditions were used. Test specimen 120A1.6P, having cap and base plates, did not have a smaller buckling load than other tests conducted on 120 in. specimens with one interconnector and Tee end connectors. It is considered that a number of variables contribute to possible differences in the buckling load and that the length of the end connector is not as significant as some of the other variables, such as the initial imperfections.

#### 6.6 FORCES IN THE INTERCONNECTOR

Theoretical values for the forces in the interconnectors are determined to be used for the purposes of designing the interconnectors and the fastening to the individual angles. Experimentally it is determined that the forces in the interconnector are not large and that the method of the fastening does affect the failure mode of the specimen.

The type E interconnector had a very small amount of weld fastening the interconnector to the individual angles compared to the type A interconnector (see Table 3). Test 120E2.1 shows the same failure mode and only a slight reduction in the failure load as compared to tests 120A2.1 and 120A2.2.

Specimens 120F2.1 and 120G2.1 had the interconnectors bolted to the individual angles and had considerably reduced failure loads as compared to tests 120A2.1 and 120A2.2. The failure mode was about a combination of the two principal axes. These specimens with bolted connections simulate spaced columns, that is, the interconnectors acted only as spacers and did not transfer any shear or bending forces.

These three tests indicate that there is a need to develop shear and bending forces in the interconnector. If no shear force or bending moment is transferred by the interconnector then the starred angle strut acts as a spaced column.

The same principals used to analyze the forces in the battens of a battened column (Fig. 22) were used to determine the forces in the interconnector as given in Appendix C. The forces that need to be considered are the vertical shear force and corresponding bending moment which are functions of the axial force in the strut. It is recommended that the following forces, as detailed in Appendix C, be used:

$$Q = 0.01 * C_f$$

(6.1)



$$F_z = \frac{Qd}{nb} \quad (6.2)$$

$$M_u = \frac{F_z b}{2} \quad (6.3)$$

where  $C_f$  = the axial load in the strut;  $Q$  = the shear force in the strut;  $F_z$  = the shear force in the interconnector; and  $M_u$  = the bending moment in the interconnector.

#### 6.7. REVIEW OF THE REQUIREMENTS OF THE DESIGN STANDARDS

All the standards examined have different requirements for the number and design of the interconnectors and the related fastening to the individual angles of starred angle compression members. Apparently research has been insufficient to establish the actual behaviour of the starred angle strut and hence no consistent set of design rules exists.

The present Canadian Standards, CSA S16 (6), require that the slenderness ratio of the individual angles between points of interconnection not exceed the slenderness ratio of the member as a whole. The relationship of the geometric properties for the equal leg angles results in the Canadian Standards requiring only one interconnector.

The present British and German Standards have requirements which are more conservative than the Canadian Standards. The minimum requirement of both standards is that two interconnectors are required. Both of these standards also require specific shear and bending forces to be resisted.

The results of this research clearly indicate that the requirements of the Canadian Standards for the interconnection of starred angle compression members is inadequate and should be changed.

## Chapter 7

### CONCLUSIONS AND RECOMMENDATIONS

#### 7.1 CONCLUSIONS

The following conclusions are based on the discussion of the theoretical and experimental results:

- a) the relationship between the geometric properties of the individual angles and the geometric properties of the built-up section is  $r_v/r_u = 1.96$ ,
- b) members with zero or one interconnector fail by bending about the U-U axis, whereas, members having two or more interconnectors fail by bending about the V-V axis,
- c) there is a corresponding increase in failure load with the change in the failure mode,
- d) the optimum number of interconnectors for the starred angle compression members is two, located at the third points,
- e) the length of the end connector has a negligible effect on the failure load when two interconnectors are used because the starred angle compression member fails about the V-V axis, and

- i) some shear force and bending moment should be considered in the design of the interconnectors and their fastening to the individual angles to ensure that bending about the V-V axis controls.

## 7.2 RECOMMENDATIONS

As the objective is to determine suitable design rules the following recommendations are made:

- a) design of the starred angle members should be based on the properties of the built-up section,
- b) two interconnectors, in addition to the end connectors, placed at the third points, should be used for any equal leg angle used to construct starred angle compression members, and
- c) the interconnector should be designed for shear and bending using the following equations:

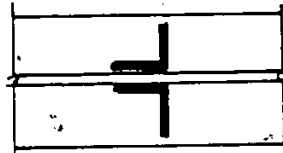
- i)  $F_z = C_f * L / 1000b$

- ii)  $M_u = C_f * L / 2000$

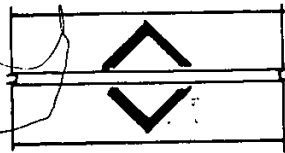
### 7.3 FURTHER RESEARCH

There are several questions raised that should be the basis of further research as follows:

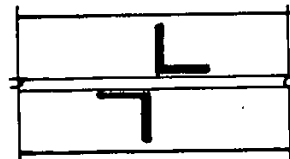
- a) the effects of interconnection on other arrangements of double angles, particularly the box arrangement,
- b) a general study of the effects of the out-of-straightness in one plane on the load-displacement in the perpendicular plane, and
- c) further study on the short and intermediate lengths of starred angle compression members.



a) BACK-TO-BACK



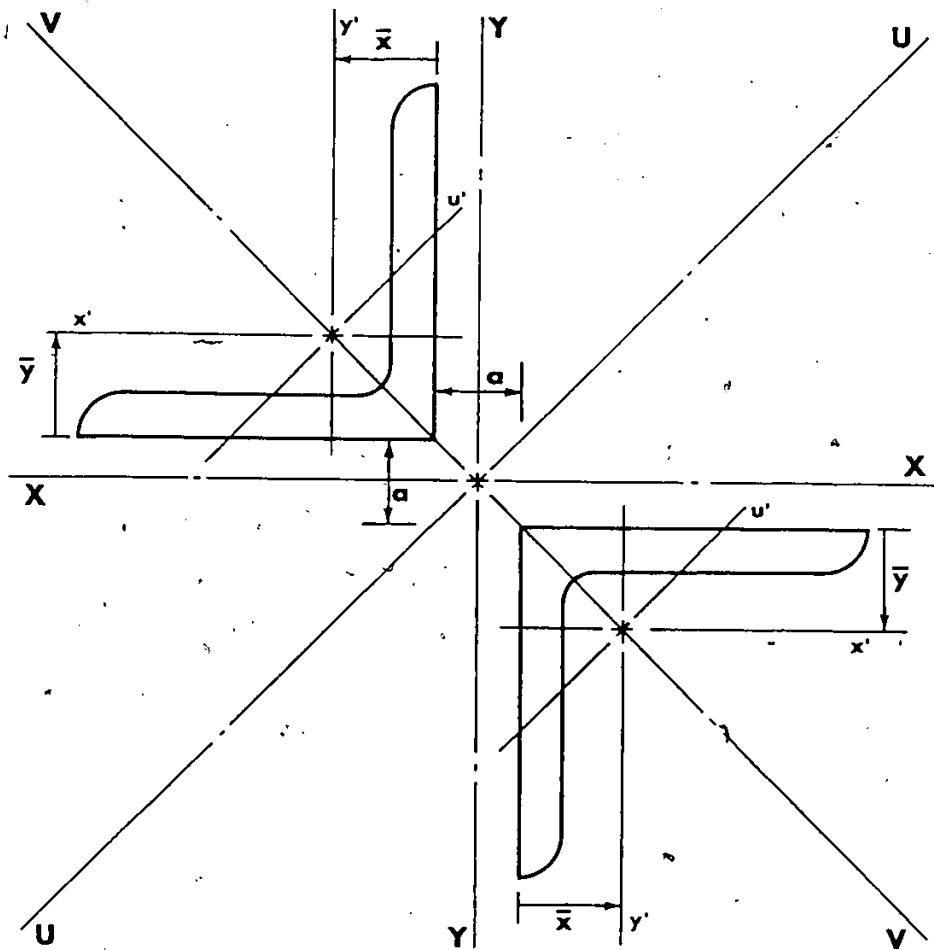
b) BOX



c) STARRED

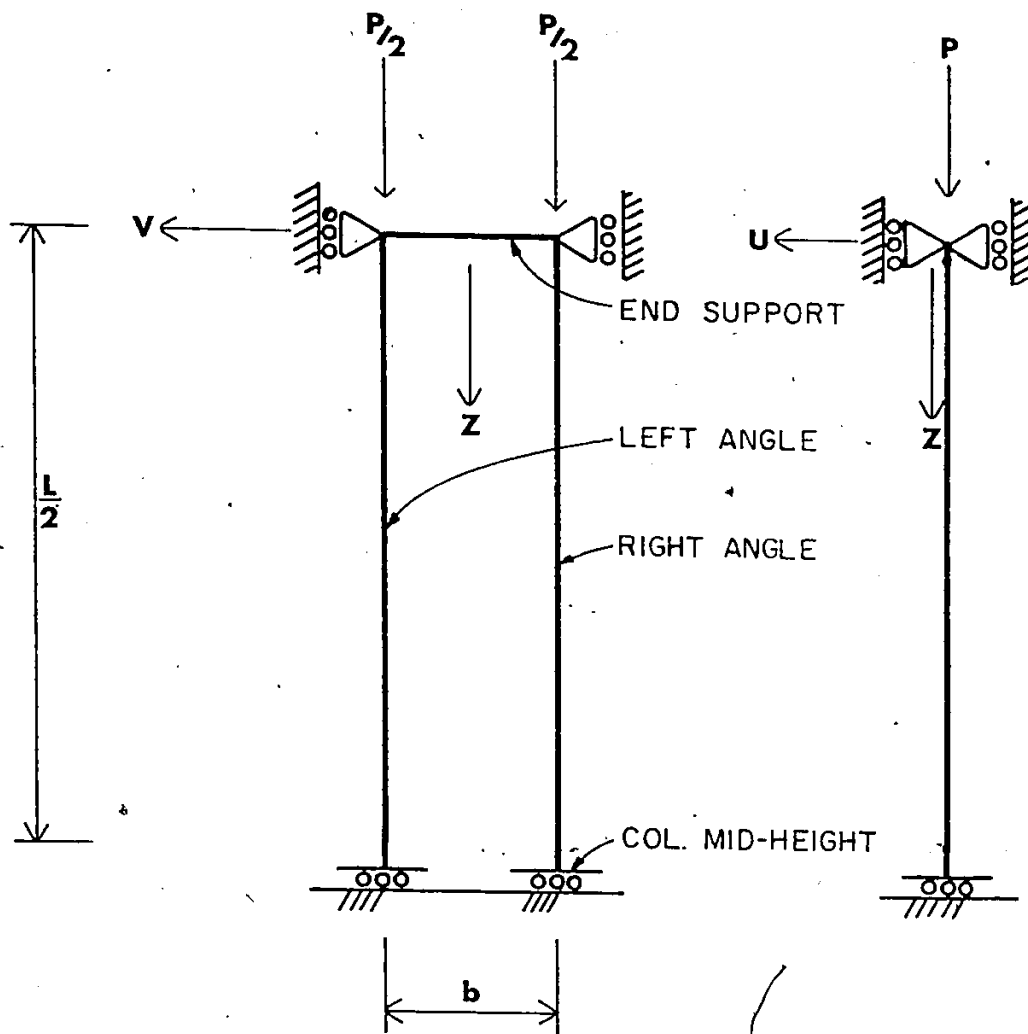
ARRANGEMENTS OF DOUBLE ANGLES

FIGURE 1



STARRED ANGLE GEOMETRY

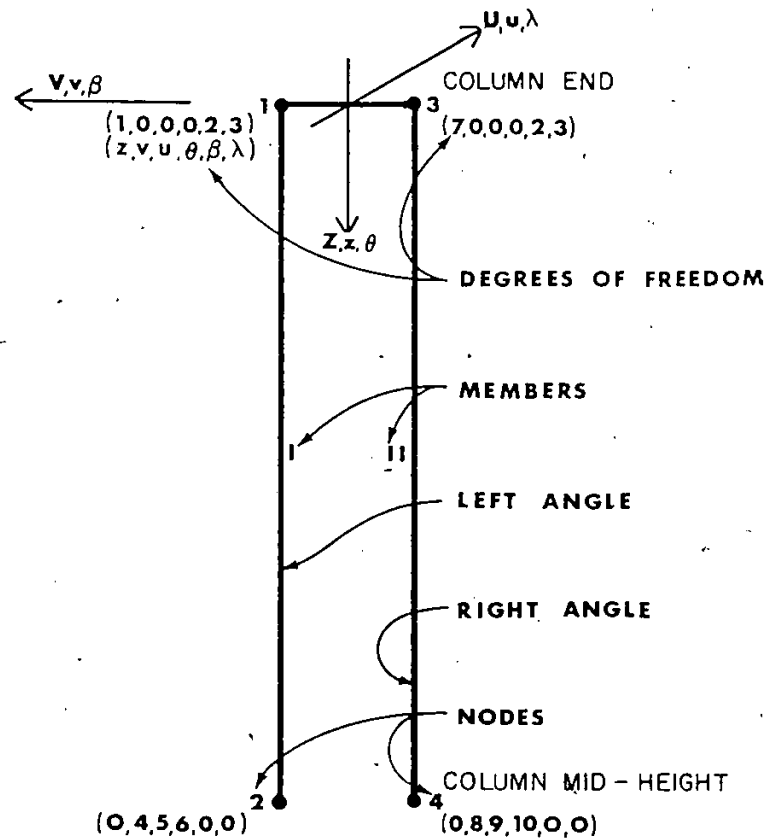
FIGURE 2



MODEL OF STARRED ANGLE

FIGURE 3



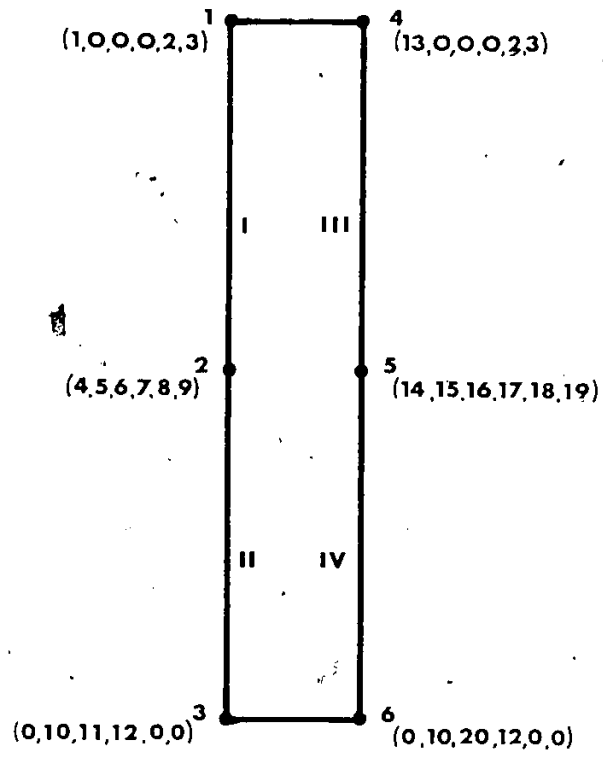


NOTE: THE COMMENTS ON FIG. 4a APPLY TO FIGS. 4a TO 4f

a) 0 INTERCONNECTORS

FINITE ELEMENT MODEL

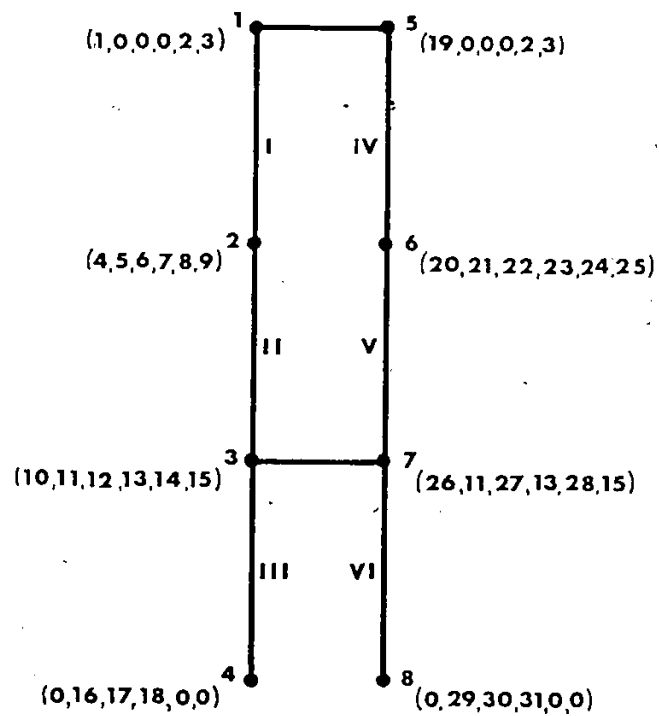
FIGURE 4



b) I INTERCONNECTOR

FINITE ELEMENT MODEL

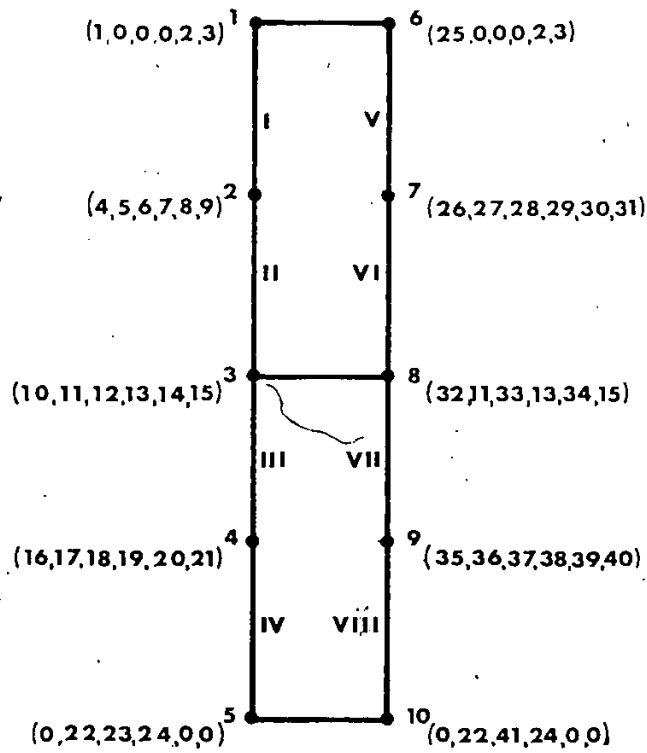
FIGURE 4



c) 2 INTERCONNECTORS

FINITE ELEMENT MODEL

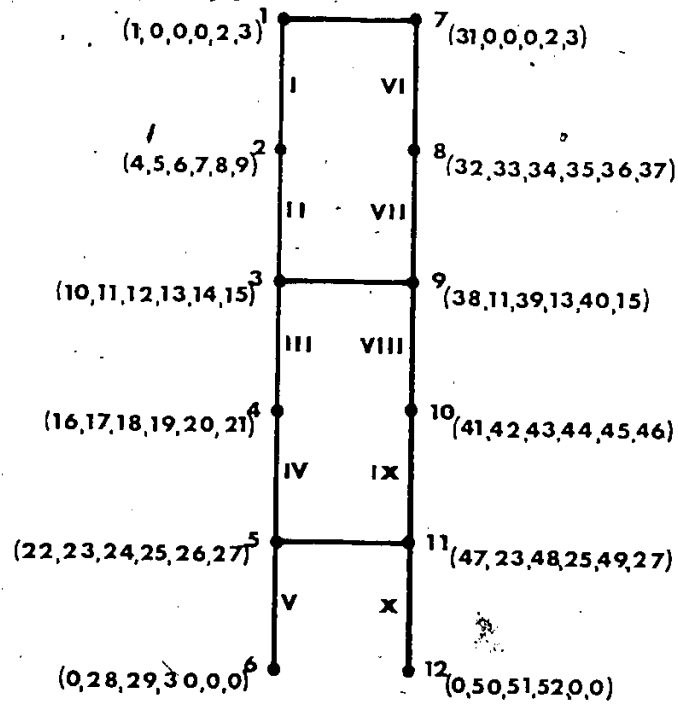
FIGURE 4



d) 3 INTERCONNECTORS

FINITE ELEMENT MODEL

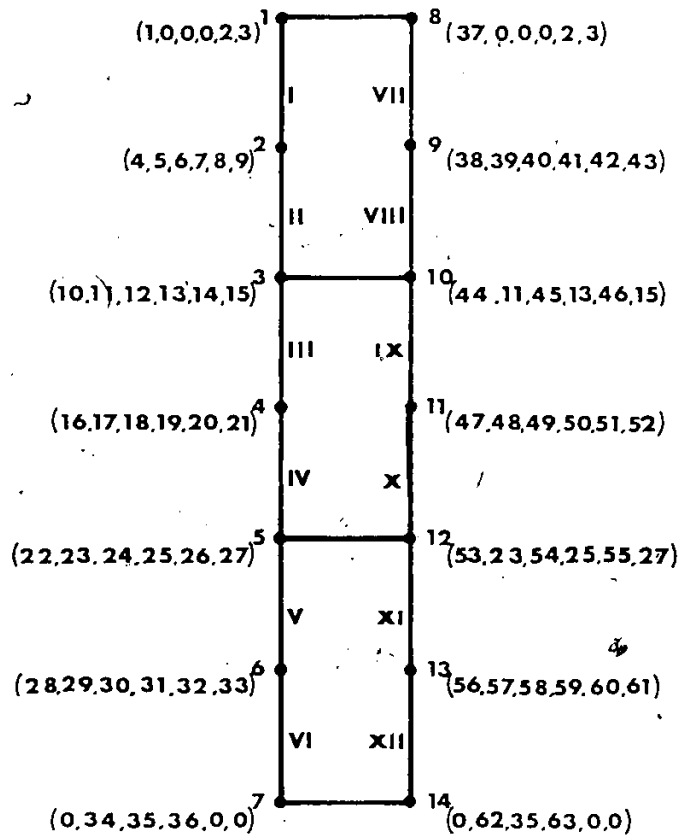
FIGURE 4



e) 4 INTERCONNECTORS

FINITE ELEMENT MODEL

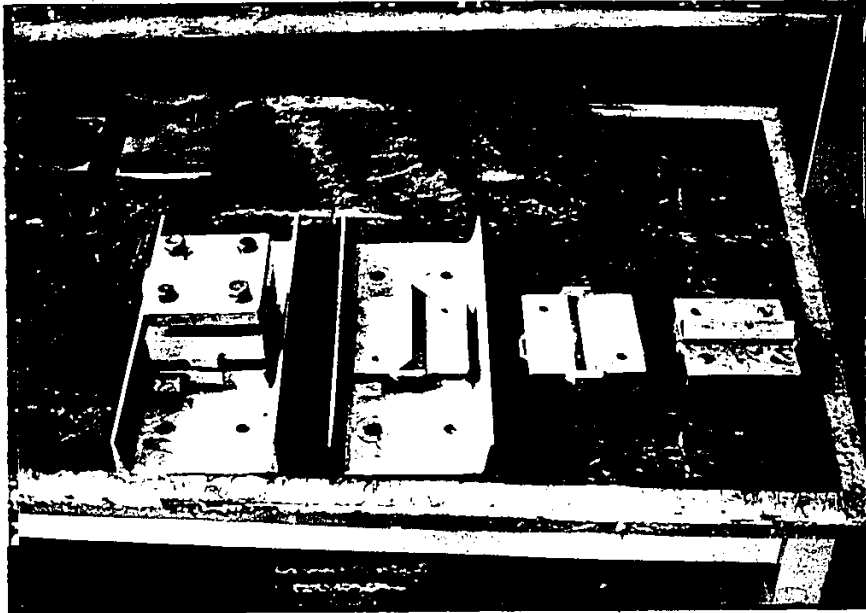
FIGURE 4



f) 5 INTERCONNECTORS

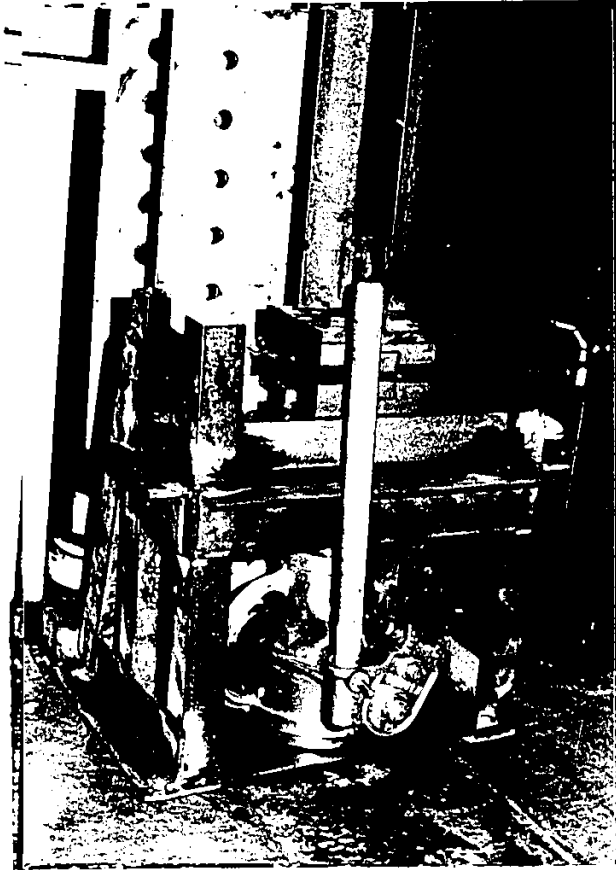
FINITE ELEMENT MODEL

FIGURE 4



KNIFE EDGE ASSEMBLY

FIGURE 5

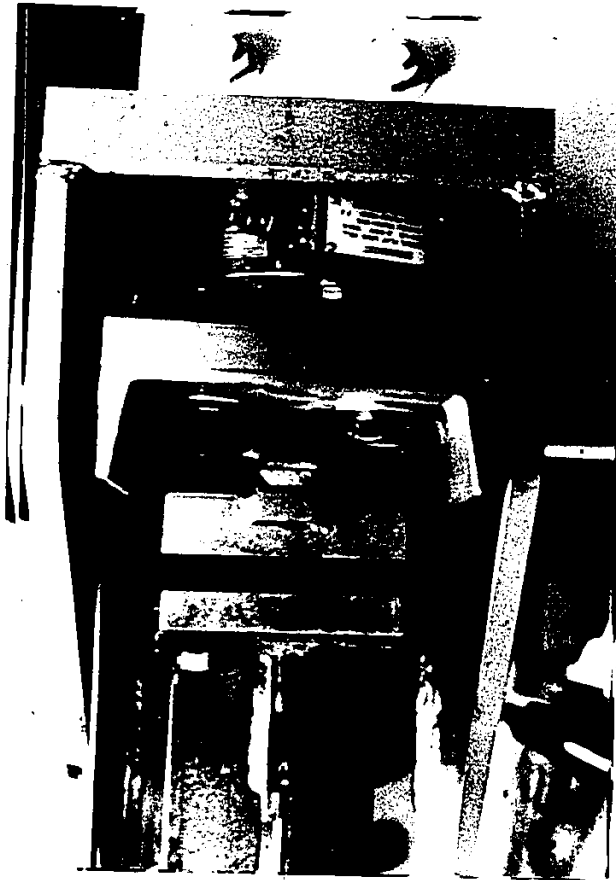


a) BOTTOM FIXTURE

END FIXTURES

FIGURE 6





b) TOP FIXTURE

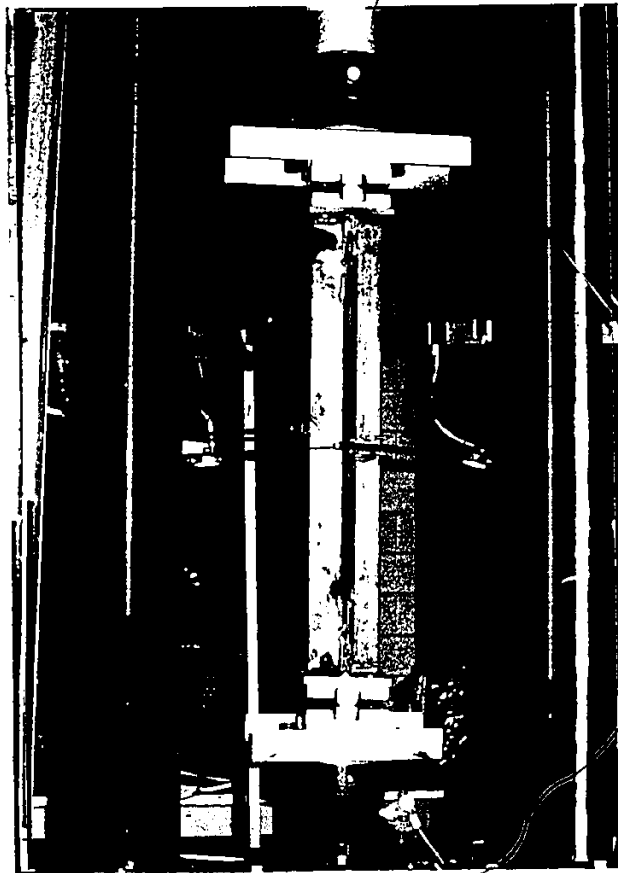
END FIXTURES

FIGURE 6



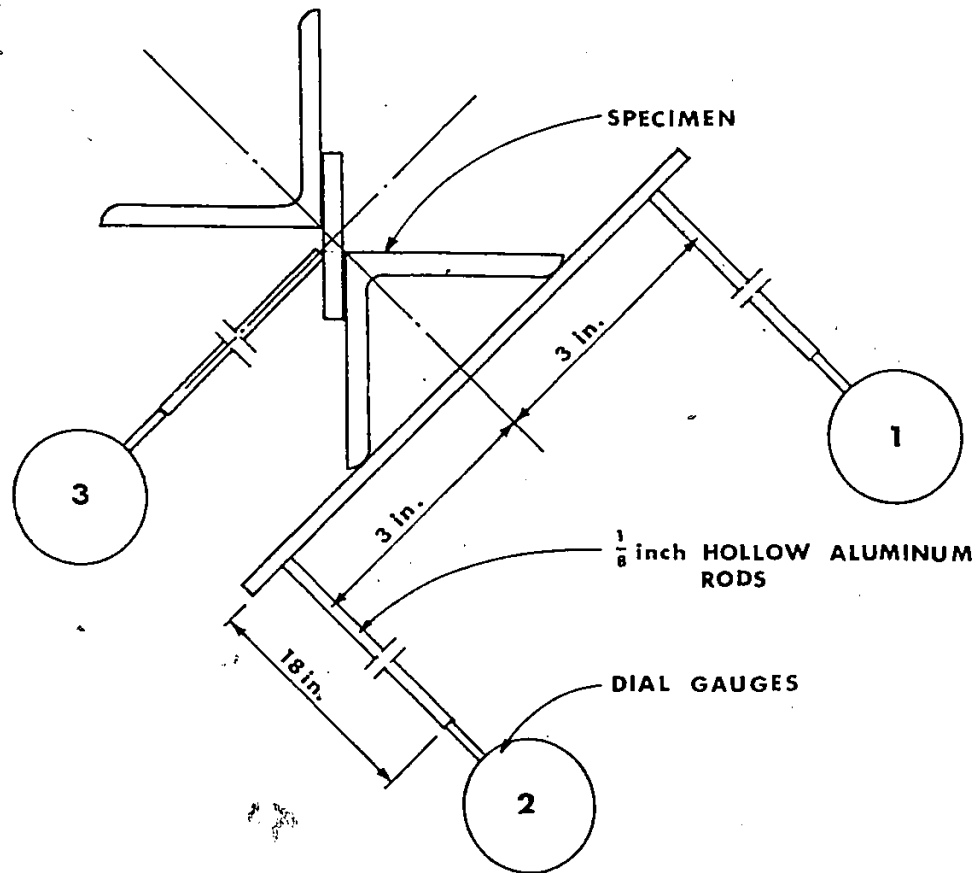
SET-UP OF 120 INCH SPECIMEN

FIGURE 7



SET-UP OF 80 & 40 INCH SPECIMENS

FIGURE 8



a) DIAL INDICATORS AT INTERCONNECTOR

INSTRUMENTATION

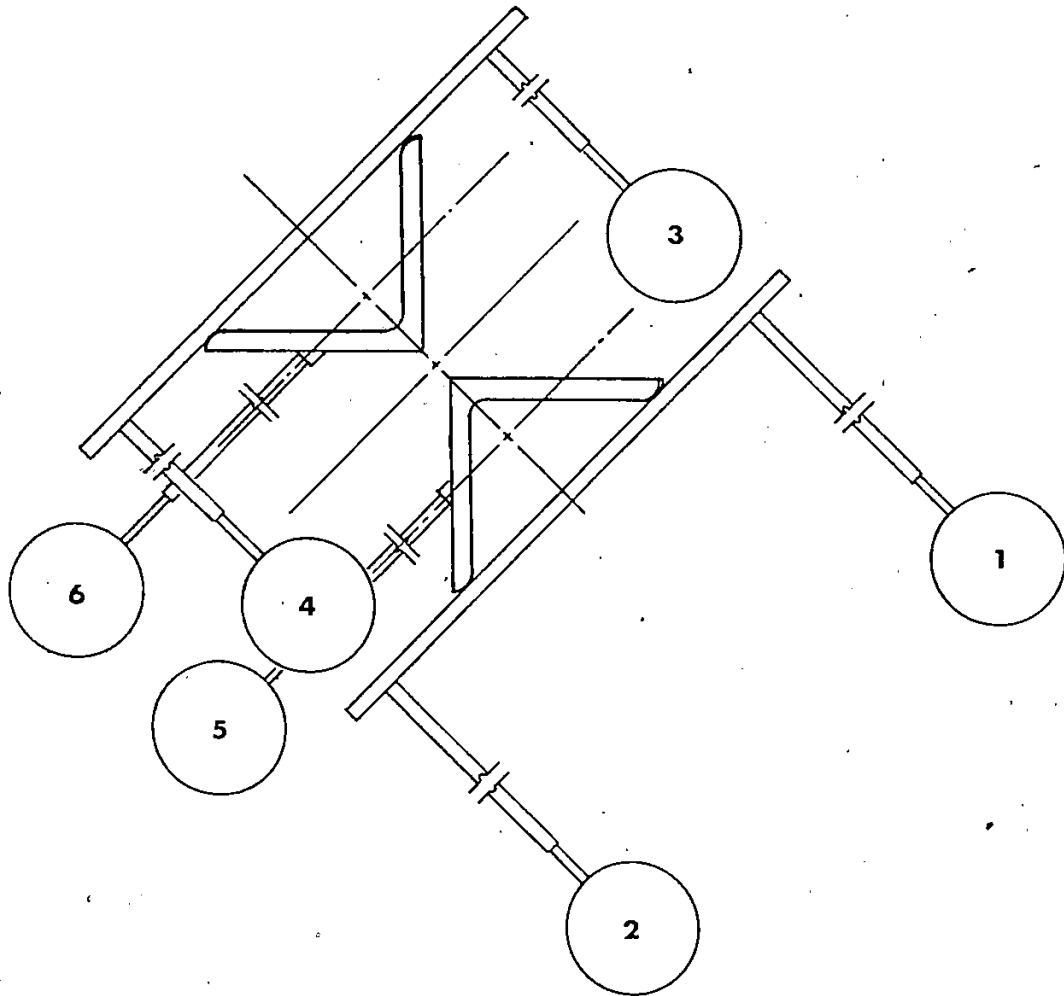
FIGURE 9



b) PHOTOGRAPH OF INSTRUMENTATION  
AT INTERCONNECTORS

INSTRUMENTATION

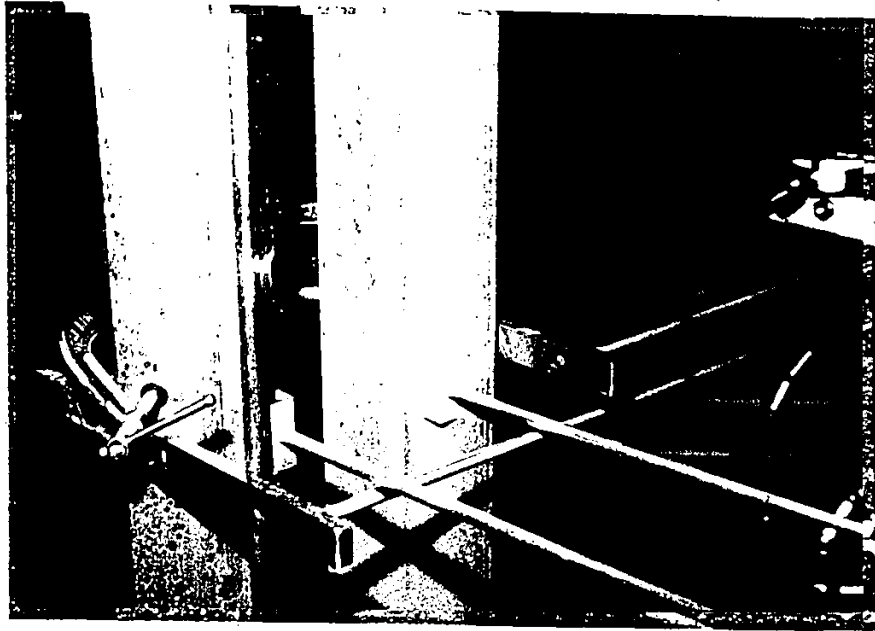
FIGURE 9



c) DIAL INDICATORS BETWEEN INTERCONNECTORS

INSTRUMENTATION

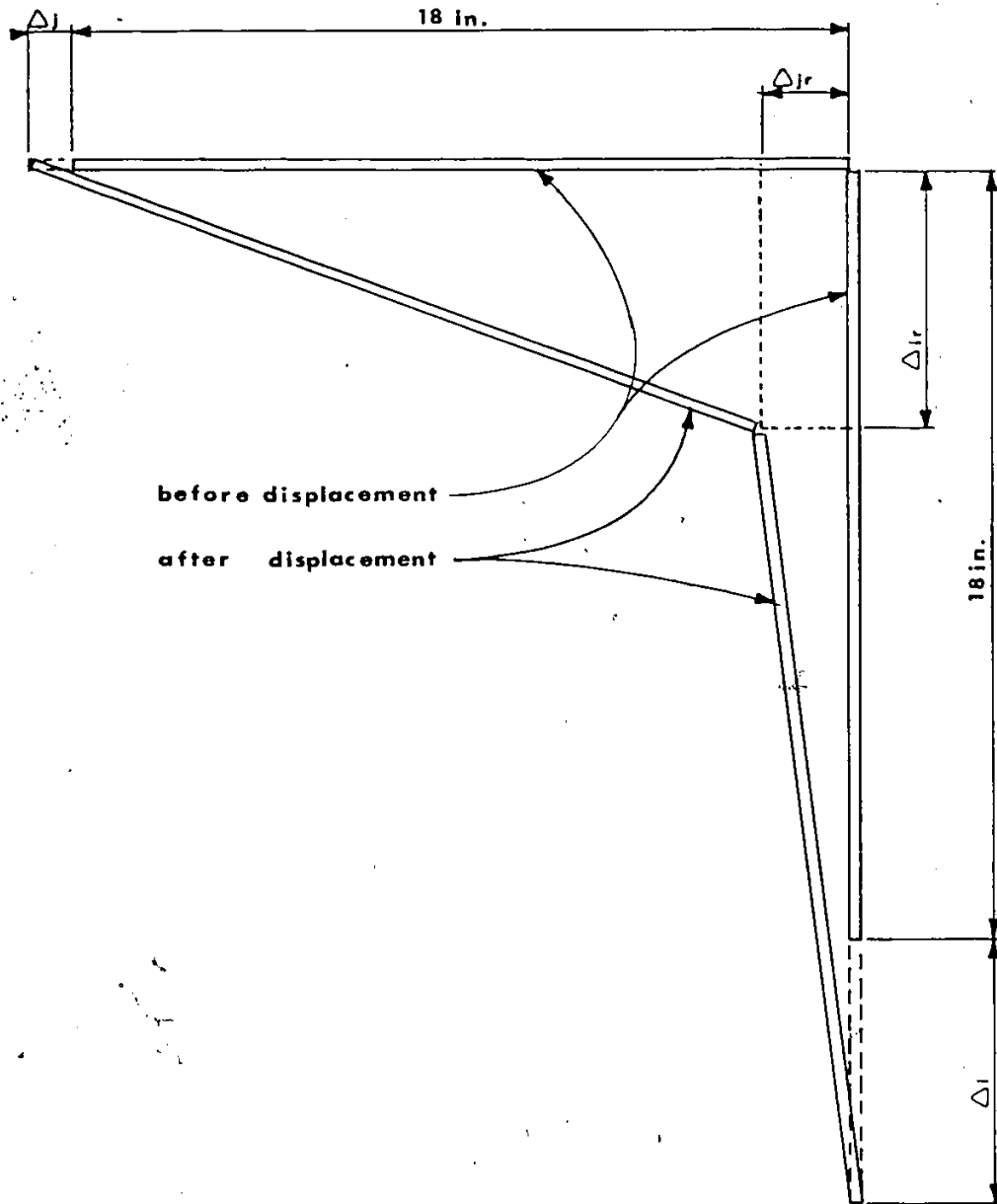
FIGURE 9



d) PHOTOGRAPH OF INSTRUMENTATION  
BETWEEN INTERCONNECTORS

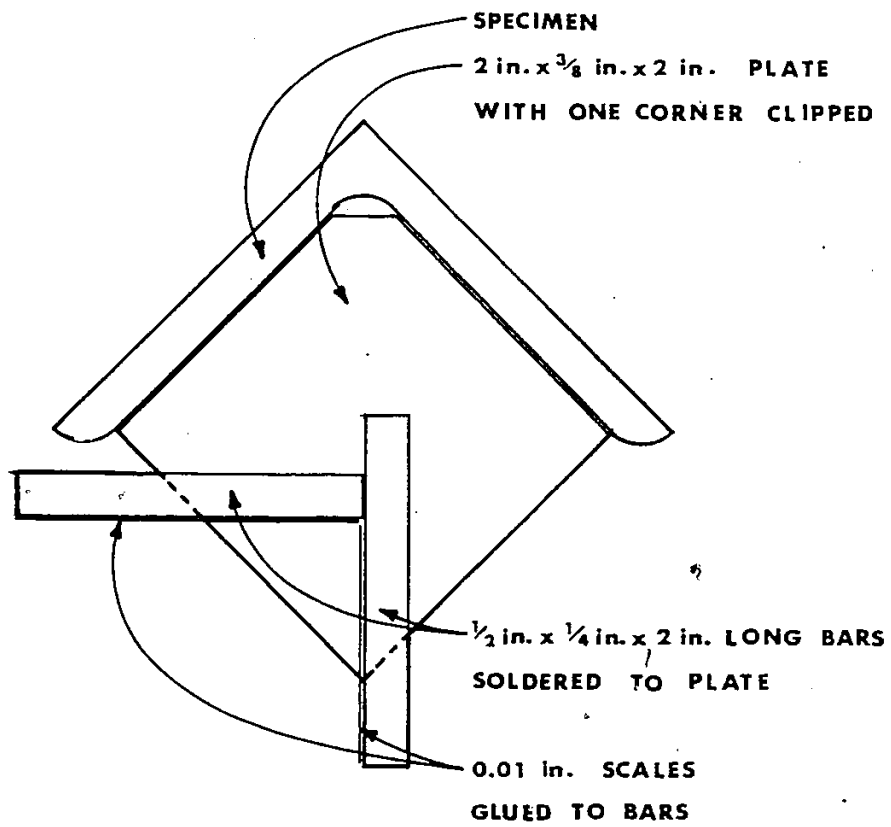
INSTRUMENTATION

FIGURE 9



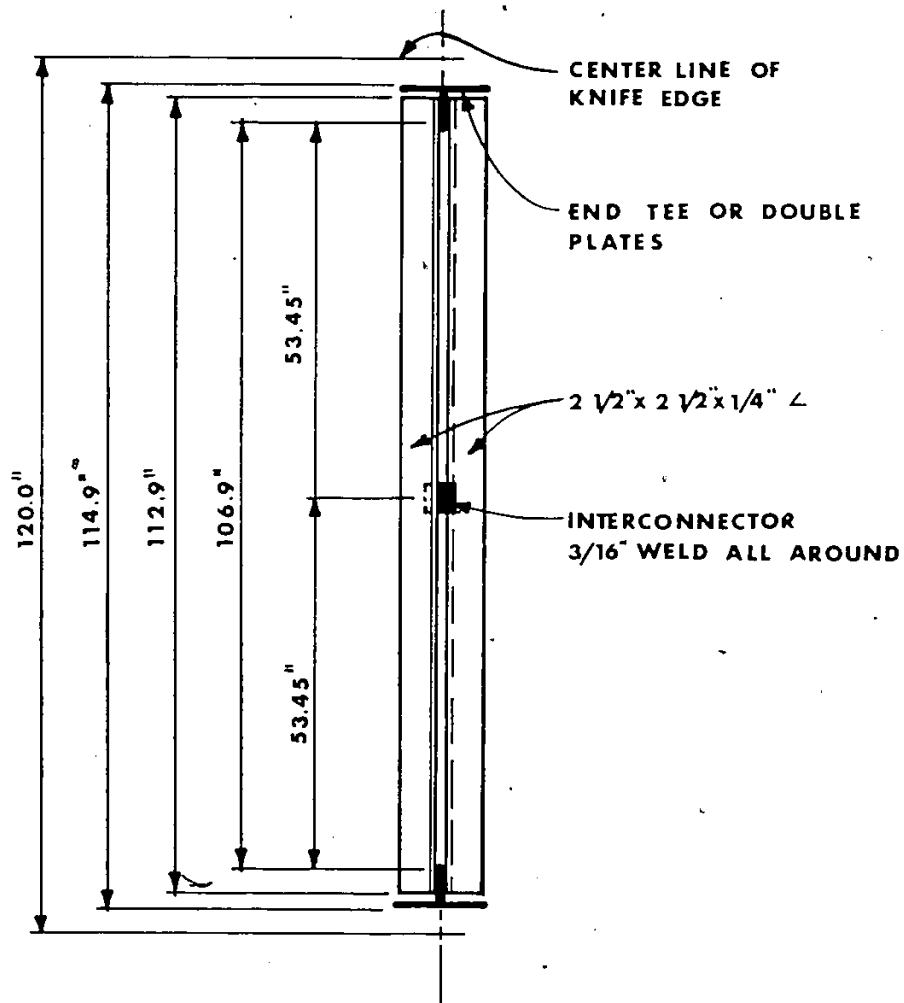
EFFECT OF RODS ON MEASURED  
DISPLACEMENTS  
FIGURE 10





OUT OF STRAIGHTNESS GAUGE

FIGURE II

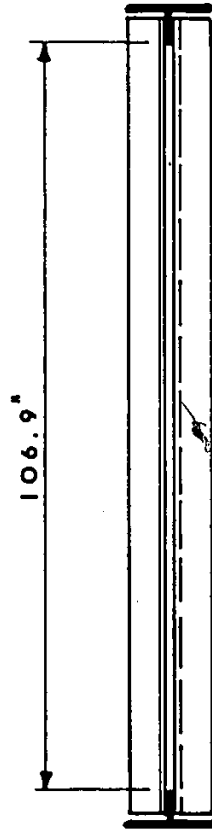


NOTE INFORMATION ON FIG. 12a IS TYPICAL FOR FIGS. 12b TO 12i

a) TYPICAL 120 INCH TEST SPECIMENS

120 INCH TEST SPECIMENS

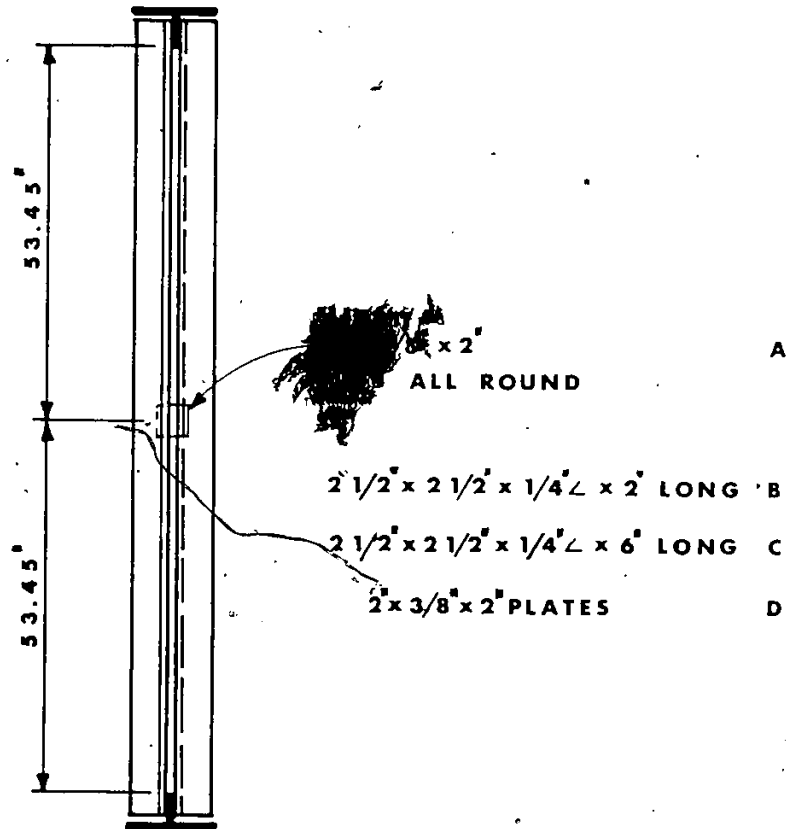
FIGURE 12



b) SPECIMENS 120A0.1 & 120A0.2

120 INCH TEST SPECIMENS

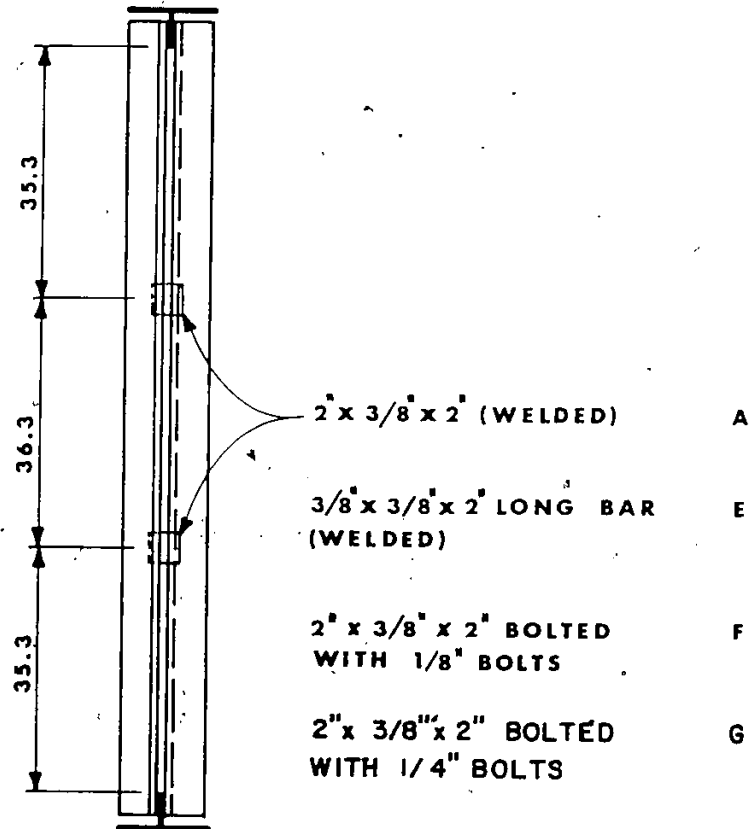
FIGURE 12



c) SPECIMENS 120A1.1 , 120A1.2 , 120B1.1 ,  
120C1.1 & 120D1.1

120 INCH TEST SPECIMENS

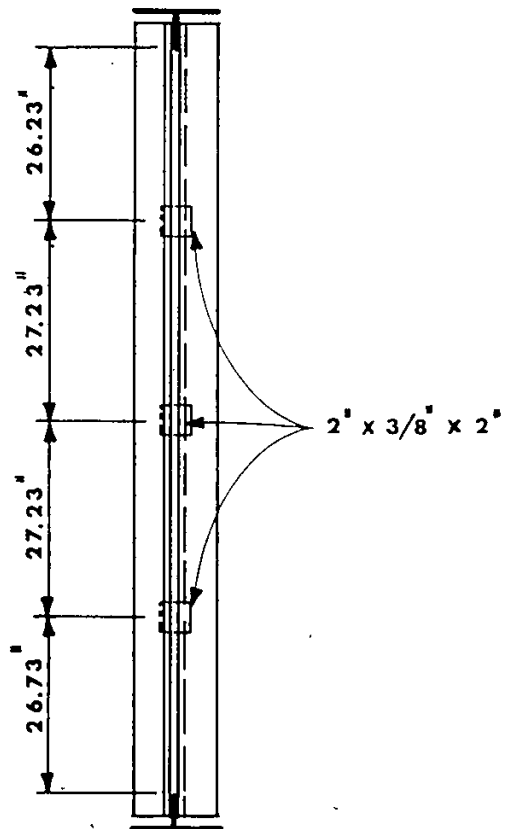
FIGURE 12



d) SPECIMENS I20A2.1 , I20A2.2 , I20E2.1  
I20F2.1 & I20G2.1

I20 INCH TEST SPECIMENS

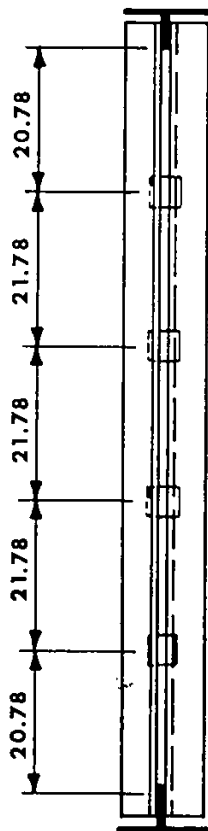
FIGURE 12



e) SPECIMENS 120A3.1 & 120A3.2

120 INCH TEST SPECIMENS

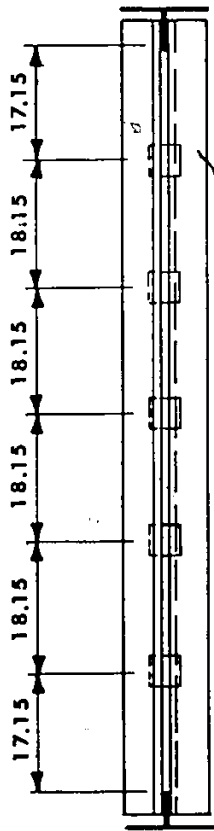
FIGURE 12



f) SPECIMEN 120A4.1 , 120A4.2 & 120A4.3

120 INCH TEST SPECIMENS

FIGURE 12

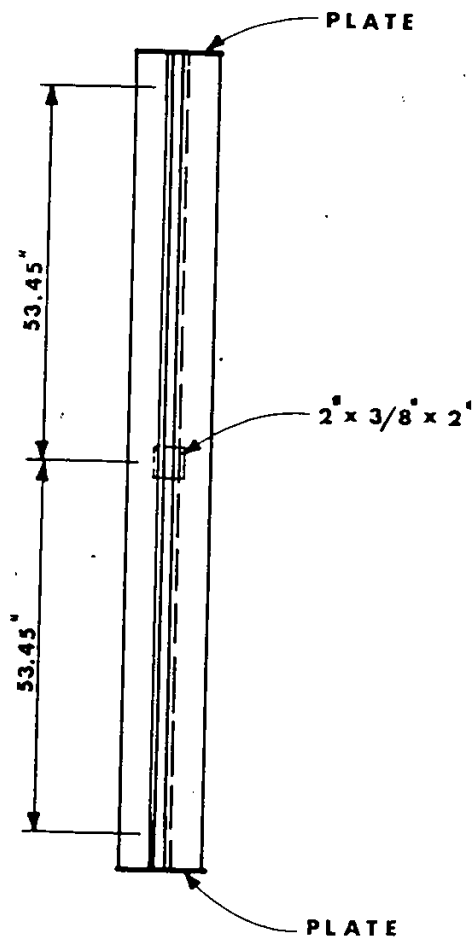


g) SPECIMEN I20A5.1

I20 INCH TEST SPECIMENS

FIGURE I2

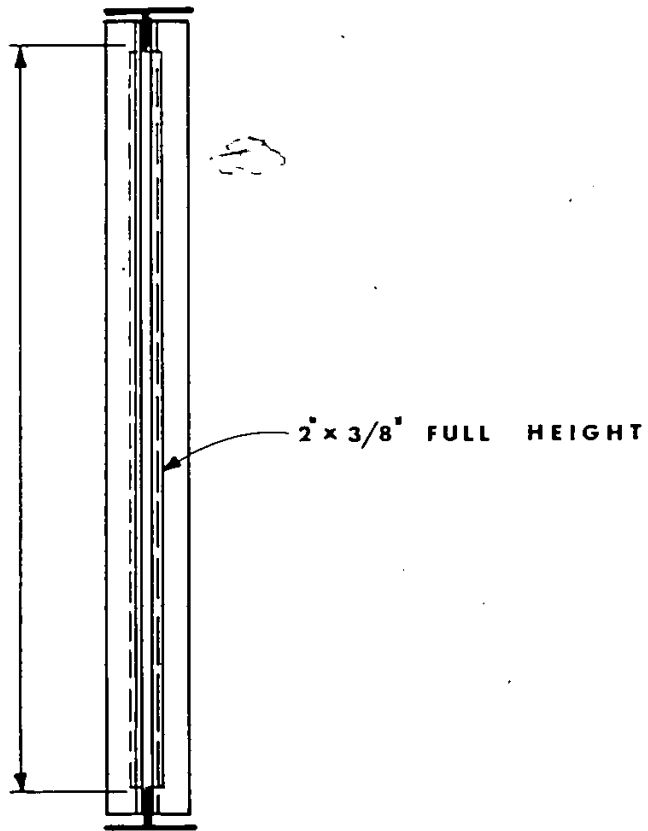




h) SPECIMEN 120AI.6P

120 INCH TEST SPECIMENS

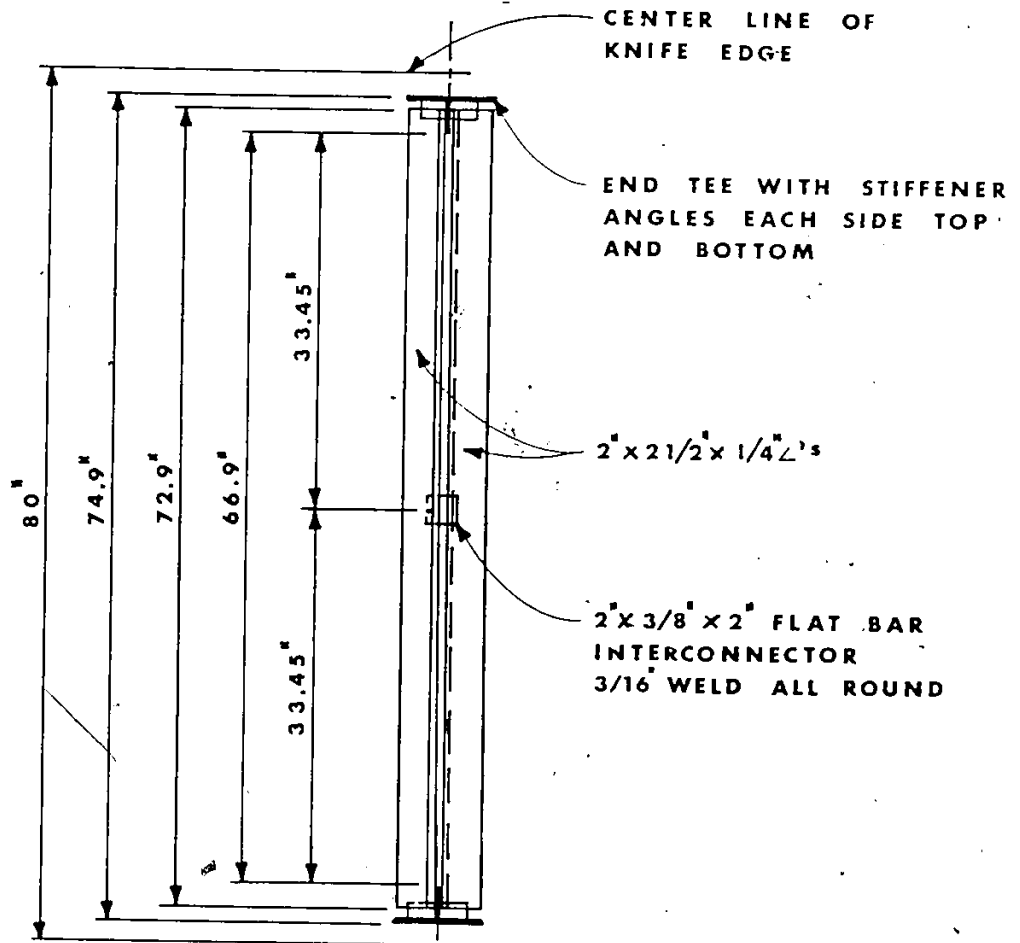
FIGURE 12



i) SPECIMEN 120AF

120 INCH TEST SPECIMENS

FIGURE 12

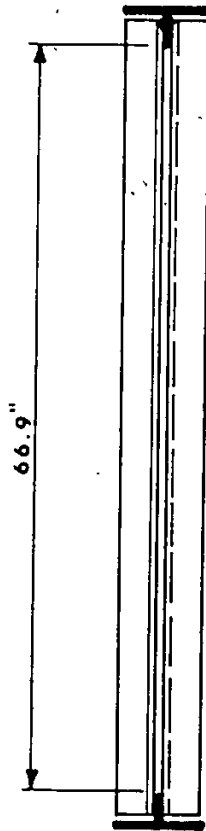


NOTE: INFORMATION ON FIG. 13a APPLIES TO FIGS. 13a TO 13b

a) TYPICAL 80 INCH SPECIMEN

80 INCH TEST SPECIMENS

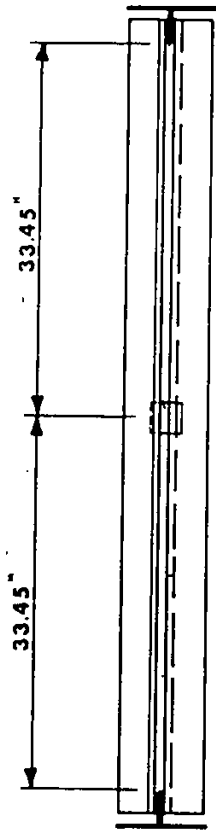
FIGURE 13



b) SPECIMEN 80AO.1

80 INCH TEST SPECIMENS

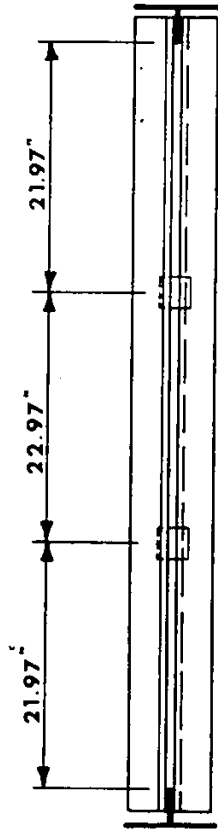
FIGURE 13



c) SPECIMENS 80A1.1 & 80A1.2

80 INCH TEST SPECIMEN

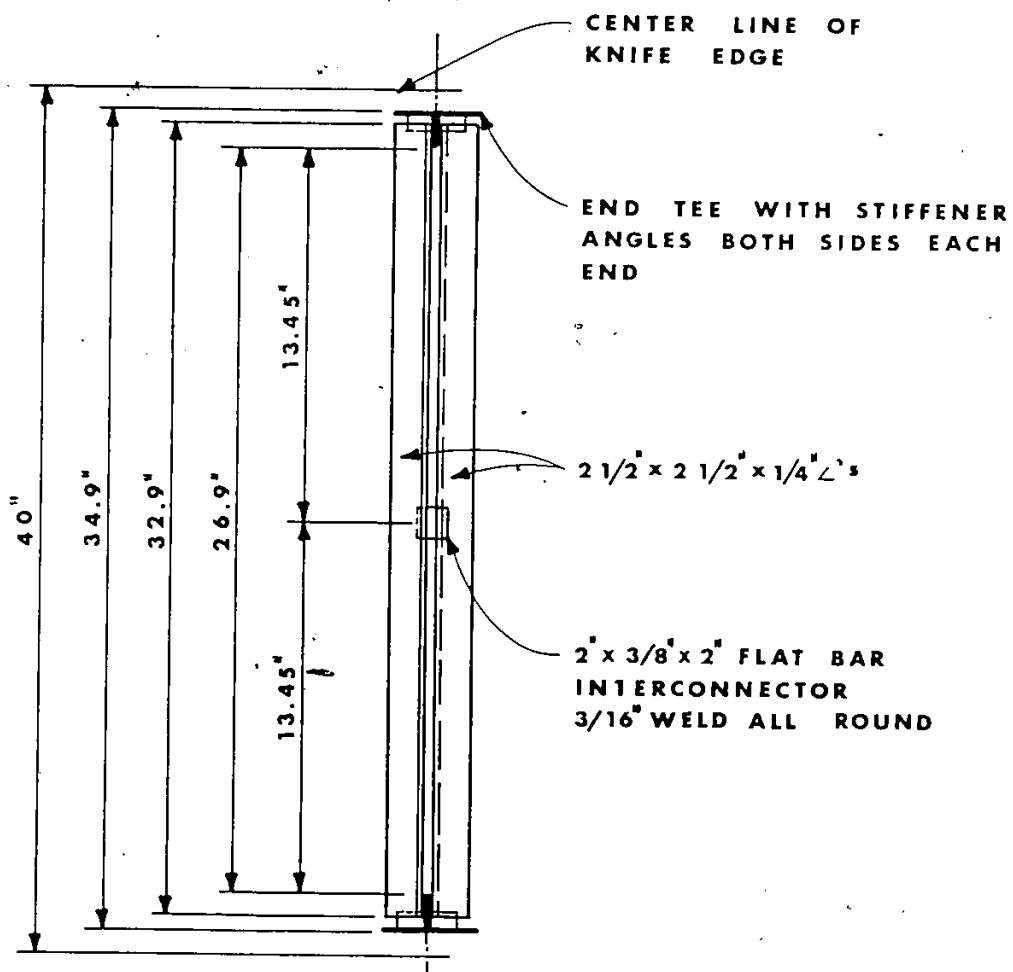
FIGURE 13



d) SPECIMENS 80A2.1, 80A2.2 & 80A2.3

80 INCH TEST SPECIMENS

FIGURE 13

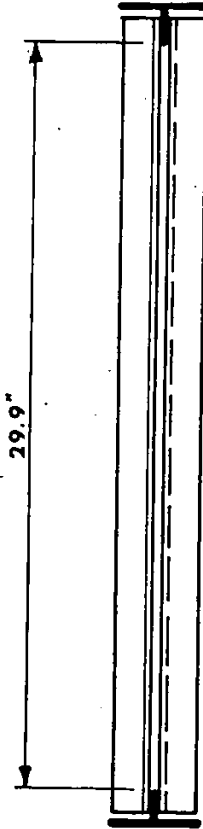


NOTE: THE INFORMATION ON FIG. 14a APPLIES TO FIGS. 14b TO 14d

d) TYPICAL 40 INCH TEST SPECIMENS

40 INCH TEST SPECIMENS

FIGURE 14

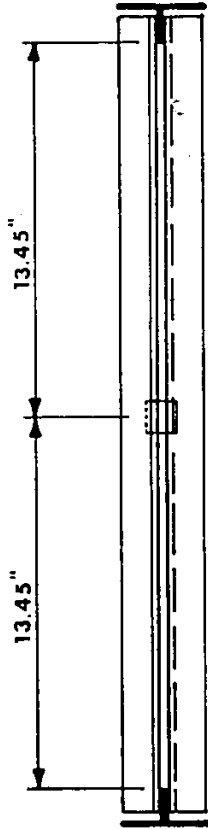


b) SPECIMEN 40A0.1

40 INCH TEST SPECIMENS

FIGURE 14

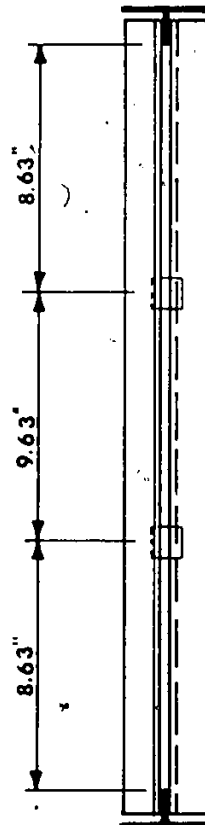




c) SPECIMEN 40A1.1

40 INCH TEST SPECIMENS

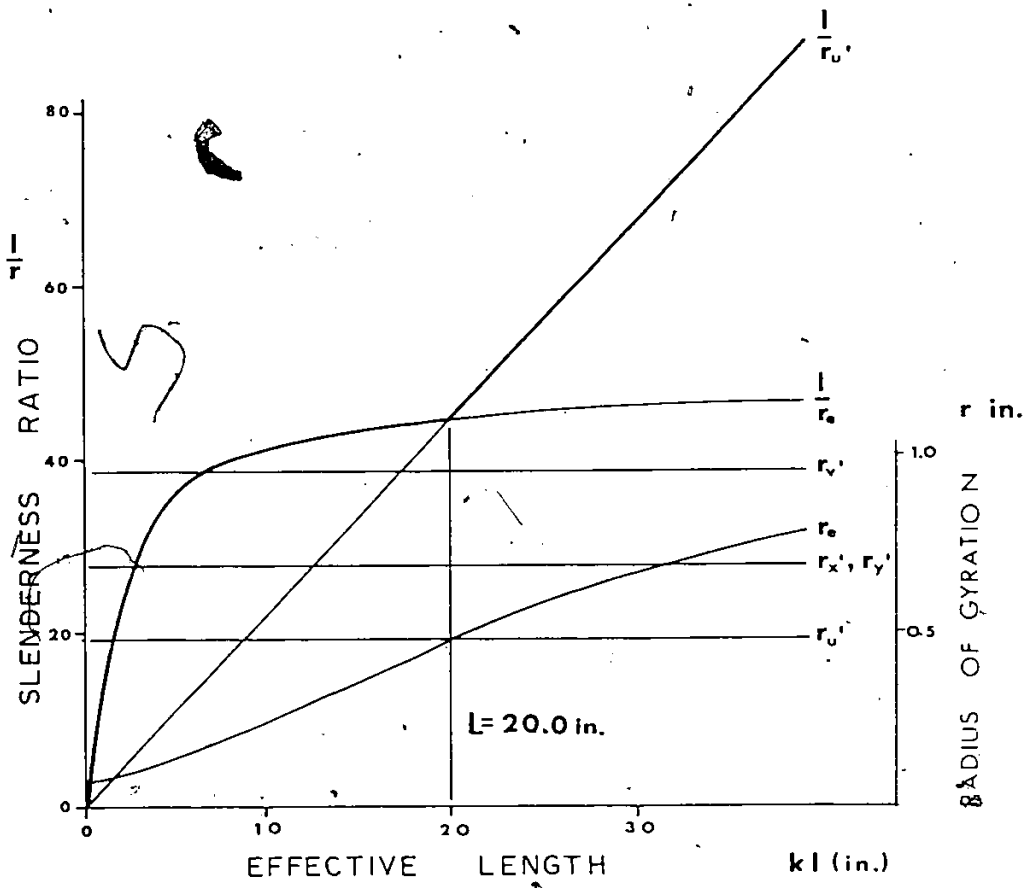
FIGURE 14



d) SPECIMENS 40A2.1 & 40A2.2

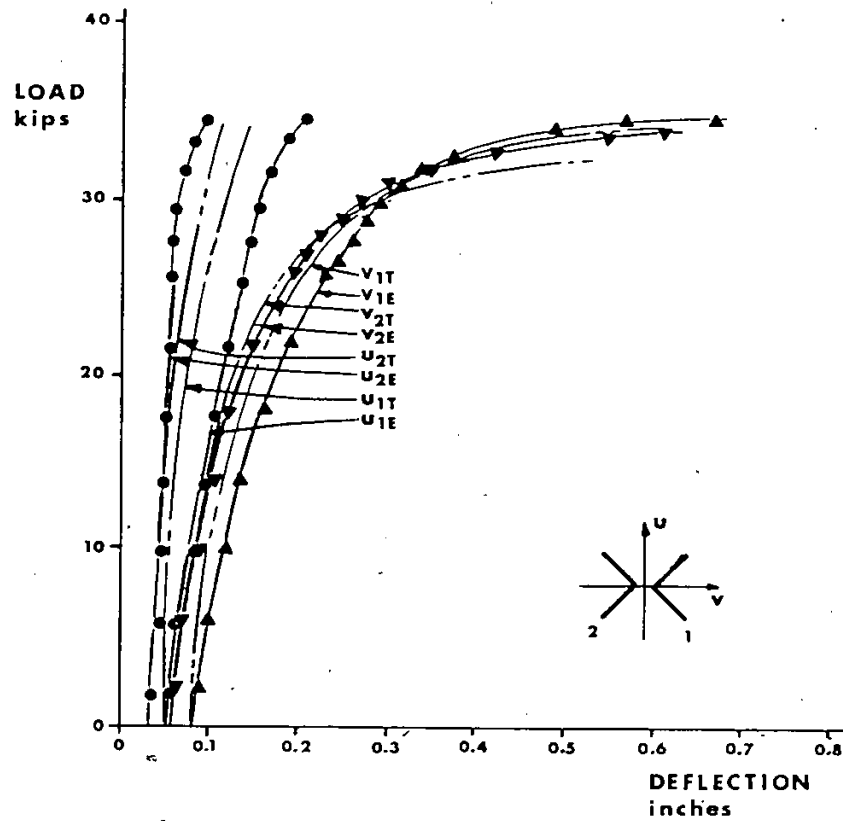
40 INCH TEST SPECIMENS

FIGURE 14



PLOT OF SLENDERNESS RATIO TO EFFECTIVE LENGTH FOR SINGLE ANGLE

FIGURE 15

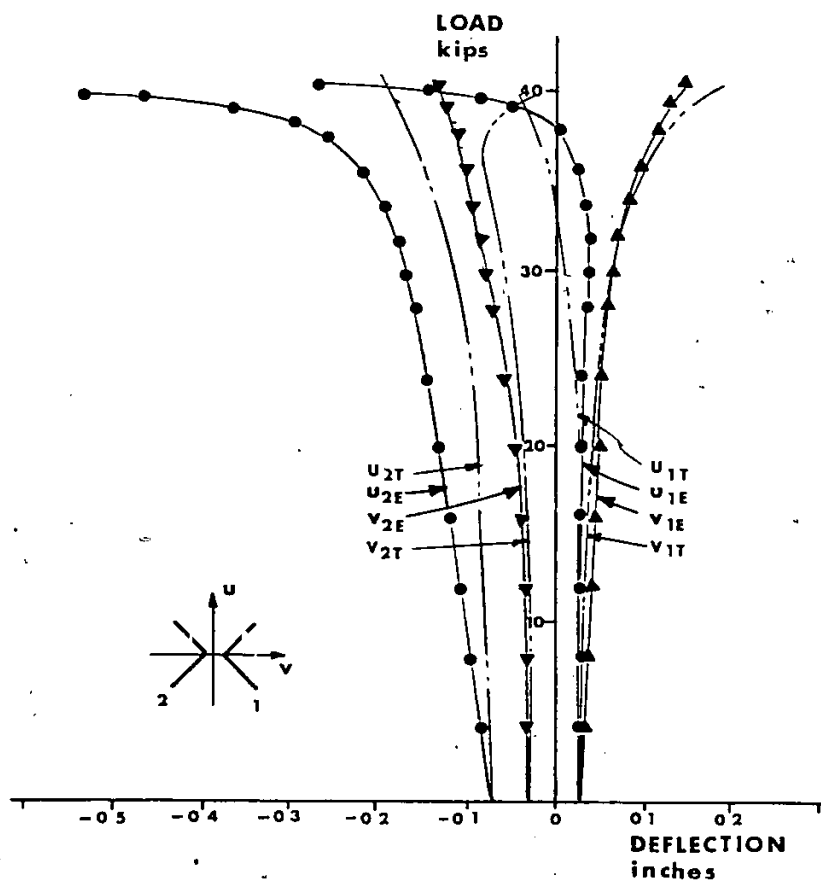


NOTE: SUBSCRIPTS 1 AND 2 REPRESENT ANGLES 1 OR 2.  
 SUBSCRIPTS T AND E INDICATE THEORETICAL OR  
 EXPERIMENTAL CURVES TYPICAL FIGS. 16, 17 AND 18

a) TEST 120A0.1

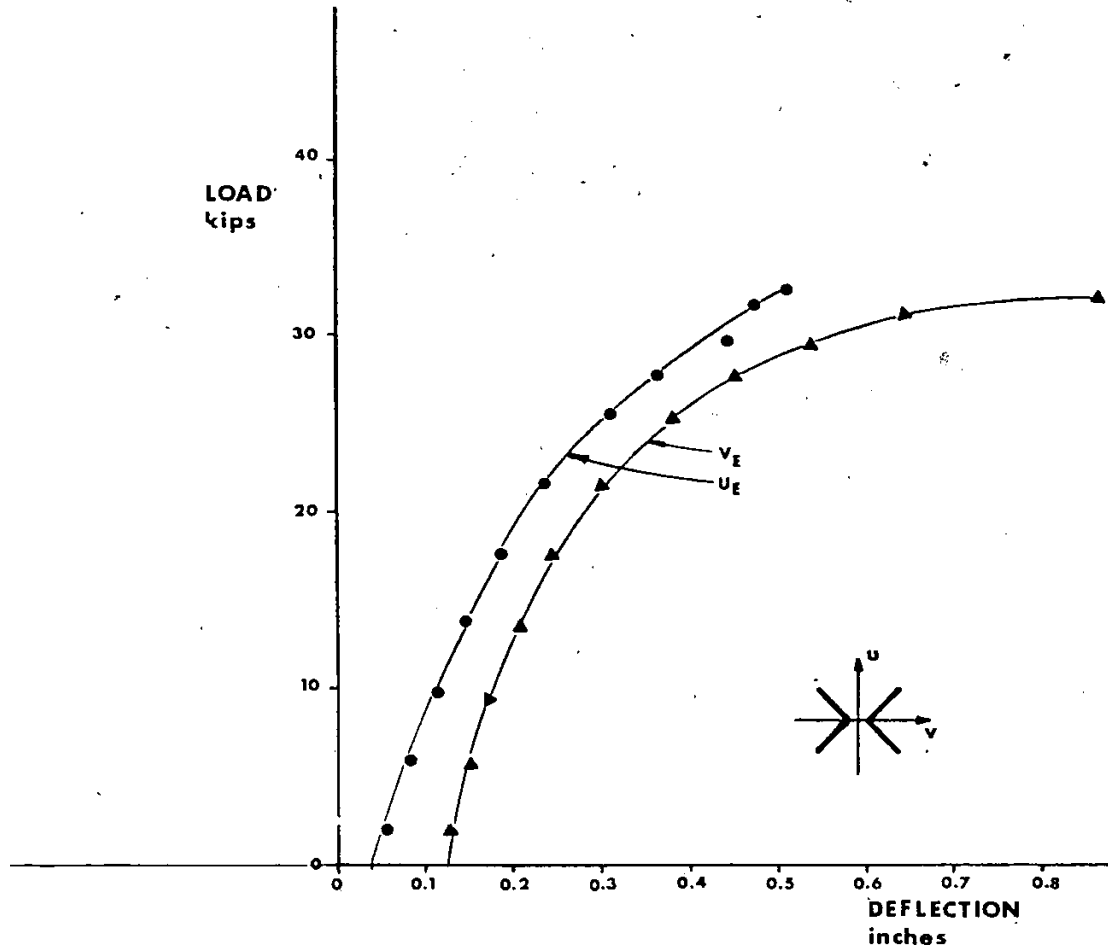
LOAD DEFLECTION CURVES FOR  
 120 INCH TEST SPECIMENS

FIGURE 16



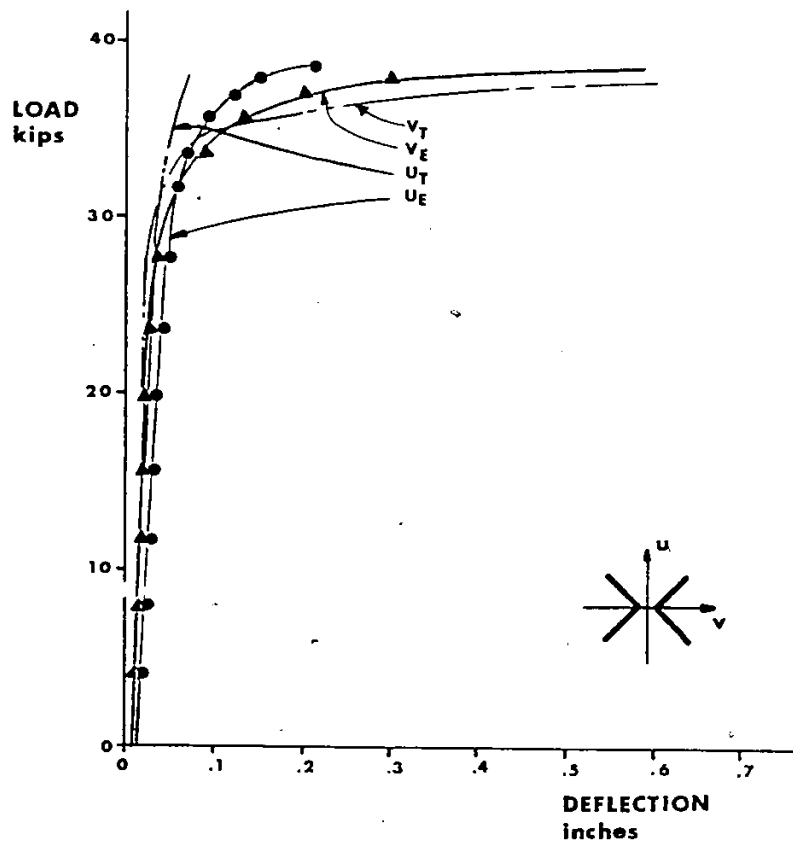
b) TEST 120A0.2.  
 LOAD DEFLECTION CURVES FOR  
 120 INCH TEST SPECIMENS

FIGURE 16



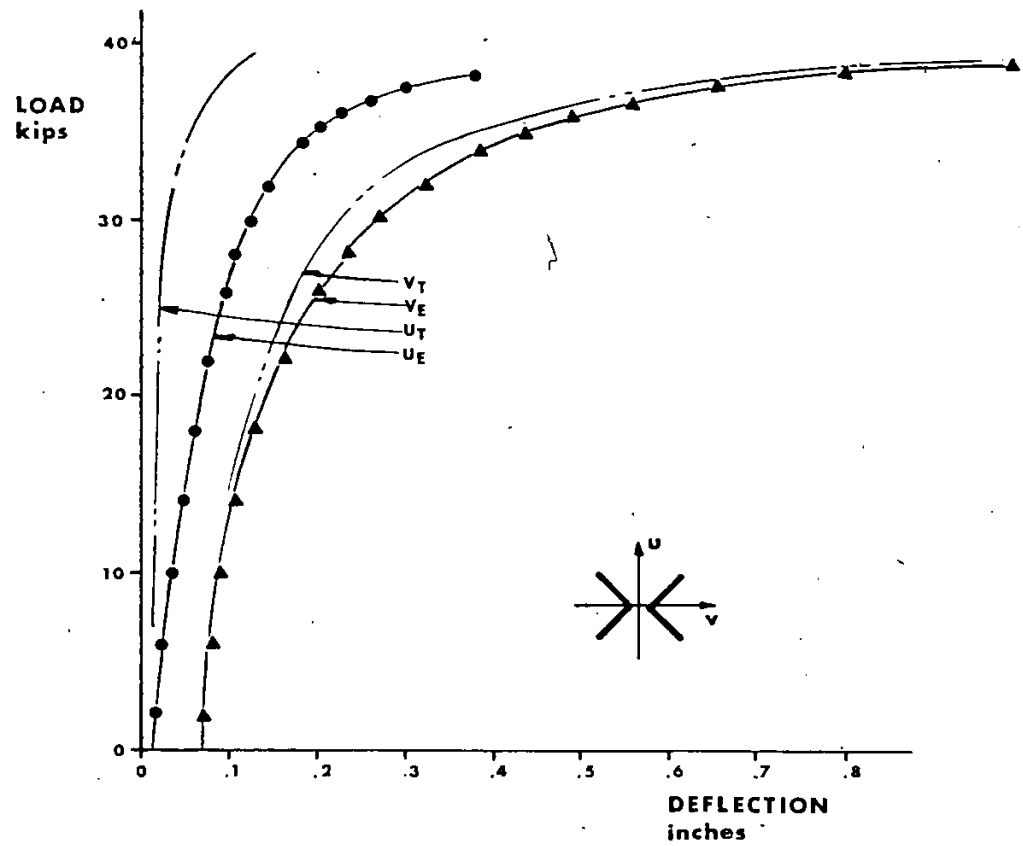
c) TEST 120A1.2  
LOAD DEFLECTION CURVES FOR  
120 INCH TEST SPECIMENS

FIGURE 16



d) TEST 120A1.3  
LOAD DEFLECTION CURVES FOR  
120 INCH TEST SPECIMENS

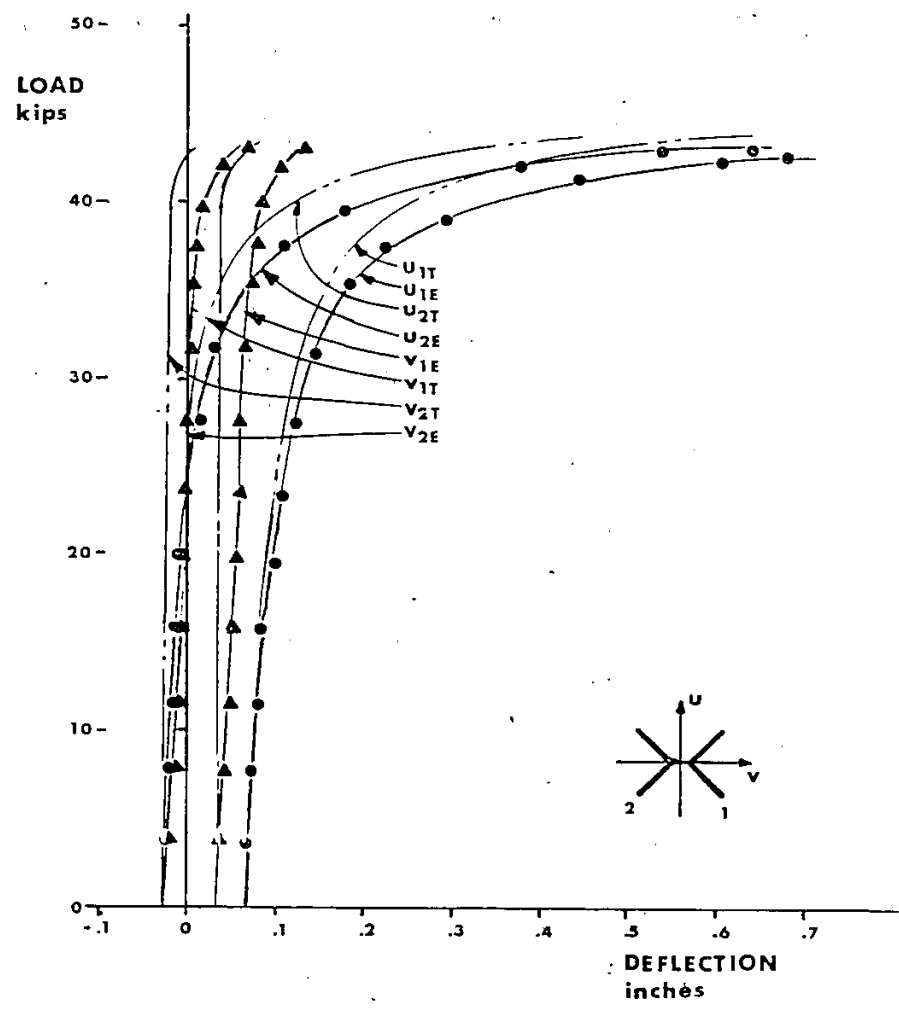
FIGURE 16



e) TEST 120A1.5  
LOAD DEFLECTION CURVES FOR  
120 INCH TEST SPECIMENS

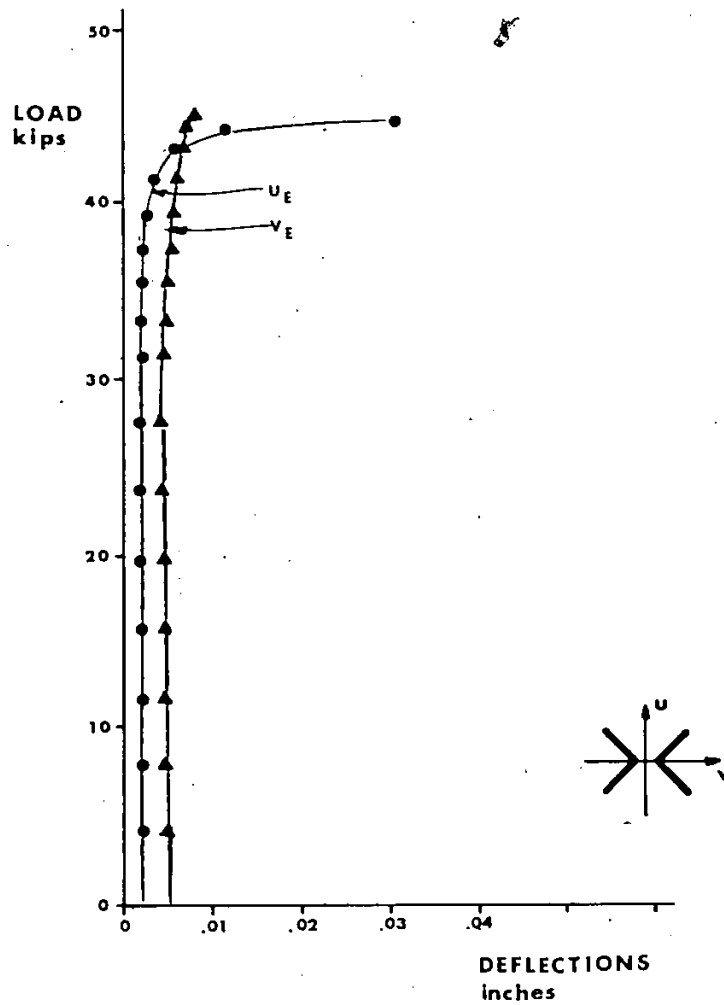
FIGURE 16





f) TEST 120A2.1  
LOAD DEFLECTION CURVES FOR  
120 INCH TEST SPECIMENS

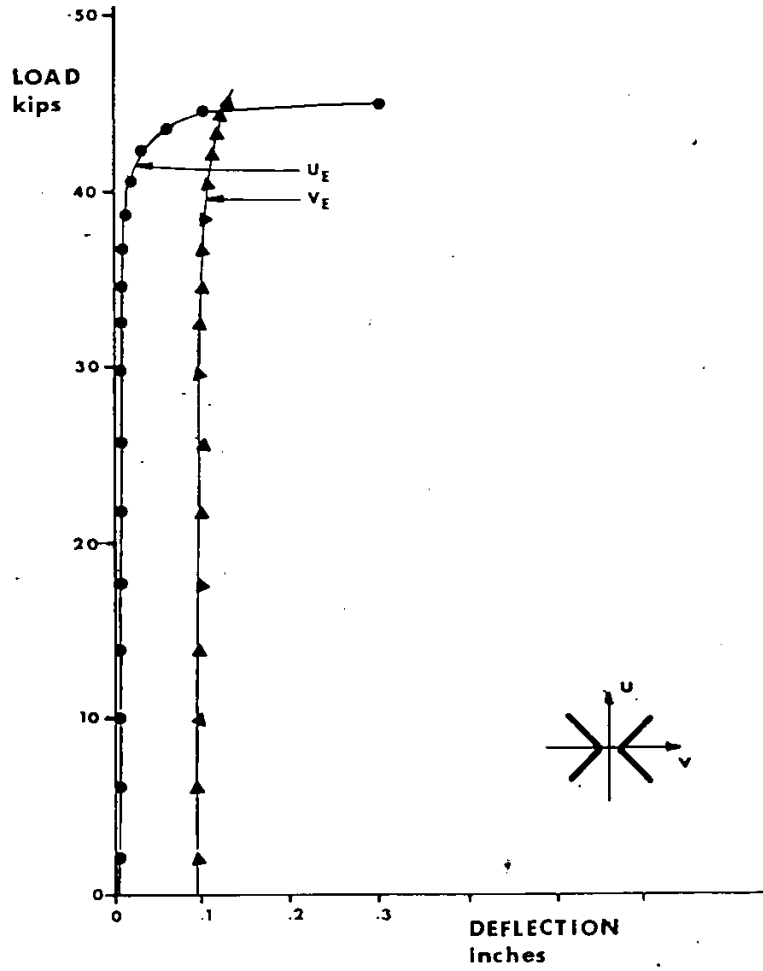
FIGURE 16



g) TEST 120A3.1

LOAD DEFLECTION CURVES FOR  
120 INCH TEST SPECIMENS

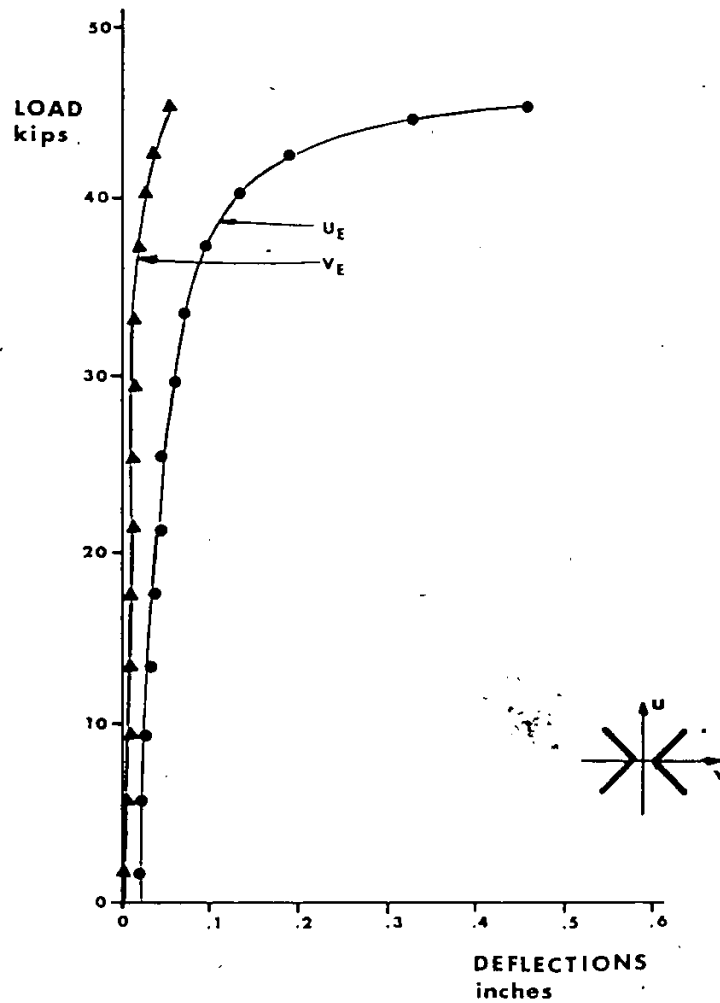
FIGURE 16



h) TEST 120A3.2

LOAD DEFLECTION CURVES FOR  
120 INCH TEST SPECIMENS

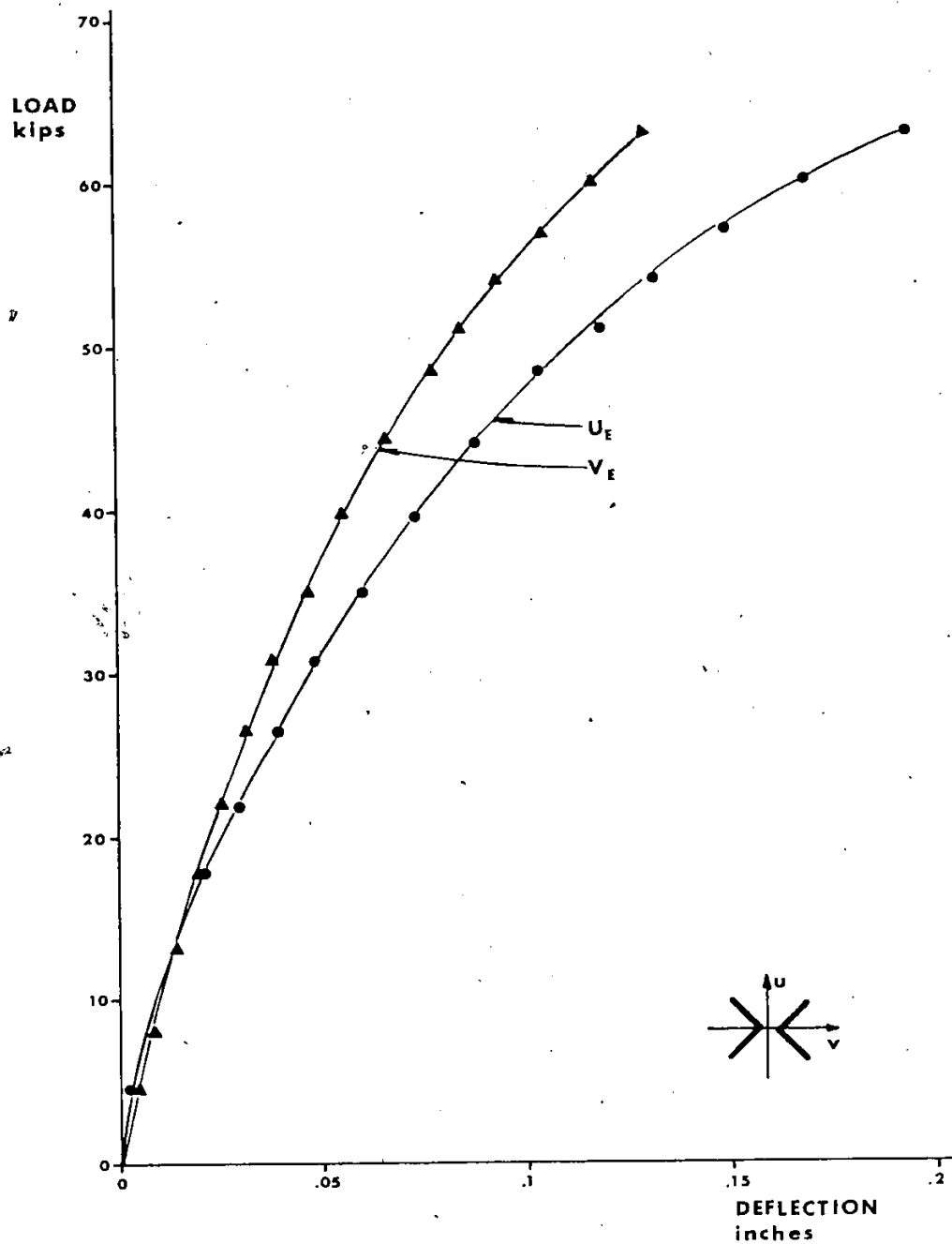
FIGURE 16



1) TEST 120A5.1

LOAD DEFLECTION CURVES FOR  
120 INCH TEST SPECIMENS

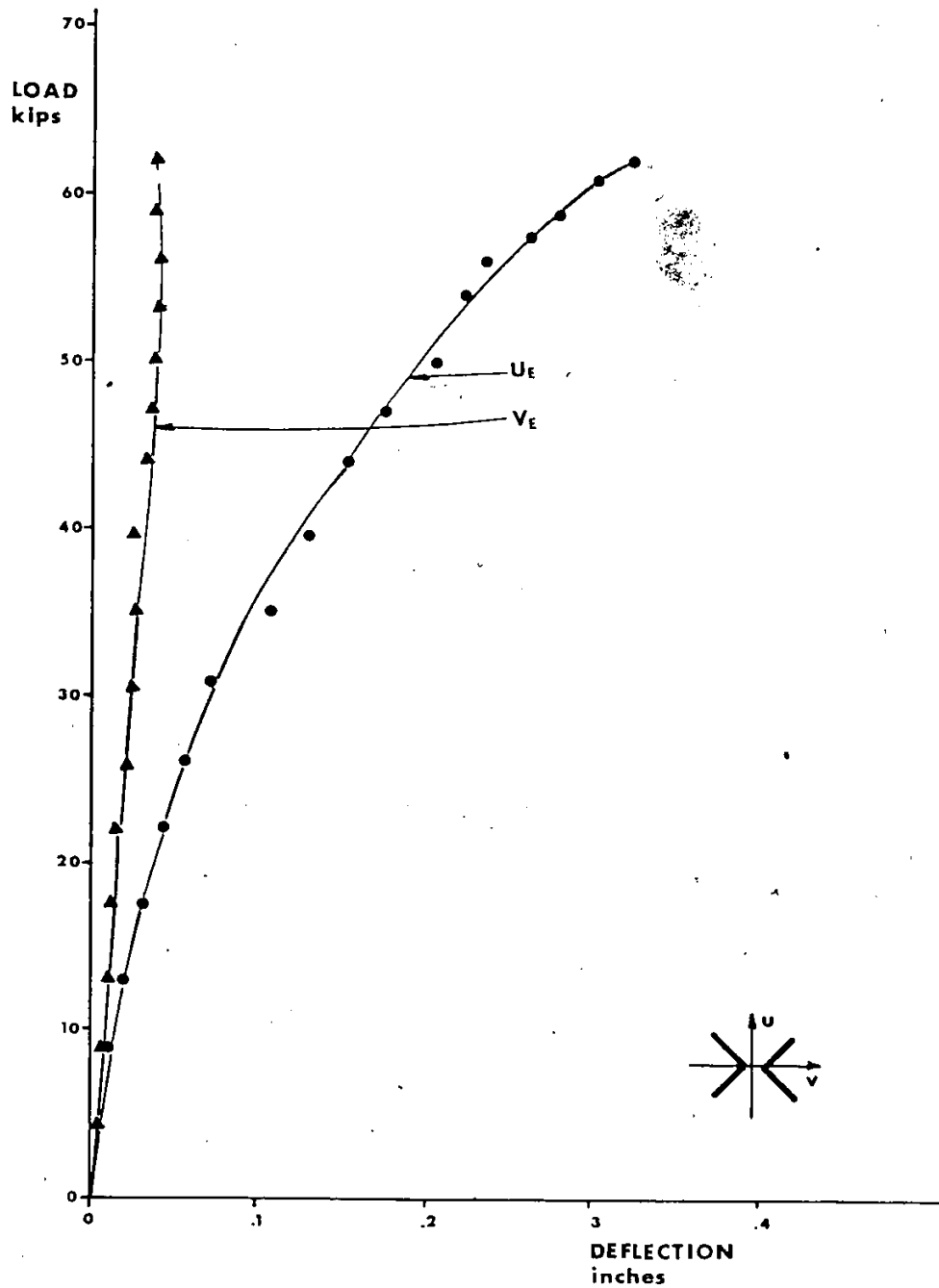
FIGURE 16



a) TEST 80A1.2

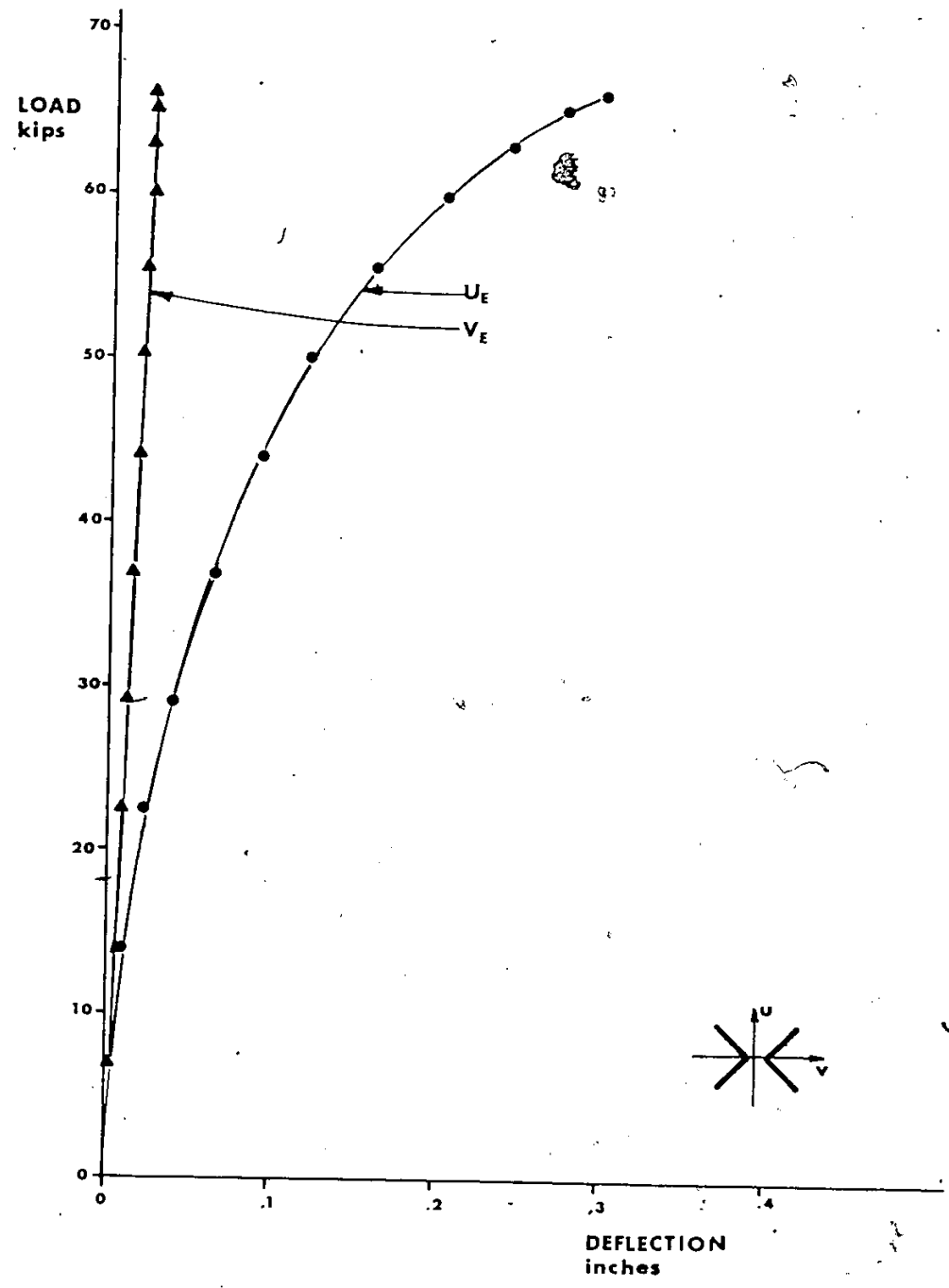
LOAD DEFLECTION CURVES FOR  
80 INCH TEST SPECIMENS

FIGURE 17

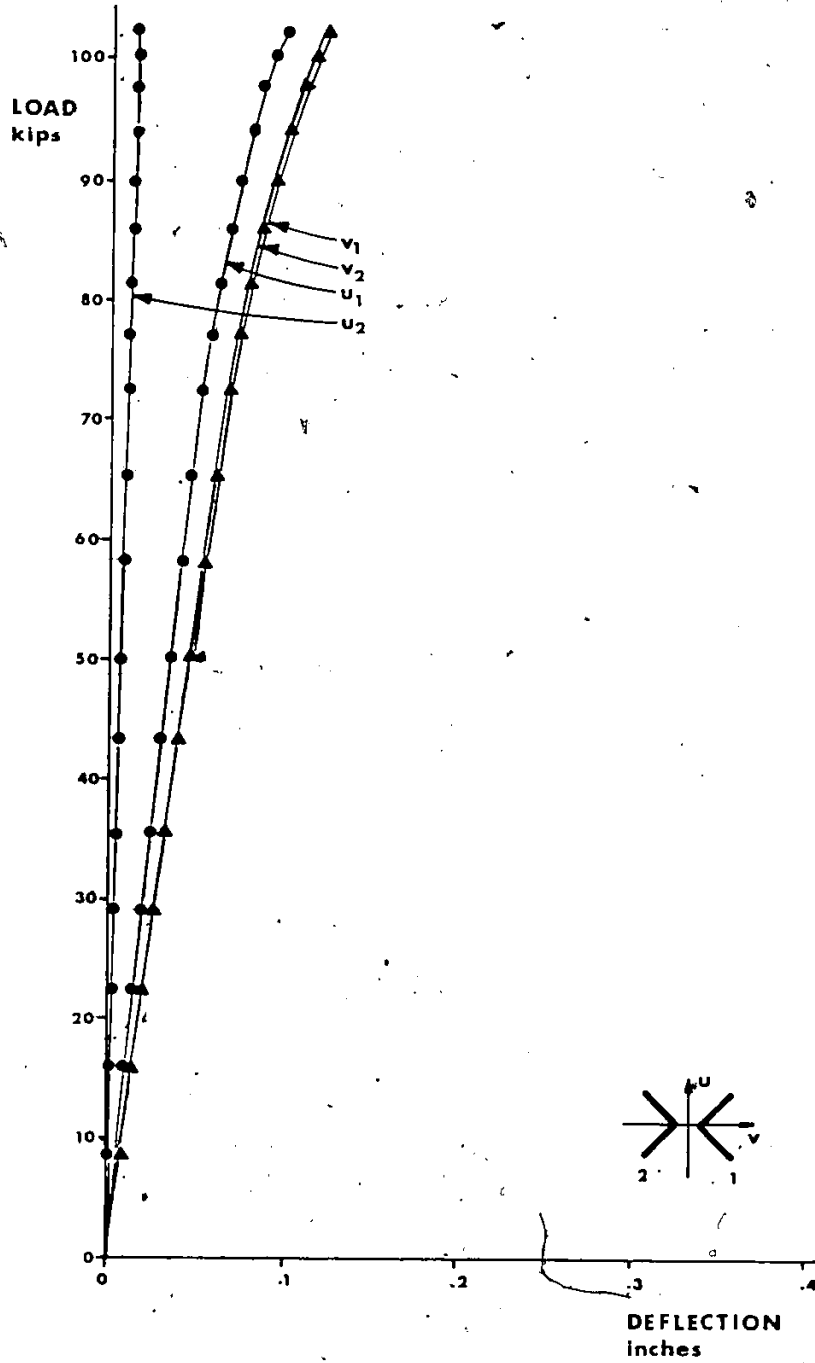


b) TEST 80A2.2  
LOAD DEFLECTION CURVES FOR  
80 INCH TEST SPECIMENS

FIGURE 17

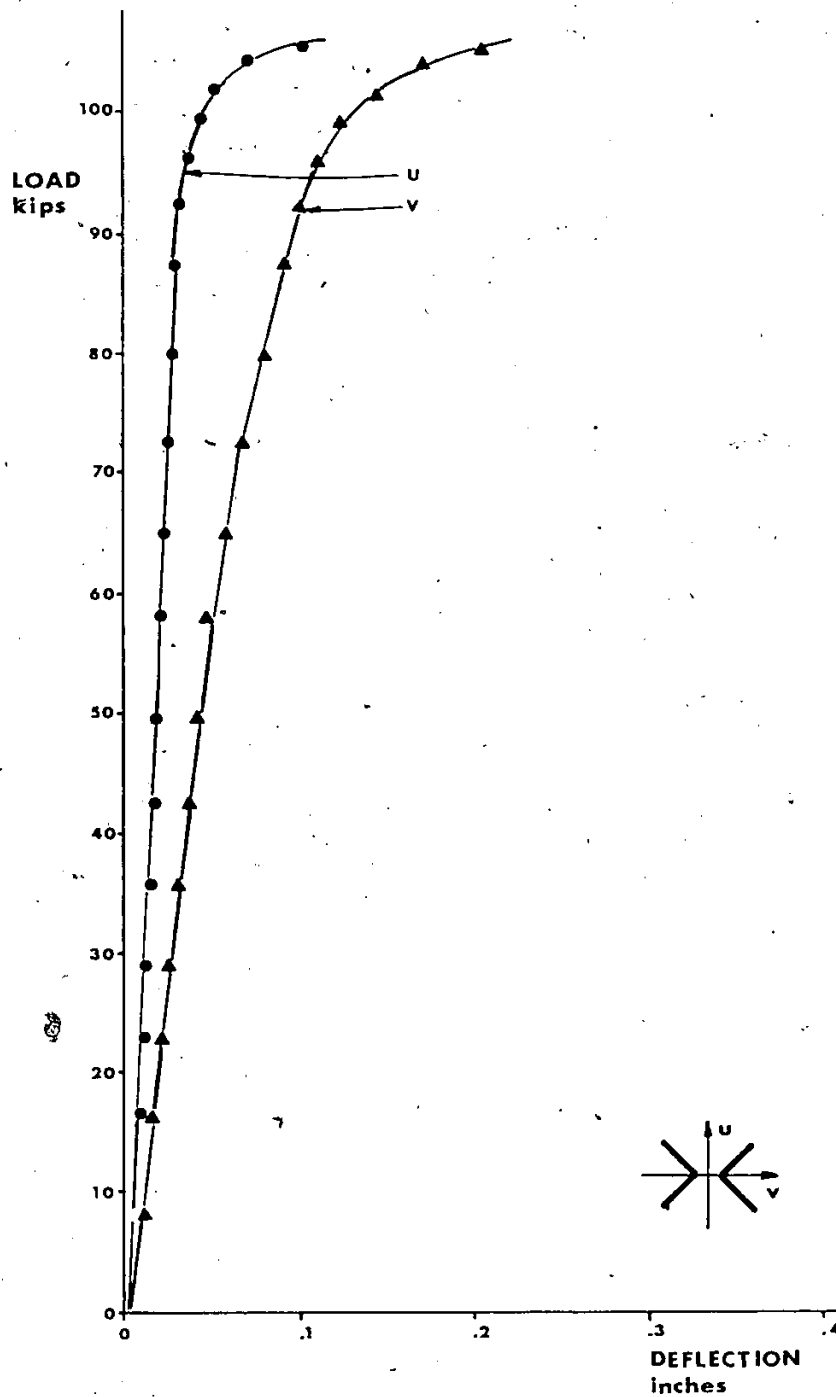


c) TEST 80A2.3  
LOAD DEFLECTION CURVES FOR  
80 INCH TEST SPECIMENS  
FIGURE 17

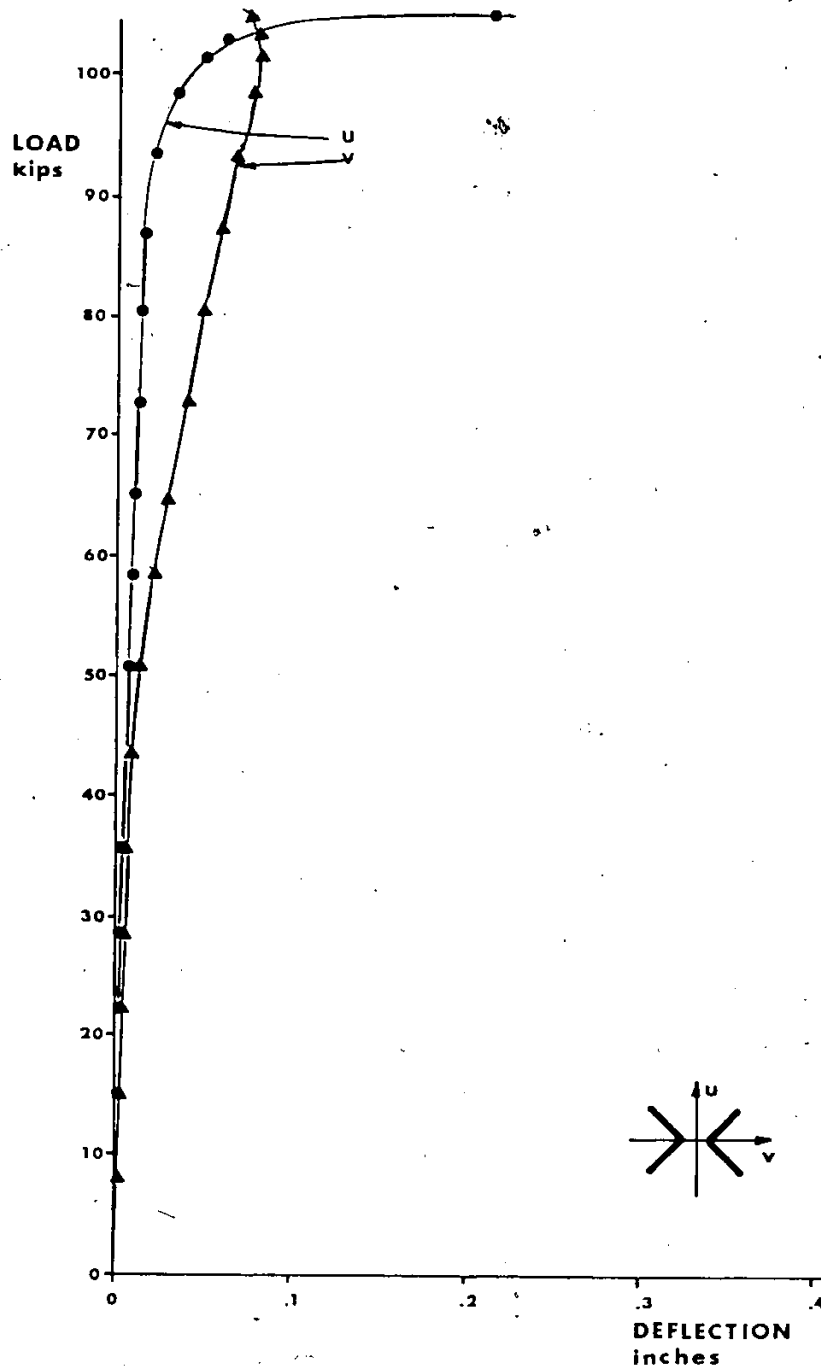


d) TEST / 40A0.I  
 LOAD DEFLECTION CURVES FOR  
 40 INCH TEST SPECIMENS  
 FIGURE 18

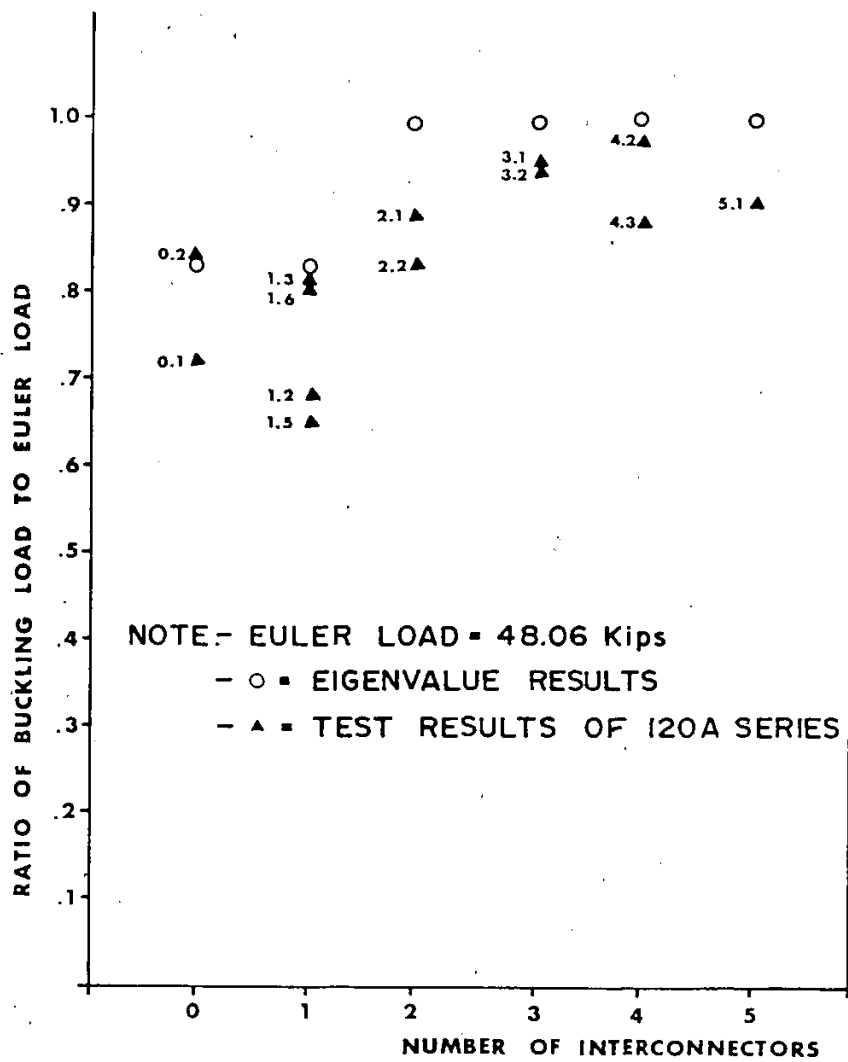




b) TEST 40A1.2  
LOAD DEFLECTION CURVES FOR  
40 INCH TEST SPECIMENS  
FIGURE 18

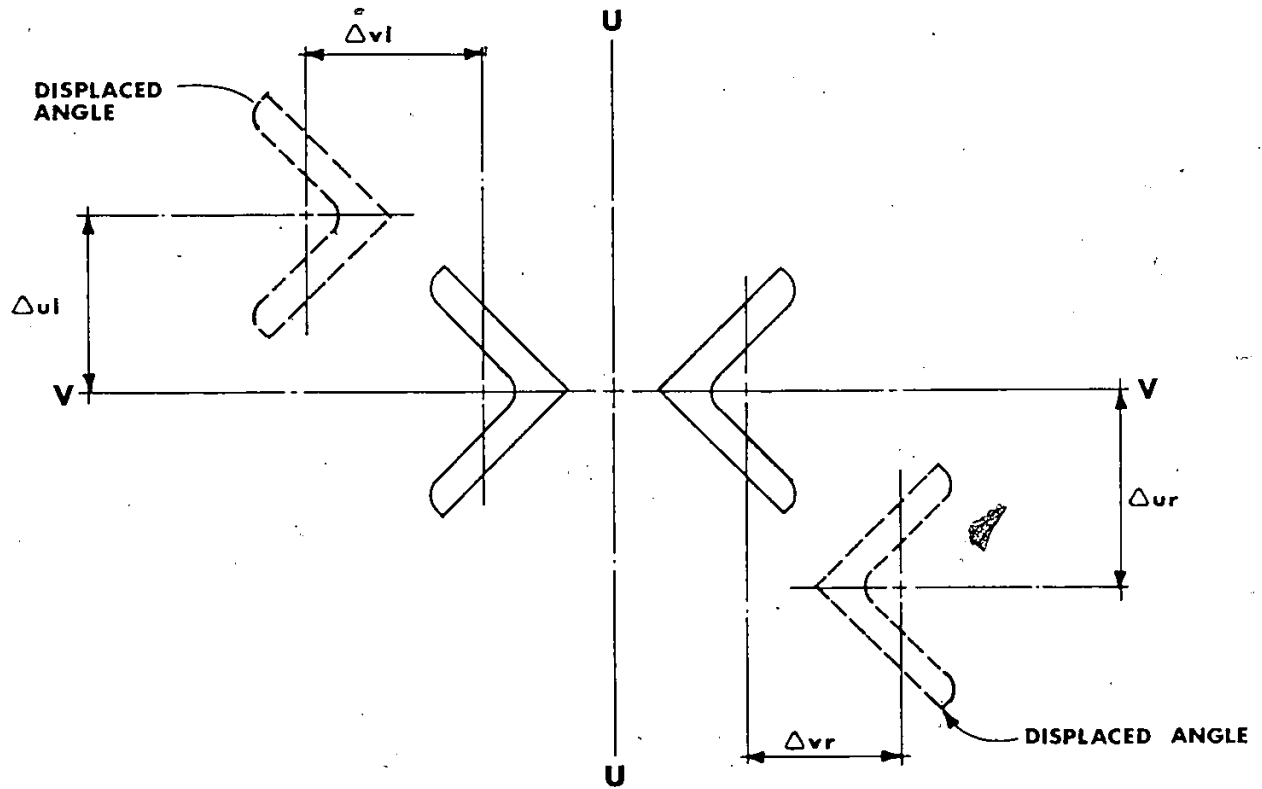


c) TEST 40A2.2  
LOAD DEFLECTION CURVES FOR  
40 INCH TEST SPECIMENS  
FIGURE 18



LOAD VERSUS NUMBER OF INTERCONNECTORS

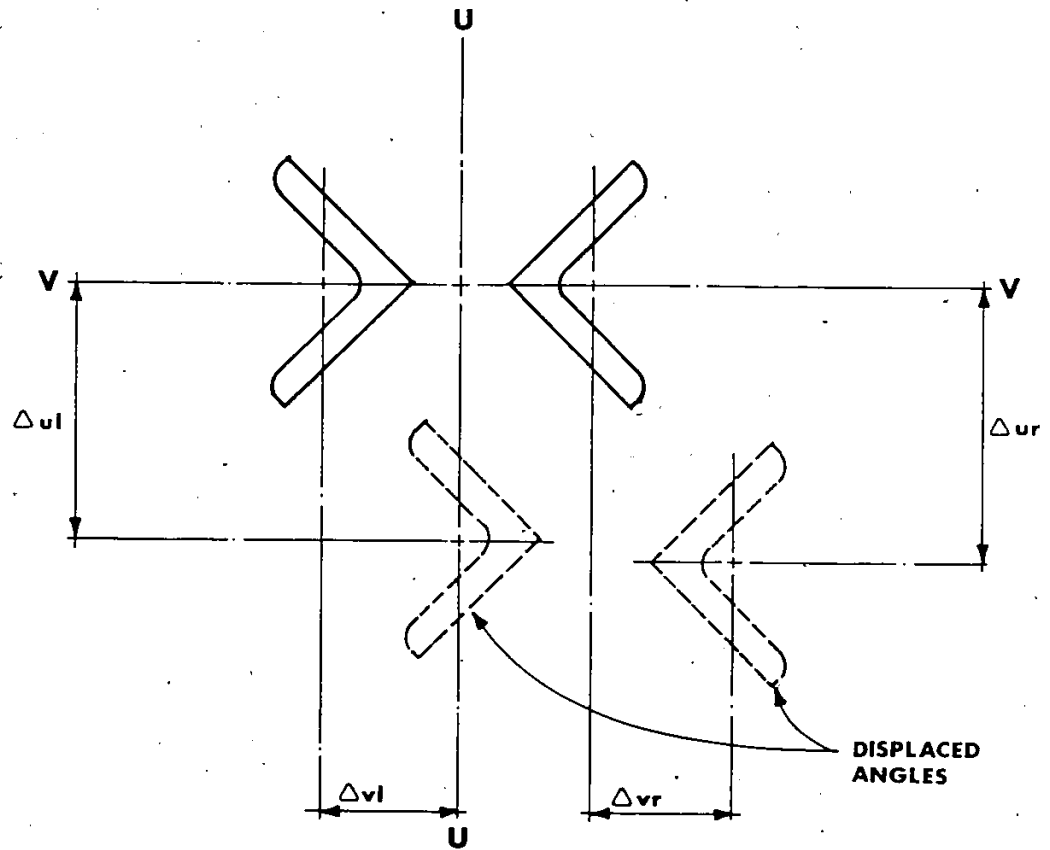
FIGURE 19



d) OPPOSITE DIRECTION

POSSIBLE DISPLACED SHAPES OF  
THE ANGLES OF THE STRUT

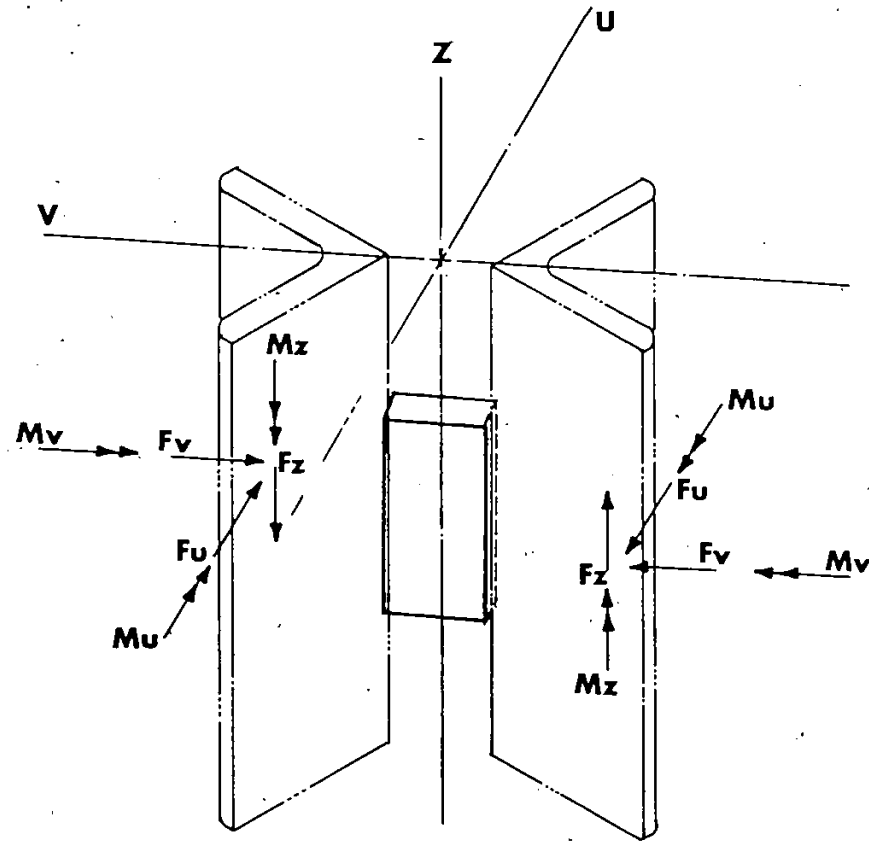
FIGURE 20



b) SAME DIRECTION

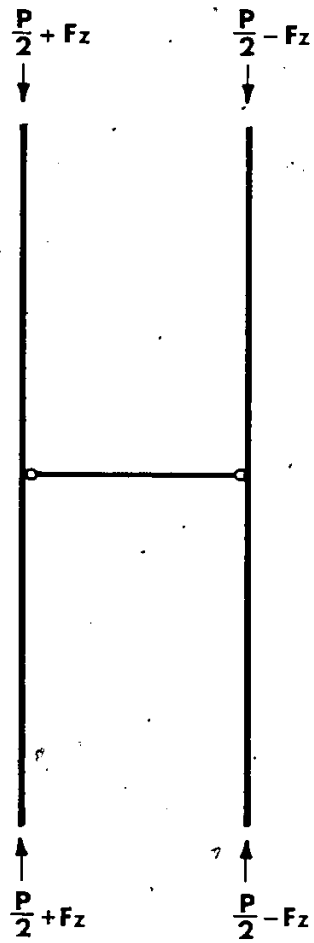
POSSIBLE DISPLACED SHAPES OF  
THE ANGLE OF THE STRUT

FIGURE 20

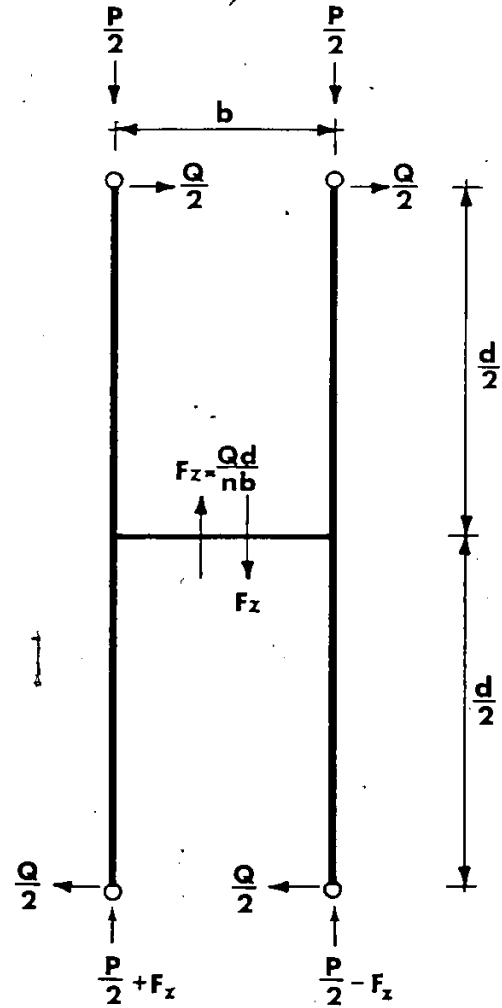


POTENTIAL FORCES IN AN INTERCONNECTOR

FIGURE 21



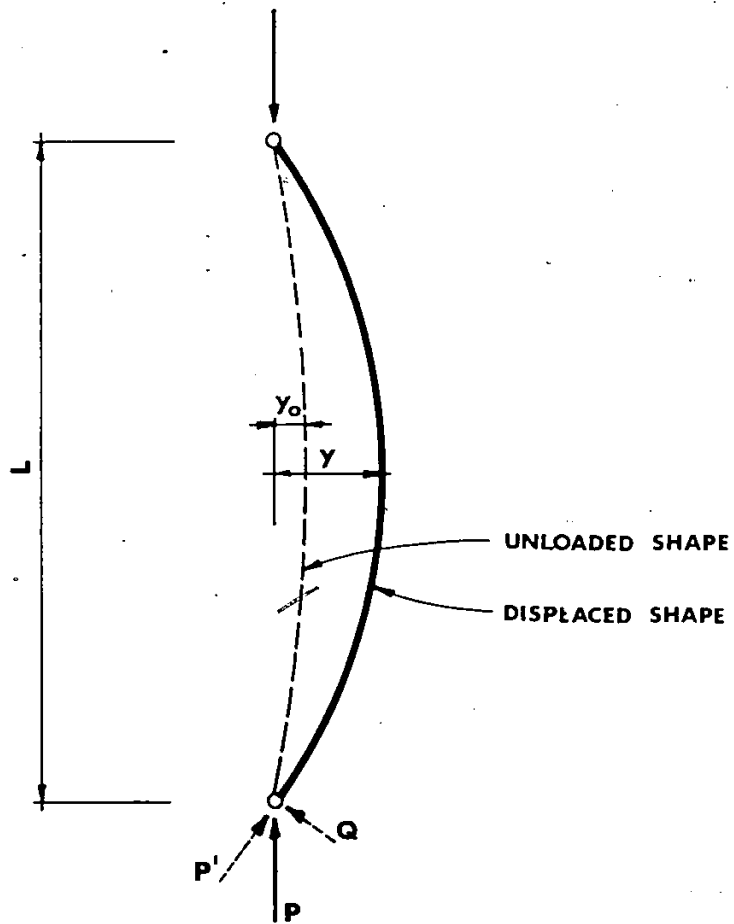
a) SPACED COLUMN



b) BATTENED COLUMN

SPACED AND BATTENED COLUMN INTERCONNECTOR FORCES

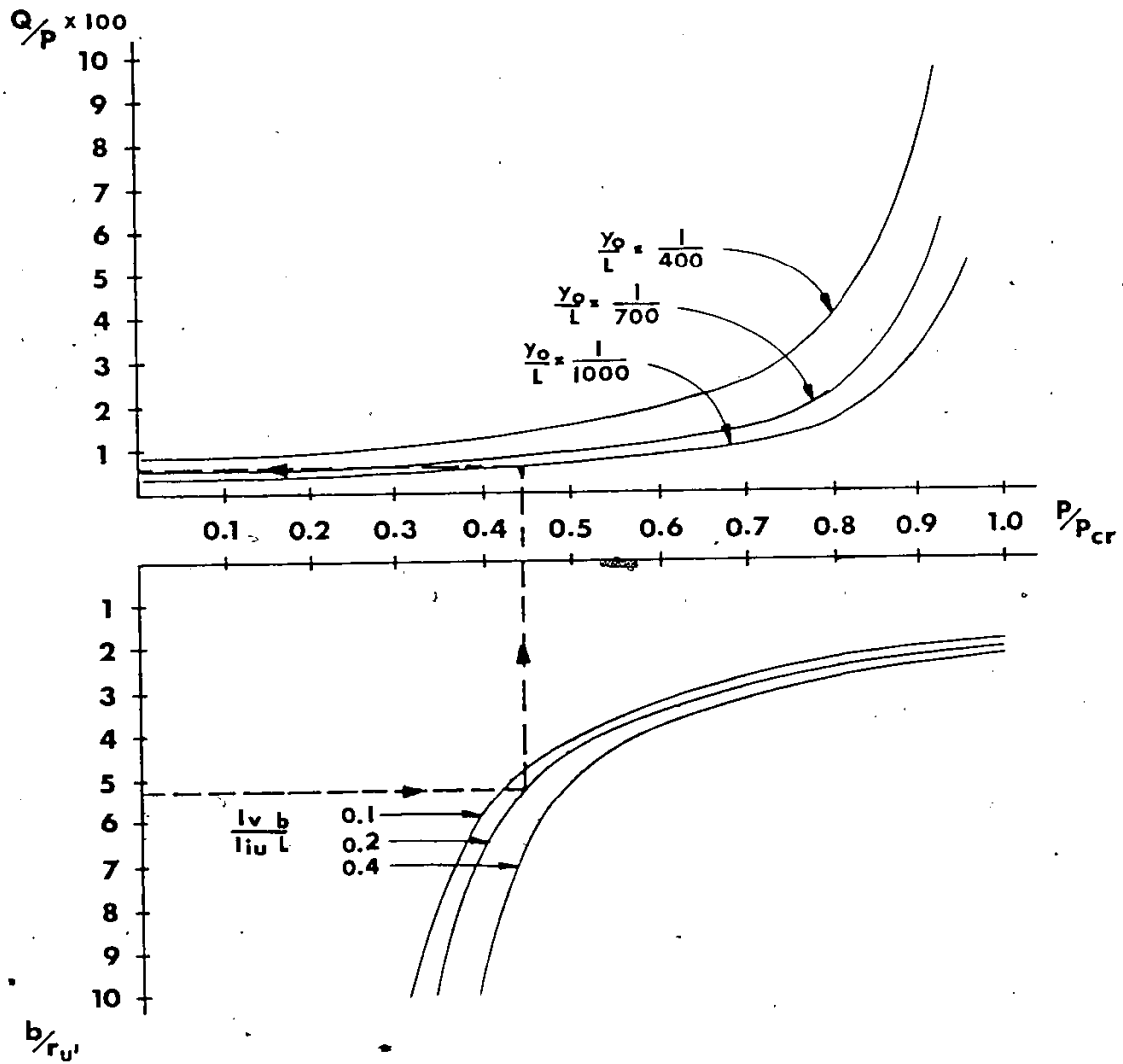
FIGURE 22



SHEAR FORCE IN A COLUMN

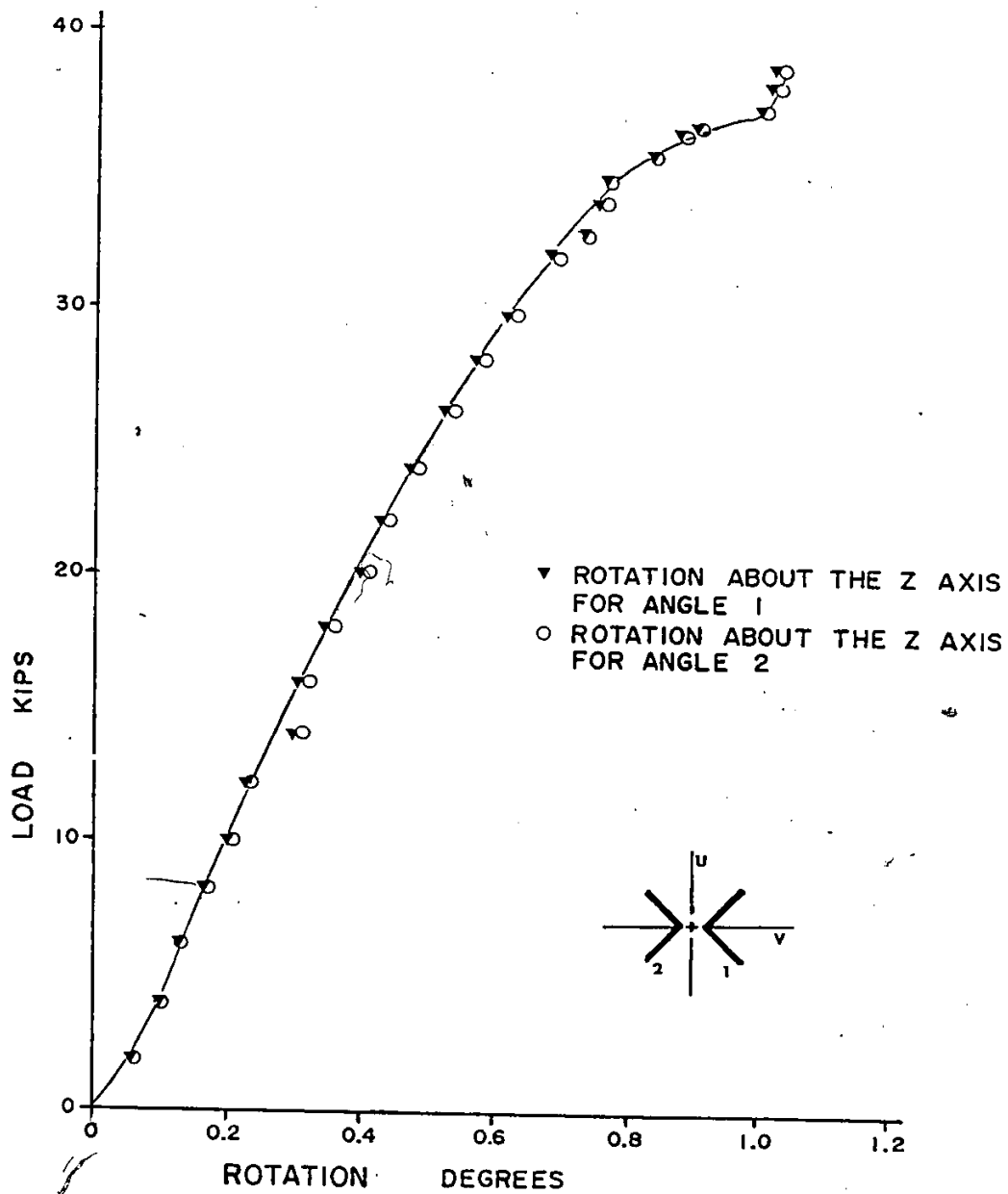
FIGURE 23





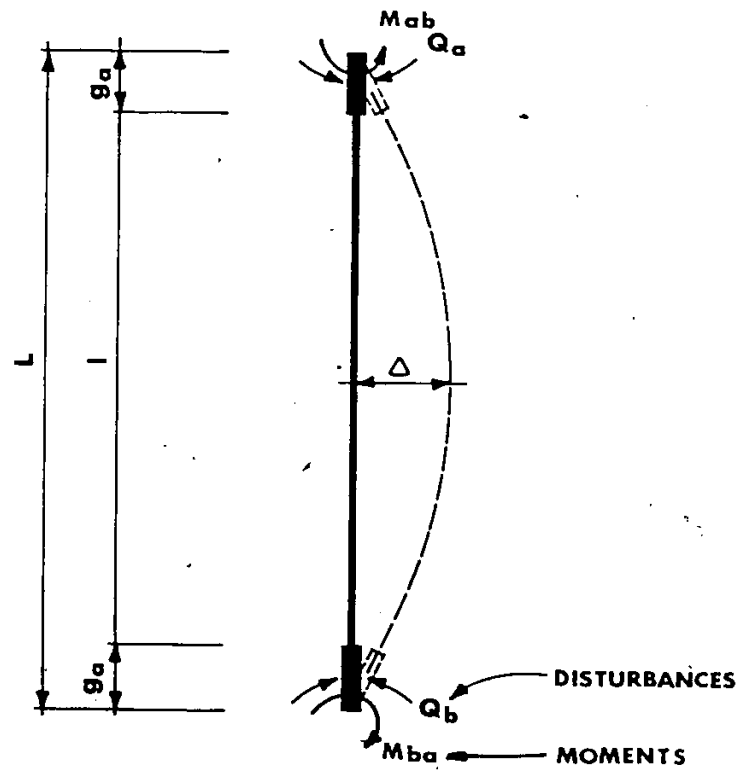
PERCENT SHEAR VERSUS AXIAL LOAD  
FOR THE STARRED ANGLES

FIGURE 24



LOAD VERSUS ROTATION TEST 120A1.3

FIGURE 25



SIMPLE COLUMN WITH END STIFFENERS

FIGURE 26

TABLE 1  
Theoretical Results

(Results in Kips)

Number of Interconnectors	Spaced Column	Battened Column	Eigenvalue
0	40.18(U)	N/A	39.77(U)
1	40.18(U)	42.90(U)	39.55(U)
2	N/A	61.25(U)	48.07(V)
3			48.04(V)
4			49.23(V)
5			47.65(V)

- NOTE: 1. Results tabulated are for a 120 in. starred angle strut made of two 2-1/2 x 2-1/2 x 1/4 in. angles.
2. Euler buckling load about the V-V axis = 48.9 kips.
3. The letter in brackets indicates the axis about which buckling is predicted.
4. Both spaced and battened column theories predict buckling about the U-U axis. Buckling about the V-V axis must be checked as well using appropriate theories to determine about which axis the smaller buckling load occurs. In the case of the battened column with 2 interconnectors the Euler load about the V-V axis is smaller and governs.

TABLE 2  
Geometric Properties

Property	Units	Nominal	Actual	Percent Difference
$A_o$	in. <sup>2</sup>	1.19	1.25	4.8
$I_{x'} \text{ or } I_{y'}$	in. <sup>4</sup>	0.70	0.76	
$r_{x'} \text{ or } r_{y'}$	in.	0.77	0.78	
$r_{u'}$	in.	0.49	0.50	
$x \text{ or } y$	in.	0.72	0.73	
$t$	in.	0.25	0.26	
$A$	in. <sup>2</sup>	2.38	2.5	4.8
$I_x \text{ or } I_y$	in. <sup>4</sup>	3.37	3.63	
$r_x \text{ or } r_y$	in.	1.19	1.20	
$I_u$	in. <sup>4</sup>	4.49	4.83	
$r_u$	in.	1.38	1.39	
$I_v$	in. <sup>4</sup>	2.25	2.42	
$r_v$	in.	0.97	0.98	
$J$	in. <sup>4</sup>	0.17	0.22	
$I_p$	in. <sup>4</sup>	6.55	8.13	
$r_t$	in.		0.033L	

NOTE: 1. The allowable percent difference in the cross sectional area for rolled angles is  $\pm 2.5$  percent of the theoretical or the specified amount (7,38).

TABLE 3

## Types of Interconnectors

Type of Connector	Description
A	2" x 3/8" x 2" plate with 3/16" weld all around.
B	2-1/2" x 2-1/2" x 1/4" angle 2" long with 3/16" weld all around.
C	2-1/2" x 2-1/2" x 1/4" angle 6" long with 3/16" weld all around.
D	2" x 3/8" x 2" plate placed horizontally with 3/16" weld all around.
E	3/8" x 3/8" x 2" long bar with 3/16" weld all around.
F	2" x 3/8" x 2" plate with 1/8" mild steel bolt through one leg of each angle.
G	2" x 3/8" x 2" plate with 1/4" high strength bolt in one leg of each angle.
AF	2" x 3/8" flat bar installed for the full height of the specimen with 3/16" staggered weld 3" long at 9" centers.

TABLE 4  
Experimental Results

Test Number	Failure Load (kips)	Maximum Out-of-Straightness (in.)	Failure mode	Remarks
120A0.1	34.59	0.05	U-U	
120A0.2	40.41	0.07	Combined	
120A1.2	32.73	0.13	U-U	
120A1.3	38.92	0.05	U-U	
120A1.4	23.2	0.08	U-U	
120A1.5	31.40	0.25	U-U	
120A1.6P	38.43	----	U-U	see note 5
120B1.1	36.72	0.10	U-U	
120C1.1	36.32	----	U-U	see note 5
120D1.1	35.23	----	U-U	see note 5
120A2.1	42.95	0.07	V-V	
120A2.2	39.96	0.08	V-V	
120E2.1	35.30	----	V-V	see note 5
120F2.1	29.68	----	Combined	see note 5
120G2.1	29.58	----	Combined	see note 5
120A3.1	45.43	0.05	V-V	
120A3.2	44.96	0.08	V-V	
120A4.2	46.38	----	V-V	see note 5
120A4.3	42.39	----	V-V	see note 5
120A5.1	43.39	0.07	V-V	
80A0.1	62.84	0.026	U-U	
80A1.2	66.07	0.015	U-U	
80A2.1	66.47	0.014	V-V	
80A2.2	62.83	0.067	V-V	
80A2.3	68.95	0.071	V-V	
40A0.1	104.24	----	U-U	see note 6
40A1.1	107.47	----	U-U	see note 6
40A2.1	110.56	----	V-V	see note 6
40A2.2	106.29	----	V-V	see note 6

- NOTE: 1. The principal axis of failure is the axis about which failure occurred.
2. Test specimen 120A2.1 indicates that the length of the member was 120 in., a type A interconnector was used, there were 2 interconnectors and the .1 indicates that this was the first specimen with 2 type A interconnectors.
3. See Table 3 for description of interconnector types.

4. Failure modes shown are the principal axis about which the specimens failed.
5. These out-of-straightnesses were not found as the tests were conducted to determine the failure load and the failure mode only.
6. The tests on the 40 in. long specimens did not have the initial out-of-straightness measured as other effects such as residual stresses were felt to have a greater effect on the inelastic failure of these specimens.



TABLE 5

## Tensile Test Specimen Results

Specimen	1	2	3	4	Average
Area Sq. In.	0.19	0.19	0.19	0.19	
Modulus of Elasticity (ksi)	30,300.	29,700.	29,300.	29,500.	29,700.
Yield Stress (ksi)	48.2	53.8	54.1	54.7	52.7
Ultimate Stress (ksi)	68.8	80.6	80.3	80.7	77.6
Percent Elongation	36	32	33	33	

Appendix A

ELASTIC AND GEOMETRIC STIFFNESS MATRICES

Following are the element stiffness matrices used and are written in the form consistent with that used by Gallagher (9) and Hatout (13).

$$[K_e] = \begin{bmatrix}
 \frac{EA}{L} & 0 & 0 & 0 & 0 & 0 & -\frac{EA}{L} & 0 & 0 & 0 & 0 & 0 \\
 \frac{12EI_2}{L^3} & 0 & 0 & 0 & \frac{6EI_2}{L^2} & 0 & -\frac{12EI_2}{L^3} & 0 & 0 & 0 & \frac{6EI_2}{L^2} \\
 \frac{12EI_2}{L^3} & 0 & -\frac{6EI_2}{L^2} & 0 & 0 & 0 & -\frac{12EI_2}{L^3} & 0 & -\frac{6EI_2}{L^2} & 0 & 0 \\
 \frac{GJ}{L} & 0 & 0 & 0 & 0 & 0 & -\frac{GJ}{L} & 0 & 0 & 0 & 0 \\
 \frac{4EI_2}{L} & 0 & 0 & 0 & \frac{6EI_2}{L^2} & 0 & \frac{2EI_2}{L} & 0 & 0 & 0 & 0 \\
 \frac{4EI_2}{L} & 0 & -\frac{6EI_2}{L^2} & 0 & 0 & 0 & 0 & 0 & \frac{2EI_2}{L} & 0 & 0 \\
 \frac{EA}{L} & 0 & 0 & 0 & 0 & 0 & 0 & 0 & 0 & 0 & \frac{EA}{L} \\
 \text{SYMMETRICAL} & & & & & & \frac{12EI_2}{L^3} & 0 & 0 & 0 & -\frac{6EI_2}{L^2} \\
 & & & & & & \frac{12EI_2}{L^3} & 0 & \frac{6EI_2}{L^2} & 0 & 0 \\
 & & & & & & \frac{GJ}{L} & 0 & 0 & 0 & 0 \\
 & & & & & & & \frac{4EI_2}{L} & 0 & 0 & 0 \\
 & & & & & & & & \frac{4EI_2}{L} & 0 & 0
 \end{bmatrix}$$

$$\begin{bmatrix}
 0 & 0 & 0 & 0 & 0 & 0 & 0 & 0 & 0 & 0 & 0 & 0 \\
 & \frac{6}{5L} & 0 & 0 & 0 & 0.1 & 0 & -\frac{6}{5L} & 0 & 0 & 0 & 0.1 \\
 & & \frac{6}{5L} & 0 & -0.1 & 0 & 0 & 0 & -\frac{6}{5L} & 0 & -0.1 & 0 \\
 & & & 0 & 0 & 0 & 0 & 0 & 0 & 0 & 0 & 0 \\
 & & & & \frac{2L}{15} & 0 & 0 & 0 & 0.1 & 0 & -\frac{L}{30} & 0 \\
 & & & & & \frac{2L}{15} & 0 & -0.1 & 0 & 0 & 0 & -\frac{L}{30} \\
 & & & & & & 0 & 0 & 0 & 0 & 0 & 0 \\
 & & & & & & & & \frac{6}{5L} & 0 & 0 & 0 & -0.1 \\
 & & & & & & & & & \frac{6}{5L} & 0 & 0.1 & 0 \\
 & & & & & & & & & & 0 & 0 & 0 \\
 & & & & & & & & & & & \frac{2L}{15} & 0 \\
 & & & & & & & & & & & & \frac{2L}{15}
 \end{bmatrix}$$

[Kg]-F

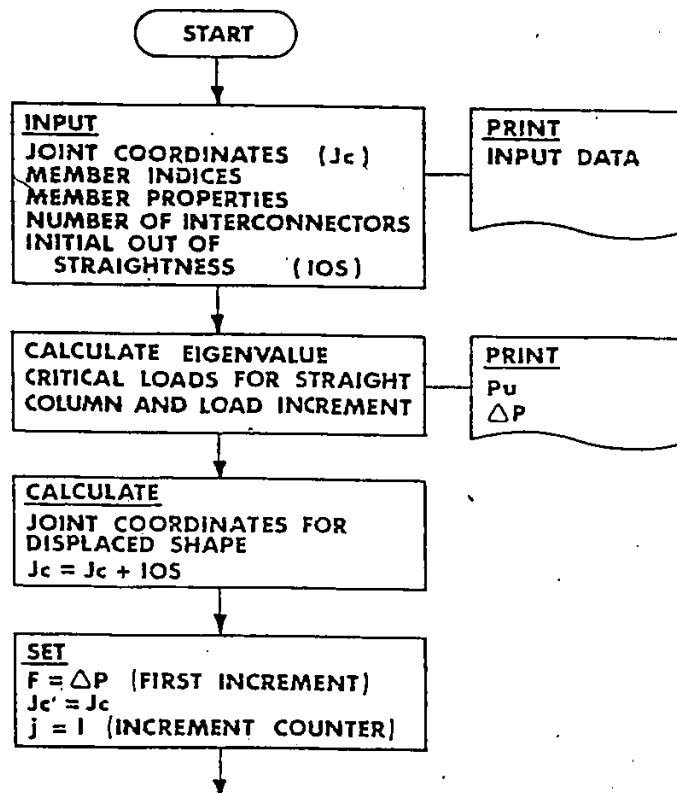
SYMETRICAL

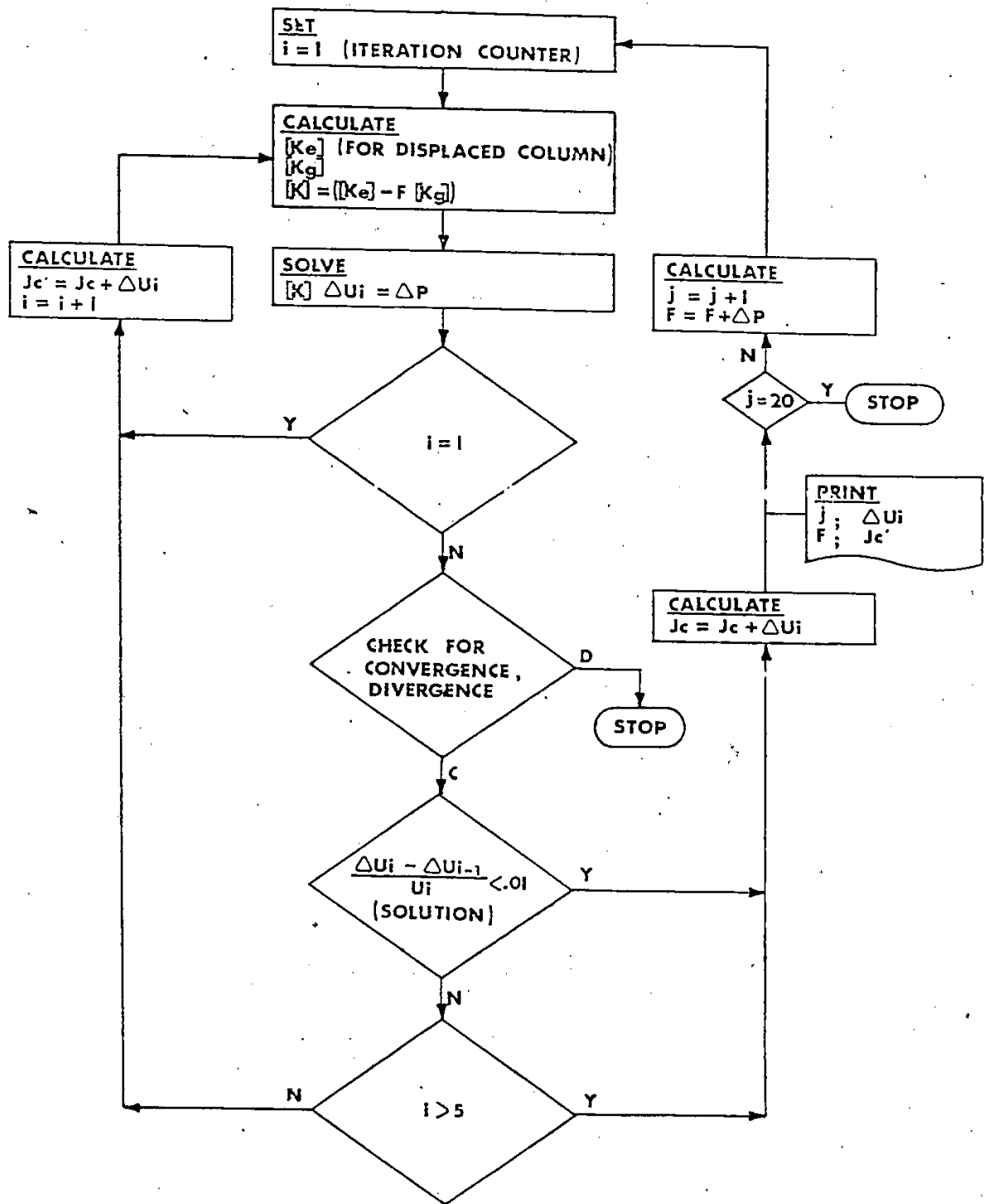
where  $L$  = the length of the member,  $d/2$ ;  $A$  = the area of the member,  $A_0$ ;  $J$  = the St. Venant torsional constant;  $I_2'$  = the moment of inertia about the  $V'-V'$  axis,  $I_{V'}$ ; and  $I_3'$  = the moment of inertia about the  $U'-U'$  axis,  $I_{U'}$ .

Appendix B

COMPUTER PROGRAM FLOW CHART AND LISTING

The flow chart shows the process used in the computer program to solve the linear iterative-incremental problem. Following the flow chart is the complete program listing with a sample of the input data and output.





FORTRAN IV G LEVEL 21

MAIN

DATE = 83003

20/36/40

## PURPOSE:

- 1) TO CALCULATE THE FIRST BUCKLING LOAD OF SLENDER, CLOSE-SPACED, 2 MEMBER, COLUMNS TIED TOGETHER BY RIGID INTERCONNECTORS.
- 2) CALCULATE THE DISPLACEMENTS BY A LINEAR INCREMENTAL ITERATIVE PROCEDURE.

## USAGE:

INPUT IS REQUIRED ON TWO CARDS  
 CARD 1 CONTAINS NUMBER OF INTERCONNECTORS, LENGTH,  
 SPACING, INITIAL OUT OF STRAIGHTNESS FOR EACH MEMBER  
 IN PERPENDICULAR DIRECTIONS AT MID HEIGHT  
 CARD 2 CONTAINS THE PROPERTIES OF THE MEMBERS

## NOTATION:

GLK1	-ELASTIC STIFFNESS MATRIX
GLK2	-GEOMETRIC STIFFNESS MATRIX
TOTL	-SUM OF STIFFNESS MATRICES
TRAN	-DEPENDANT DEGREES OF FREEDOM TRANSFORMATION MATRIX
TRAN	-TRANSPOSE OF TRAN
CNN	-JOINT COORDINATES
CN	-REVISED COORDINATES
DC	-DIRECTION COSINES
MN	-MEMBER INDICES
IVC	-VARIABLE CORRELATION TABLE
RIOS	-INITIAL OUT OF STRAIGHTNESS
AA	-AREA VECTOR
E	-MODULOUS OF ELASTICITY
G	-MODULOUS OF RIGIDITY
LGTH	-LENGTH VECTOR
ZI	-MOMENT OF INERTIA S3 AXIS
YI	-MOMENT OF INERTIA S2 AXIS
XI	-TORSION CONSTANT J
XL	-VECTOR OF EIGENVALUES
X	-VECTOR OF EIGENVECTORS
ALPHA	-ORIENTATION VECTOR GENERAL MEMBER ANGLE OF S3 AXIS TO GLOBAL HORIZ. VERTICAL MEMBER ANGLE OF S3 AXIS TO Z AXIS
M	-NUMBER OF MEMBERS
N	-NUMBER OF JOINTS
NDF	-NUMBER OF DEGREES OF FREEDOM
NN	-NUMBER OF INTERCONNECTORS
NDDF	-NUMBER OF DEPENDANT DEGREES OF FREEDOM
IGEN	-INDICATOR IF 1 PROGRAM CALCULATES THE EIGEN VALUES AND VECTORS FOR FIRST MODE BUCKLING
INC	-INDICATOR IF 1 PROGRAM CALCULATES LOAD DEFLECTION CURVES USING A ITERATIVE INCREMENTAL
MEM	-INDICATOR IF 1 PROGRAM SETS ALL DATA TO DEFINE CNN, MN, IVC, RIOS, M, N, NDF, NDDF GIVEN THE NUMBER OF INTERCONNECTORS, LENGTH, AND SPACING. IF NOT 1 THEN THE DATA IS REQUIRED AND THE TRANSFORMATION MATRIX TRAN IS NOT USED.
IPLT	-INDICATOR IF 1 THEN PLOTS OF THE LOAD DEFLECTION ARE PRINTED. THIS INDICATOR MUST BE 0 IF INC IS 0
IPRT	-INDICATOR IF 1 THEN ALL OUTPUT IS PRINTED. IF IPRT IS 0 THEN ONLY THE INPUT DATA, EIGEN VALUE, EIGEN VECTOR AND FINAL LOAD DISPLACEMENT VALUES ARE PRINTED.

## REMARKS:

THIS PROGRAM WAS DEVELOPED FOR JOINTS ARRANGED TO FORM A CRUCIFORM, WITH ONLY SLIGHT MODIFICATION IT COULD BE USED FOR OTHER SECTIONS. THE INTER CONNECTION OF THE INTERCONNECTORS IS ASSUMED TO BE RIGID AND THE INITIAL OUT OF STRAIGHTNESS IS ASSUMED TO BE A SINE CURVE.

## SUBROUTINES AND FUNCTION SUBPROGRAMS REQUIRED:

SIN, COS, SQR, ARRY, EIGEN, IFIX, FLOAT, ABS

## METHOD:

THIS PROGRAM IS BASED ON THE FINITE ELEMENT APPROACH AND THE GEOMETRIC STIFFNESS MATRIX IS BASED ON THE WORK OF F. C. MARTIN

FORTRAN IV G LEVEL 21

MAIN

DATE = 83003

20/36/40

```

0001      DIMENSION TRAN(100,100), TRANT(100,100), TEMP(100,100)
0002      DIMENSION GLK1(100,100), GLK2(100,100), TOTL(100,100), P(100), U(100)
0003      DIMENSION CN(50,3), DC(50,3), MN(50,2), IVC(50,12)
0004      DIMENSION GX1(20), GY1(20), GZ1(20), GY2(20), GZ2(20), LGTH(50)
0005      DIMENSION RIOS(50,2)
0006      DIMENSION XL(100), X(10000), GLK1V(10000), GLK2V(10000)
0007      DIMENSION CNN(50,3), UX(100), PY(100)
0008      INTEGER DOOF(50)
0009      REAL L
0010      REAL MK, LGTH, M1
0011      PI=4.0*ATAN(1.0)

C
C      INPUT INDICATORS
0012      READ(5,503) IGEN, INC, MEM, IPLT, IPRT
0013      FORMAT(5I2)
0014      IF (INC.NE.1) IPLT=0

C
C      INPUT OF DATA
0015      IF (MEM.NE.1) GOTO4000
0016      READ(5,500) NN, L, B, Y1, Y2, Z1, Z2
0017      FORMAT(15,6F10.5)
0018      S=L/(2*(NN+1))
0019      N=(NN+2)*2
0020      M=(NN+1)*2
0021      NDF=(NN+1)*10+IFIX(FLOAT(NN)/2.0)
0022      NDOF=1+NN+IFIX(FLOAT(NN)/2.0)
0023      WRITE(6,723)
0024      WRITE(6,700) NN, L, B, Y1, Y2, Z1, Z2, N, M, NDF, NDOF
0025      GOTO4001
0026      4000 READ(5,503) N, M, NDF
0027      WRITE(6,722) N, M, NDF
0028      4001 CONTINUE

C
C      JOINT COORDINATES
0029      IF (MEM.NE.1) GOTO4002
0030      N2=N/2
0031      DO20 I=1, N2
0032      I1=I+N/2
0033      CNN(I,1)=(I-1)*S
0034      CNN(I,2)=B/2
0035      CNN(I,3)=0.0
0036      CNN(I1,1)=CNN(I,1)
0037      CNN(I1,2)=-CNN(I,2)
0038      CNN(I1,3)=0.0

C
C      INITIAL OUT OF STRAIGHTNESS
0039      RIOS(I,1)=Y1*SIN(PI/L*CNN(I,1))
0040      RIOS(I,2)=Z1*SIN(PI/L*CNN(I,1))
0041      RIOS(I1,1)=Y2*SIN(PI/L*CNN(I,1))
0042      RIOS(I1,2)=Z2*SIN(PI/L*CNN(I,1))
0043      CONTINUE
0044      4002 CONTINUE
0045      WRITE(6,701)
0046      DO40 I=1, N
0047      IF (MEM.NE.1) READ(5,504) (CNN(I,J), J=1,3)
0048      WRITE(6,702) I, (CNN(I,J), J=1,3)
0049      CONTINUE
0050      40 WRITE(6,714)
0051      DO10 I=1, N
0052      IF (MEM.NE.1) READ(5,502) (RIOS(I,J), J=1,2)
0053      WRITE(6,702) I, (RIOS(I,J), J=1,2)
0054      CONTINUE

C
C      MEMBER INDICES
0055      WRITE(6,703)
0056      IF (MEM.NE.1) GOTO4004
0057      M2=M/2
0058      DO60 I=1, M2
0059      I1=I+M2
0060      MN(I,1)=I
0061      MN(I,2)=I+1
0062      MN(I1,1)=I+N/2
0063      MN(I1,2)=I+1+N/2

```

```

FORTRAN IV G LEVEL 21                MAIN                DATE = 83003                20/36/40
0064      50  CONTINUE
0065      4004 CONTINUE
0066      DO70I=1,M
0067      IF (MEM.NE.1)READ(5,503)(MN(I,J),J=1,2)
0068      WRITE(6,704)I,(MN(I,J),J=1,2)
0069      70  CONTINUE
C
C      VARIABLE CORELATION TABLE
0070      IF (MEM.NE.1)GOTO4005
0071      CALL VCTABL(IVC,M,NN)
0072      4005 CONTINUE
0073      WRITE(6,705)
0074      DO190I=1,M
0075      IF (MEM.NE.1)READ(5,504)(IVC(I,J),J=1,12)
0076      504  FORMAT(12I2)
0077      WRITE(6,706)I,(IVC(I,J),J=1,12)
0078      190  CONTINUE
C
C      INPUT MECHANICAL PROPERTIES
0079      WRITE(6,707)
0080      READ(5,502)E,G,AA,ZI,YI,XI,ALPHA
0081      502  FORMAT(7F10,4)
0082      WRITE(6,708)E,G,AA,ZI,YI,XI,ALPHA
C
C      DEPENDANT DEGREES OF FREEDOM
0083      IF (MEM.NE.1)GOTO4006
0084      DDOF(1)=3
0085      I=1
0086      IF (NN.EQ.0)GOTO320
0087      300  I2=I+1
0088      I3=I+2
0089      I4=I+3
0090      IF (I2.EQ.NDOF)GOTO310
0091      DDOF(I2)=DDOF(I)+10
0092      DDOF(I3)=DDOF(I2)+1
0093      DDOF(I4)=DDOF(I3)+1
0094      I=I4
0095      IF (I.EQ.NDOF)GOTO320
0096      GOTO300
0097      310  DDOF(I2)=DDOF(I)+9
0098      320  CONTINUE
0099      WRITE(6,715)(DDOF(I),I=1,NDOF)
C
C      TRANSFORMATION MATRIX
0100      JJ=NDF-NDOF
0101      IF (IPRT.EQ.1)WRITE(6,719)
0102      KTR2=1
0103      FACT=0.0
0104      IF (R.NE.0.0)FACT=1.0/D
0105      DO290I=1,NDF
0106      JO=I+KTR2
0107      DO200J=1,JJ
0108      TRAN(I,J)=0.0
0109      TPANT(J,I)=0.0
0110      200  CONTINUE
0111      IF (KTR2.GT.NDOF)GOTO210
0112      IF (I.EQ.DDOF(KTR2))GOTO220
0113      210  CONTINUE
0114      TRAN(I,JO)=1.0
0115      TPANT(JC,I)=1.0
0116      GOTO281
0117      220  CONTINUE
0118      IF (KTR2.EQ.1)GOTO250
0119      DO230JN=10,12
0120      JT=JN
0121      DO230K=1,M
0122      KI=K
0123      IF (IVC(K,JN).EQ.DDOF(KTR2))GOTO240
0124      230  CONTINUE
0125      240  CONTINUE
0126      J7=9
0127      IF (JT.EQ.11)GOTO245
0128      IF (JT.EQ.12)J7=7
0129      J1=IVC(KT,JZ)

```



```

FORTRAN IV G LEVEL 21
0130 J2=IVC(KT+M2,JZ)
0131 J3=0.0
0132 GOTC260
0133 245 CONTINUE
0134 J3=IVC(KT+M2,11)
0135 GOTQ260
0136 250 CONTINUE
0137 J1=IVC(1,1)
0138 J2=IVC(M/2+1,1)
0139 J3=0.0
0140 260 CONTINUE
0141 DD270JCH=1,NDDF
0142 JCHECK=NDDF-JCH+1
0143 IF (J1.GE.DDOF(JCHECK)) J1=J1-1
0144 IF (J2.GE.DDOF(JCHECK)) J2=J2-1
0145 IF (J3.EQ.0) GOTQ270
0146 IF (J3.GE.DDOF(JCHECK)) J3=J3-1
0147 270 CONTINUE
0148 KTR2=KTR2+1
0149 IF (J3.EC.0) GOTQ275
0150 TRAN(I,J3)=1.0
0151 TRANT(J3,1)=1.0
0152 GOTQ280
0153 275 CONTINUE
0154 TRAN(I,J1)=-FACT
0155 TRAN(I,J2)=FACT
0156 TRANT(J1,1)=-FACT
0157 TRANT(J2,1)=FACT
0158 280 CONTINUE
0159 281 CONTINUE
0160 IF (IPRT.EQ.1) WRITE(6,720)(TRAN(I,JP),JP=1,JJ)
0161 290 CONTINUE
0162 4006 CONTINUE

C
C
C CHECK INDICATOR IGEN IF EQUAL TO 1 THEN CALCULATE EIGEN VALUES
C AND EIGEN VECTORS
0163 IF (IGEN.NE.1) GOTC305

C
C DIRECTION COSINES FOR STRAIGHT COLUMN
0164 CALL COSINE(M,MM,CNN,LGTH,DC)

C
C EIGEN VALUE
0165 CALLELAKM(M,XI,YI,ZI,AA,F,G,LGTH,DC,NDF,IVC,ALPHA1,GLK1)
0166 CALL GECKM(M,LGTH,DC,NDF,IVC,ALPHA1,GLK2)
0167 IF (MEM.NE.1) GOTQ4013
0168 CALL MATMUL(GLK1,TRAN,TEMP,NDF,NDF,JJ)
0169 CALL MATMUL(TRAN,TEMP,GLK1,JJ,NDF,JJ)
0170 CALL MATMUL(GLK2,TRAN,TEMP,NDF,NDF,JJ)
0171 CALL MATMUL(TRAN,TEMP,GLK2,JJ,NDF,JJ)
0172 GOTQ4014
0173 4013 CONTINUE
0174 JJ=NDF
0175 4014 CONTINUE
0176 CALL ARRAY(2,JJ,JJ,100,100,GLK1V,GLK1)
0177 CALL ARRAY(2,JJ,JJ,100,100,GLK2V,GLK2)
0178 CALL NROOT(JJ,GLK2V,GLK1V,XL,X)
0179 I1=1
0180 CL1=2.0/XL(I1)
0181 IF (MEM.NE.1) CL1=CL1/2.
0182 WRITE(6,709)I1
0183 WRITE(6,710)CL1
0184 DD304I=1,JJ
0185 U(I)=X(I)
0186 304 CONTINUE
0187 IF (MEM.EQ.1) CALL VECT(TRAN,U,UX,JJ,NDF)
0188 WRITE(6,724)
0189 DD303I=1,NDF
0190 IF (MEM.EQ.1) WRITE(6,702)I,UX(I)
0191 IF (MEM.NE.1) WRITE(6,702)I,U(I)
0192 303 CONTINUE
0193 305 CONTINUE

C
C CHECK INDICATOR INC
0194 IF (INC.NE.1) GOTQ420

```

DATE = 83003

20/36/40

FORTRAN IV G LEVEL 21

MAIN

DATE = 53003

20/36/40

```

0195          C
0196          C
          C      CALCULATE THE LOAD INCRMENT
          C
          C      READ(5,502)PDEL
          C      IF(PDEL.EQ.0.0)PDEL=CL1/40.0
          C
          C      JOINT COORDINATES FOR INITIALLY CUT OF STRAIGHT COLUMN
          C
          C      WRITE(6,701)
          C      DO 42 I=1,N
          C      CN(I,1)=CNN(I,1)
          C      DO 41 J=2,3
          C      CN(I,J)=CNN(I,J)+RIDS(I,J-1)
          C      CN(I,J)=CN(I,J)
          C      CONTINUE
          C      WRITE(6,702)I,(CN(I,J),J=1,3)
          C      CONTINUE
          C
          C      INITIALIZE LOAD AND DISPLACEMENT VECTORS
          C
          C      DO 355 I=1,NDF
          C      P(I)=0.0
          C      UX(I)=0.0
          C      CONTINUE
          C      IF(MEM.EQ.1)P(IVC(N/2+1,1))=PDEL
          C      IF(MEM.EQ.1)P(IVC(1,1))=PDEL
          C      IF(MEM.NE.1)P(IVC(N,7))=-PDEL
          C      IF(MEM.EQ.1)CALL VECT(TRAN,P,PT,NDF,JJ)
          C      NDC=N/2-1
          C      PA=0.0
          C
          C      INCREMENTING THE PROBLEM FOR LOAD VERSUS DEFLECTION
          C
          C      DO 400 KTR=1,20
          C      PA=PA+PDEL
          C      A=PA
          C      A2=A
          C      IF(MEM.EQ.1)A2=A+2
          C      IF(MEM.NE.1)GOTO 4007
          C      CLSTY2=CN(N,2)-CNN(N,2)
          C      CLSTZ2=CN(N,3)-CNN(N,3)
          C      NO=N/2
          C      CONTINUE
          C      IF(MEM.NE.1)NO=(N+2)/2
          C      CLSTY1=CN(NO,2)-CNN(NO,2)
          C      CLSTZ1=CN(NO,3)-CNN(NO,3)
          C
          C      ITERATE AT LOAD TO GET DISPLACEMENTS
          C      IF(IPRT.EQ.1)WRITE(6,711)
          C      DO 390 ITERAT=1,5
          C
          C      DIRECTION COSINES FOR DISPLACED COLUMN
          C      CALL COSINE(M,MN,CN,LGTH,DC)
          C
          C      ELASTIC AND CECMETRIC STIFFNESS MATRICES
          C      CALLELAXM(M,XI,YI,ZI,AA,E,G,LGTH,DC,NDF,IVC,ALPHA1,GLK1)
          C      CALL GECKM(M,LGTH,DC,NDF,IVC,ALPHA1,GLK2)
          C
          C      SET UP TOTAL MATRIX
          C      DO 370 I=1,NDF
          C      DO 370 J=1,NDF
          C      TOTL(I,J)=GLK1(I,J)-GLK2(I,J)*A
          C      CONTINUE
          C
          C      TRANSFORM THE TOTAL STIFFNESS MATRIX
          C      IF(MEM.NE.1)GOTO 400A
          C      CALL MATMUL(TOTL,TRAN,TEMP,NDF,NDF,JJ)
          C      CALL MATMUL(TRAN,TEMP,TOTL,JJ,NDF,JJ)
          C      DO 360 I=1,JJ
          C      U(I)=PT(I)
          C      CONTINUE

```

FORTRAN IV G LEVEL 21

MAIN

DATE = 83003

20/36/40

```

C          SOLVE PROBLEM USING A GAUSSF ILLIMINATION SUBROUTINE
C
0244      CALL SOLVE (TOTL,U,JJ)
0245      CALL VECT (THAN,U,UX,JJ,NDF)
0246      GOTC4009
0247      4008 CONTINUE
0248      DC3711=1,NDF
0249      371  UX(I)=P(I)
0250      CALL SOLVE (TOTL,UX,NDF)
0251      4009 CONTINUE
0252      IF (IPRT.NE.1)GOTO3731
0253      WRITE (6,713)
0254      DC3731=1,NDF
0255      373  WRITE(6,702)I,UX(I),P(I)
0256      3731 CONTINUE
C
C          ADJUST THE JOINT COORDINATES BY THE CALCULATED DISPLACEMENTS
C
0257      IF (MEM.NE.1)GOTC4010
0258      DC3751=1,NP0
0259      I1=I+1
0260      I2=I+N/2
0261      I3=I1+N/2
0262      I4=I3-2
0263      DC375J=1,3
0264      J6=J+6
0265      IF (J.GT.1)GOTO374
0266      CN(I,J)=CNN(I,J)+UX(IVC(I,I))
0267      CN(I2,J)=CNN(I2,J)+UX(IVC(I4,I))
0268      GOTO375
0269      374  CCNTINUE
0270      CN(I1,J)=CNN(I1,J)+UX(IVC(I,J6))
0271      CN(I3,J)=CNN(I3,J)+UX(IVC(I4,J6))
0272      375  CCNTINUE
0273      GOTC4015
0274      4010 CONTINUE
0275      DC376J=1,3
0276      IF (IVC(I,J).EQ.0)GOTO376
0277      CH(I,J)=CNN(I,J)+UX(IVC(I,J))
0278      376  CCNTINUE
0279      DC3721=2,N
0280      DC372J=1,3
0281      IF (IVC(I-1,J+6).EQ.0)GOTO372
0282      CH(I,J)=CNN(I,J)+UX(IVC(I-1,J+6))
0283      372  CCNTINUE
0284      4015 CONTINUE
0285      IF (IPRT.NE.1)GOTO3971
0286      WRITE (6,701)
0287      DC3971=1,N
0288      397  WRITE (6,702)I,(CN(I,J),J=1,3)
0289      3971 CONTINUE
0290      IF (MEM.NE.1)GOTO4011
C
C          CHECK % DIFFERENCE FROM PREVIOUS ITERATION
C
0291      IF (ABS(CN(N,2)).LE.1.E-6)GOTO3571
0292      CHCKY2=ABS((CLSTY2-CN(N,2))/CN(N,2))
0293      GOTC3572
0294      3571 CHCKY2=0.0
0295      3572 CLSTY2=CN(N,2)
0296      IF (ABS(CN(N,3)).LE.1.E-6)GOTO3573
0297      CHCKZ2=ABS((CLSTZ2-CN(N,3))/CN(N,3))
0298      GOTC3574
0299      3573 CHCKZ2=0.0
0300      CLSTZ2=CN(N,3)
0301      4011 IF (ABS(CN(NQ,3)).LE.1.E-6)GOTO3575
0302      CHCKZ1=ABS((CLSTZ1-CN(NQ,3))/CN(NQ,3))
0303      GOTC3576
0304      3575 CHCKZ1=0.0
0305      3576 CLSTZ1=CN(NQ,3)
0306      IF (ABS(CN(NQ,2)).LE.1.E-6)GOTO3577
0307      CHCKY1=ABS((CLSTY1-CN(NQ,2))/CN(NQ,2))
0308      GOTC3578
0309      3577 CHCKY1=0.0
0310      3578 CLSTY1=CN(NQ,2)
0311      IF (CHCKY1.LE..01.AND.CHCKZ1.LE..01)GOTO392
0312      GOTC390
0313      392  CONTINUE

```



FOURPAN IV G LEVEL 21

MAIN

DATE = 83003

20/36/40

```

0364 713 @*****,,/)
      713 FORMAT( ' ' , 'LOAD AND DISPLACEMENT'/// ' ' , 'D.O.F' DISPLACEMENT
      @NT LOAD//)
0365 714 FORMAT(/// ' ' , 'INITIAL OUT OF STRAIGHTNESS (INCHES)'/// ' ' , 'JOINT'
      @ , T12 , 'Y' , T29 , 'Z'//)
0366 715 FORMAT(/// ' ' , 'DEPENDANT DEGREES OF FREEDOM'//10I10)
0367 716 FORMAT(/// ' ' , 'CCOUNTER' , T12 , 'LOAD' , T24 , 'Y1' , T36 , 'Z1' , T48 , 'Y2' , T60 ,
      @ 'Z2' ,//)
0368 717 FORMAT( ' ' , 'IS , T10 , FS , 2 , T13 , 4F12.4)
0369 718 FORMAT(/// ' ' , 'LOAD KIPS' , T10 , F10.4/// ' ' , 'ITERATIONS' , T14 , I2)
0370 719 FORMAT(/// ' ' , 'TRANSFORMATION MAT IX (NOE X JJ)'//)
0371 720 FORMAT( ' ' , '13F9.2'// ' ' , '13F9.2'// ' ' , '10 , I2'// ' ' , 'T10 , I2F9.2)
0372 721 FORMAT( ' ' , 'FINAL NUMBER OF ITERATIONS' , 'I2' , 'PC LOAD' , F10.5 ,
      @ 'KIPS'//)
0373 722 FORMAT( ' ' , 'SINGLE PRISMATIC 3D COMPRESSION MEMBER'/// ' ' , 'NUMBER OF
      @F JCINTS' , T35 , I5// ' ' , 'NUMBER OF MEMBERS' , T35 , I5/// ' ' , 'NUMBER OF D.O
      @F' , T35 , I5///)
0374 723 FORMAT( ' ' , 'BUILT UP DOUBLE ANGLE 3D COMPRESSION MEMBER'///)
0375 724 FORMAT(/// ' ' , 'EIGEN VECTOR'/// ' ' , 'D.O.F' , T14 , 'VECTOR'//)
0376 STOP
0377 END

```

FORTRAN IV G LEVEL 21

ELAKM

DATE = 83003

20/36/40

```

0001      SUBROUTINE ELAKM(N,XI,YI,ZI,AA,F,G,EL,DC,NDF,IVC,ALPHA1,MK)
          SUBROUTINE TO CALCULATE THE MASTER ELASTIC STIFFNESS MATRIX
          DIMENSION DC(50,3),EL(50)
          DIMENSION IVC(50,12),EKL(12,12),T(12,12)
          DIMENSION EKG(12,12),U(12,12),V(12,12),MK(100,100)
          REAL MK
          PI=4.0*ATAN(1.0)
          DO10 I=1,NDF
          DO10 J=1,NDF
          MK(I,J)=0.0
10      CONTINUE
          DO10 COK=1,M
          ALPHA=ALPHA1+PI/180.
          CX=DC(K,1)
          CY=DC(K,2)
          CZ=DC(K,3)
          DO20 I=1,12
          DO20 J=1,12
          T(I,J)=0.0
20      CONTINUE
          T(1,1)=CX
          T(1,2)=CY
          T(1,3)=CZ
          IF (CX+CZ)25,27,25
          25      CONTINUE
          ELCNE=SQRT(CX**2+CZ**2)
          T(2,1)=(-CX*CY*CCS(ALPHA)-CZ*SIN(ALPHA))/ELONF
          T(2,2)=ELCNF*CCS(ALPHA)
          T(2,3)=(-CY*CZ*CCS(ALPHA)+CX*SIN(ALPHA))/ELONF
          T(3,1)=(CX*CY*SIN(ALPHA)-CZ*CCS(ALPHA))/ELONF
          T(3,2)=-ELONF*SIN(ALPHA)
          T(3,3)=(CY*CZ*SIN(ALPHA)+CX*CCS(ALPHA))/ELONE
          GOTC30
27      CONTINUE
          T(2,1)=-CY*CCS(ALPHA)
          T(2,3)=CY*SIN(ALPHA)
          T(3,1)=SIN(ALPHA)
          T(3,3)=CCS(ALPHA)
30      CONTINUE
          DO40 I=1,3
          I3=I+3
          I6=I+6
          I9=I+9
          DO40 J=1,3
          J3=J+3
          J6=J+6
          J9=J+9
          T(I3,J3)=T(I,J)
          T(I6,J6)=T(I,J)
          T(I9,J9)=T(I,J)
40      CONTINUE
          DO50 I=1,12
          DO50 J=1,12
          EKL(I,J)=0.0
50      CONTINUE
          FKL(1,1)=E*AA/EL(K)
          EKL(1,7)=-EKL(1,1)
          EKL(2,2)=12.0*E*ZI/EL(K)**3
          FKL(2,6)=6.0*L*ZI/EL(K)**2
          LKL(2,8)=-EKL(2,2)
          EKL(2,12)=EKL(2,2)
          EKL(3,3)=12.0*E*YI/EL(K)**3
          EKL(3,5)=-6.0*E*YI/EL(K)**2
          FKL(3,9)=-EKL(3,3)
          FKL(3,11)=EKL(3,5)
          EKL(4,4)=G*XI/EL(K)
          FKL(4,10)=-EKL(4,4)
          EKL(5,5)=4.0*E*YI/EL(K)
          EKL(5,9)=-EKL(3,11)
          FKL(5,11)=2.0*E*YI/EL(K)
          FKL(6,6)=4.0*L*ZI/EL(K)
          LKL(6,8)=-EKL(2,2)
          EKL(6,12)=2.0*E*ZI/EL(K)
          FKL(7,7)=EKL(1,1)
          FKL(8,8)=-EKL(2,2)
          EKL(8,12)=-EKL(2,12)

```

FORTRAN IV G LEVEL 21

ELAKM

DATE = 83003

20/36/40

```

0076      EKL(9,9)=-EKL(3,9)
0077      FKL(9,11)=-EKL(3,11)
0078      EKL(10,10)=-EKL(4,10)
0079      EKL(11,11)=EKL(5,5)
0080      EKL(12,12)=EKL(6,6)
0081      D0601=2.12
0082      I1=1-1.
0083      D060J=1.11
0084      EKL(I,J)=EKL(J,I)
0085      60  CONTINUE
0086      CALL TRANS(T,U,12,12)
0087      CALL MULT(U,EKL,V,12,12,12)
0088      CALL MULT(V,T,EKG,12,12,12)
0089      D0701=1.12
0090      IL=IVC(K,1)
0091      IF(IL.EQ.0)GOTO9C
0092      IL1=IABS(IL)
0093      JJ=IL1/IL
0094      D080J=1.12
0095      IN=IVC(K,J)
0096      IF(IN.EQ.0)GOTO80
0097      IN1=IABS(IN)
0098      KK=IN1/IN
0099      MK(IL1,IN1)=MK(IL1,IN1)+JJ*KK*EKG(I,J)
0100      80  CONTINUE
0101      90  CONTINUE
0102      100 CONTINUE
0103      RETRN
0104      -END

```

FORTRAN IV G LEVEL 21

GEOKM

DATE = 83003

20/36/40

```

0001      SUBROUTINE GEOKM(M,EL,DC,NOF,IVC,ALPHA1,MK)
          C
          C      SUBROUTINE TO CALCULATE THE MASTER GEOMETRIC STIFFNESS MATRIX
          DIMENSION EL(50),DC(50,3),IVC(50,12),GKL(12,12),GKG(12,12)
          DIMENSION T(12,12),U(12,12),V(12,12),MK(100,100)
          REAL MK
          PI=4.0*ATAN(1.0)
          DO10I=1,NOF
          DO10J=1,NOF
          MK(I,J)=0.0
10      CONTINUE
          DO100K=1,M
          ALPHA=ALPHA1*PI/180.
          CX=DC(K,1)
          CY=DC(K,2)
          CZ=DC(K,3)
          DO20I=1,12
          DO20J=1,12
          T(I,J)=0.0
20      CONTINUE
          T(1,1)=CX
          T(1,2)=CY
          T(1,3)=CZ
          IF (CX+CZ)25,27,25
25      CONTINUE
          ELONE=SQRT(CX**2+CZ**2)
          T(2,1)=(-CX*CY*COS(ALPHA)-CZ*SIN(ALPHA))/ELONE
          T(2,2)=ELCNE*COS(ALPHA)
          T(2,3)=(-CY*CZ*COS(ALPHA)+CX*SIN(ALPHA))/ELONE
          T(3,1)=(CX*CY*SIN(ALPHA)-CZ*COS(ALPHA))/ELONE
          T(3,2)=-ELONE*SIN(ALPHA)
          T(3,3)=(CY*CZ*SIN(ALPHA)+CX*COS(ALPHA))/ELONE
          GO TO 30
27      CONTINUE
          T(2,1)=-CY*COS(ALPHA)
          T(2,3)=CY*SIN(ALPHA)
          T(3,1)=SIN(ALPHA)
          T(3,3)=CCS(ALPHA)
30      CONTINUE
          DO40I=1,3
          I3=I+3
          I6=I+6
          I9=I+9
          DC40J=1,3
          J3=J+3
          J6=J+6
          J9=J+9
          T(I3,J3)=T(I,J)
          T(I6,J6)=T(I,J)
          T(I9,J9)=T(I,J)
40      CONTINUE
          DO50I=1,12
          DO50J=1,12
          GKL(I,J)=0.0
50      CONTINUE
          GKL(2,2)=6.0/(5.0*EL(K))
          GKL(2,6)=0.0
          GKL(2,8)=-GKL(2,2)
          GKL(2,12)=GKL(2,6)
          GKL(3,3)=GKL(2,2)
          GKL(3,5)=-GKL(2,6)
          GKL(3,9)=GKL(2,8)
          GKL(3,11)=GKL(3,5)
          GKL(5,5)=2.0*EL(K)/15.0
          GKL(5,9)=GKL(2,6)
          GKL(5,11)=-EL(K)/30.0
          GKL(6,6)=GKL(5,5)
          GKL(6,8)=GKL(3,5)
          GKL(6,12)=GKL(5,11)
          GKL(8,8)=GKL(2,2)
          GKL(8,12)=GKL(3,5)
          GKL(9,9)=GKL(2,2)
          GKL(9,11)=GKL(2,6)
          GKL(11,11)=GKL(5,5)
          GKL(12,12)=GKL(6,6)
          DO60I=2,12
          II=I-1

```



FURTRAN IV G LEVEL 21

GFOKM

DATE = 83003

20/36/40

```

0076      DO60J=1,11
0077      GKL(I,J)=GKL(J,I)
0078      CONTINUE
0079      60  CALLTRANS(T,U,12,12)
0090      CALL MULT(U,GKL,V,12,12,12)
0081      CALL MULT(V,T,GKG,12,12,12)
0082      DO90I=1,12
0083      IL=IVC(K,I)
0084      IF(IL.EQ.0)GOTO90
0085      IL1=IABS(IL)
0086      JJ=IL1/IL
0087      DO80J=1,12
0088      IN=IVC(K,J)
0089      IF(IN.EQ.0)GOTO80
0090      IN1=IABS(IN)
0091      KK=IN1/IN
0092      MK(IL1,IN1)=MK(IL1,IN1)+JJ*KK*GKG(I,J)
0093      CONTINUE
0094      90  CONTINUE
0095      100 CONTINUE
0096      RETURN
0097      END

```

FORTRAN IV G LEVEL 21

VCTABL

DATE = 83003

20/36/40

```

0001 SUBROUTINE VCTABL(IVC,M,NN)
0002 DIMENSION IVC(50,12)
0003 M2=M/2
0004 M21=M/2+1
0005 IVC(1,1)=1
0006 IVC(1,2)=0
0007 IVC(1,3)=0
0008 IVC(1,4)=0
0009 IVC(1,5)=2
0010 IVC(1,6)=3
0011 IVC(M21,1)=M+3+1
0012 IVC(M21,2)=0
0013 IVC(M21,3)=0
0014 IVC(M21,4)=0
0015 IVC(M21,5)=2
0016 IVC(M21,6)=3
0017 IF(NN.EQ.0)GOTOE5
0018 DO80I=2,M2
0019 DO80J=1,12
0020 IVC(I,J)=4*((I-1)+(J-1)+(I-2)*2
80 CONTINUE
0021 CONTINUE
85 CONTINUE
0022 IVC(M2,7)=0
0023 IVC(M2,8)=3*M-2
0024 IVC(M2,9)=3*M-1
0025 IVC(M2,10)=3*M
0026 IVC(M2,11)=0
0027 IVC(M2,12)=0
0028 DO90J=7,12
0029 IVC(I,J)=IVC(2,J-6)
0030 IVC(M21,J)=IVC(M21,1)+(J-6)
90 CONTINUE
0031 IF(NN.GT.0)GOTO55
0032 IVC(1,7)=0
0033 IVC(1,8)=4
0034 IVC(1,9)=5
0035 IVC(1,10)=6
0036 IVC(1,11)=0
0037 IVC(1,12)=0
95 CONTINUE
0038 M22=M/2+2
0039 KTR=2
0040 IF(NN.EQ.0)GOTO150
0041 DO140I=M22,M
0042 KTR=3-KTR
0043 DO100J=1,6
0044 J6=J+6
0045 IVC(I,J)=IVC(I-1,J6)
100 CONTINUE
0046 IF(I.EQ.M)GOTO150
0047 DO130J=7,12
0048 IF(KTR.EQ.1)GOTO110
0049 IVC(I,J)=IVC(I-1,11)+(J-6)
0050 GOTC130
110 CONTINUE
0051 IF(J.EQ.8.OR.J.EQ.10.OR.J.EQ.12)GOTO120
0052 IVC(I,J)=IVC(I,6)+(J-5)/2
0053 GOTC130
120 CONTINUE
0054 IVC(I,J)=IVC(I-M/2,J)
130 CONTINUE
0055 CONTINUE
140 CONTINUE
0056 GOTC180
150 CONTINUE
0057 IVC(M,7)=0
0058 IVC(M,11)=0
0059 IVC(M,12)=0
0060 IF(NN.EQ.0)GOTO170
0061 IF(KTR.EQ.1)GOTO160
0062 IVC(M,8)=IVC(M,5)+1
0063 IVC(M,9)=IVC(M,8)+1
0064 IVC(M,10)=IVC(M,5)+1
0065 GOTC180
160 CONTINUE
0066 IVC(M,9)=IVC(M,6)+1
0067 IVC(M,8)=IVC(M/2,8)
0068 IVC(M,10)=IVC(M/2,10)
0069 GOTC180
0070
0071
0072
0073
0074
0075
0076
0077
0078

```

FORTRAN IV G LEVEL 21

VCTABL

DATE = 83003

20/36/40

```
0079      170  CONTINUE
0080          IVC(M, 8)=8
0081          IVC(M, 9)=9
0082          IVC(M,10)=10
0083      180  CONTINUE
0084          RETURN
0085          END
```

```

FORTRAN IV G LEVEL 21          SOLVE          DATE = 83003          20/36/40
0001          SUBROUTINE SOLVE(TCTL,U,NDF)
                C
                C          GAUSS ILLIMINATION PROCEDURE TO SOLVE SYSTEM OF EQUATIONS
                C
0002          DIMENSION TOTL(100,100),U(100)
0003          DO50 I=1,NDF
0004          II=I+1
0005          IF (II.GT.NDF)GOTO15
0006          DO10 J=II,NDF
0007          IF (TOTL(I,J).EQ.0.0)GOTO10
0008          TOTL(I,J)=TOTL(I,J)/TOTL(I,I)
0009          CCONTINUE
0010          10 CONTINUE
0011          U(I)=U(I)/TOTL(I,I)
0012          TOTL(I,I)=1.0
0013          DO50 K=1,NDF
0014          IF (K.EQ.I)GOTO50
0015          IF (II.GT.NDF)GOTO35
0016          DO10 J=II,NDF
0017          IF (TOTL(K,I).EQ.0.0.OR.TOTL(I,J).EQ.0.0)GOTO30
0018          TOTL(K,J)=TOTL(K,J)-TOTL(K,I)*TOTL(I,J)
0019          CCONTINUE
0020          30 CONTINUE
0021          U(K)=U(K)-TOTL(K,I)*U(I)
0022          TOTL(K,I)=0.0
0023          50 CONTINUE
0024          RETURN
0025          END

```

```

FORTRAN IV G LEVEL 21          COSINE          DATE = 83003          20/36/40
0001          SUBROUTINE COSINE(M,MN,CN,EL,DC)
0002          DIMENSION MN(50,2),CN(50,3),EL(50),DC(50,3)
                C
                C          SOLVES FOR THE DIPECTION COSINES FOR A THREE DIMENSION PROBLEM
                C          MN IS THE MEMBER INDICES, CN IS THE JOINT COORDINATES,EL IS THE
                C          CALCULATED LENGTHS AND DC IS THE CALCULATED COSINES.
                C
0003          DO309 I=1,M
0004          K=MN(I,1)
0005          LO=MN(I,2)
0006          SUM=0.0
0007          DO307 J=1,3
0008          SUM=SUM+(CN(LO,J)-CN(K,J))**.2
0009          CCONTINUE
0010          307 EL(I)=SORT(SUM)
0011          DO308 J=1,3
0012          DC(I,J)=(CN(LO,J)-CN(K,J))/EL(I)
0013          CCONTINUE
0014          308 CONTINUE
0015          309 RETURN
0016          END

```

```

FORTRAN IV G LEVEL 21          MATMUL          DATE = 83003          20/36/40
0001          SUBROUTINE MATMUL(A,B,C,M,K,N)
0002          DIMENSION A(100,100),B(100,100),C(100,100)
0003          DO10 I=1,M
0004          DO10 J=1,N
0005          C(I,J)=0.0
0006          DO10 L=1,K
0007          IF (A(I,L).EQ.0.0.OR.B(L,J).EQ.0.0)GOTO10
0008          C(I,J)=C(I,J)+A(I,L)*B(L,J)
0009          CCONTINUE
0010          10 CONTINUE
0011          RETURN
                END

```

```

FORTRAN IV G LEVEL 21          MULT          DATE = 8300340          20/36/40
0001          SUBROUTINE MULT(A,B,C,M,K,N)
          C
          C          THE PRODUCT OF MATRICES A X B IS STORED IN MATRIX C
          C
0002          DIMENSION A(M,K),B(K,N),C(M,N)
0003          DO10 I=1,M
0004          DO10 J=1,N
0005          C(I,J)=0.0
0006          DO10 L=1,K
0007          IF(A(I,L).EQ.0.0.OR.B(L,J).EQ.0.0)GOTO10.
0008          C(I,J)=C(I,J)+A(I,L)*B(L,J)
0009          10 CONTINUE
0010          RETURN
0011          END

```

```

FORTRAN IV G LEVEL 21          VECT          DATE = 83003          20/36/40
0001          SUBROUTINE VECT(A,E,C,M,N)
          C
          C          THIS ROUTINE MULTIPLIES A MATRIX BY A VECTOR AND STORES THE
          C
0002          DIMENSION A(100,100),B(100),C(100)
0003          DO2 I=1,N
0004          SUM=0.0
0005          DO1 J=1,M
0006          IF(A(I,J).EQ.0.0.OR.B(J).EQ.0.0)GOTO1
0007          SUM=SUM+A(I,J)*E(J)
0008          1 CONTINUE
0009          C(I)=SUM
0010          2 CONTINUE
0011          RETURN
0012          END

```

```

FORTRAN IV G LEVEL 21          TRANS          DATE = 83003          20/36/40
0001          SUBROUTINE TRANS(U,V,K,L)
          C
          C          THE TRANSPOSE OF MATRIX U IS STORED IN MATRIX V
          C
0002          DIMENSION U(L,K),V(K,L)
0003          DO10 I=1,K
0004          DO10 J=1,L
0005          V(I,J)=U(J,I)
0006          10 CONTINUE
0007          RETURN
0008          END

```

BUILT UP DOUBLE ANGLE 3D COMPRESSION MEMBER

NUMBER OF INTERCONNECTORS 0  
 TOTAL LENGTH (INCHES) 120.00  
 SPACING (INCHES) 2.50  
 INITIAL OUT OF STRAIGHTNESS Y1 0.08 Y2 0.06  
 INITIAL OUT OF STRAIGHTNESS Z1 -0.05 Z2 -0.03  
 NUMBER OF JOINTS 4  
 NUMBER OF MEMBERS 2  
 NUMBER OF DEGREES OF FREEDOM 10  
 NUMBER OF DEPENDANT D.O.F. 1

JOINT COORDINATES (INCHES)

JOINT	X	Y	Z
1	0.0	1.2950	0.0
2	60.0000	1.2950	0.0
3	0.0	-1.2950	0.0
4	60.0000	-1.2950	0.0

INITIAL OUT OF STRAIGHTNESS (INCHES)

JOINT	Y	Z
1	0.0	0.0
2	0.0800	-0.0500
3	0.0	0.0
4	0.0800	-0.0500

MEMBER INDICES

MEMBER	P	Q
1	1	2
2	3	4

VARIABLE CORRELATION TABLE

MEMBER	1	2	3	4	5	6	7	8	9	10	11	12
1	1	0	0	0	2	3	0	4	5	6	0	0
2	7	0	0	0	2	3	0	8	9	10	0	0

MEMBER PROPERTIES (KIPS, INCHES AND DEGREES)

MEMBER	MODULUS OF ELASTICITY	MODULUS OF RIGIDITY	AREA	MOMENT OF INERTIA S3 AXIS	MOMENT OF INERTIA S2 AXIS	TORSION CONSTANT J	ROTATION
	29710.00	11776.00	1.2521	0.3160	1.1800	0.0248	0.0

DEPENDANT DEGREES OF FREEDOM

CRITICAL LOAD 1 39.7746 KIPS

## EIGEN VECTOR

D.O.F. VECTOR

1	-0.0083
2	0.0
3	0.0064
4	0.7070
5	0.0
6	0.0
7	0.0
8	0.0083
9	0.7071
10	0.0
	0.0

## JOINT COORDINATES (INCHES)

JOINT	X	Y	Z
1	0.0	1.2950	0.0
2	60.0000	1.3750	-0.0500
3	0.0	-1.2950	0.0
4	60.0000	-1.2350	-0.0300

COUNTER	LOAD	Y1	Z1	Y2	Z2
1	1.99	0.0836	-0.0515	0.0631	-0.0314
2	3.93	0.0877	-0.0532	0.0665	-0.0329
3	5.97	0.0921	-0.0550	0.0704	-0.0345
4	7.95	0.0971	-0.0565	0.0748	-0.0363
5	9.94	0.1027	-0.0591	0.0798	-0.0383
6	11.93	0.1090	-0.0614	0.0855	-0.0405
7	13.92	0.1162	-0.0640	0.0921	-0.0430
8	15.91	0.1246	-0.0669	0.1000	-0.0457
9	17.90	0.1343	-0.0701	0.1093	-0.0488
10	19.89	0.1450	-0.0737	0.1207	-0.0523
11	21.88	0.1597	-0.0778	0.1349	-0.0563
12	23.86	0.1769	-0.0825	0.1532	-0.0610
13	25.85	0.1986	-0.0880	0.1776	-0.0665
14	27.84	0.2275	-0.0943	0.2121	-0.0730
15	29.83	0.2697	-0.1018	0.2683	-0.0810
16	31.82	0.3469	-0.1104	0.3901	-0.0908
17	33.81	0.4369	-0.1217	0.5271	-0.1038
18	35.80	1.2194	-0.1023	0.5723	-0.0598
19	37.79	1.1168	-0.3009	0.2717	-0.2773
20	39.77	1.2083	-0.3422	0.4681	-0.3418

## Appendix C

### FORCES IN THE INTERCONNECTORS

#### C.1 GENERAL

The determination of the forces in the interconnectors requires a knowledge of the behaviour of the starred angle strut. Studying the possible displaced shapes of the angles without interconnectors gives some insight into the forces that the interconnectors must develop to cause the angles to act together. Two possible combinations of displaced shapes are shown in Figs. 20(a) and 20(b). Without the interconnectors the angles buckle about the U-U axis, but with two or more interconnectors joining the angles at the third points then buckling occurs about the V-V axis as was determined from the theoretical and experimental results.

For the interconnector to cause the system to act as a whole the interconnector must prevent the individual angles from taking different buckled shapes. From this the forces in the interconnectors can be determined. The forces are calculated for a strut with two interconnectors only as this was determined to be the minimum number of interconnectors required to force the strut to buckle about the V-V axis. The six potential forces that the interconnector might have to resist are shown in Fig. 21.



Assuming that the interconnectors lie in the V-Z plane only, as is shown in Fig. 21, and as the interconnector is rigidly fastened to the individual angles, the calculation of the forces is simplified by applying the battened column theory to determine the forces in the interconnectors.

Fig. 22 shows the forces in the interconnector when each of the spaced column and the battened column theories is applied. From Fig. 22 it is seen that the interconnector in spaced columns does not resist any forces and that the interconnector in battened columns resists bending and shear.

If the starred angle strut is prevented from displacing in the direction of the U axis then, using the battened column theory, a critical load of 61.3 kips could be realized. On the other hand, if the strut is prevented from displacing in the direction of the V axis then, using the Euler load, a critical load of 48.9 kips would be realized. The latter displaced shape, buckling about the V-V axis, precludes any forces from acting on the interconnectors based on the battened column theory.

Since displacements are realized in both of the principal axes then there must be forces in the interconnector. The measured displacements in the direction of the V axis for tests on specimens with two interconnectors are in the order of one-tenth the displacements observed in tests on specimens with one interconnector. Based on this observa-

tion the forces determined using the battened column theory should be reduced accordingly. Based on references (3,20,36,37) on the shearing stresses in battened columns a value for the shear in the starred angle strut can be calculated based on the axial load and the initial out-of-straightness.

### C.2 SHEAR FORCE IN A COLUMN

An equation to calculate the shear force based on the works of Young (36,37), Bleich (3) and Koenigsberger and Mohsin (20) is derived in this section.

The shear in a simple column is a function of the axial force and the slope of the column and therefore the maximum shear force is at the ends of the column as shown in Fig. 23. Bleich (3) shows the shear force at the end of the column as:

$$Q = P \frac{\pi}{L} y \quad (C.1)$$

where  $y$  = the total displacement at the mid-height of the column having a sinusoidal deflected shape.

Substituting Eq. 5.9, for the mid-height displacement,  $y$ , into Eq. C.1:

$$Q = P \frac{\pi}{L} \frac{y_0}{1 - P/P_{cr}} \quad (C.2)$$

Eq. C.2 is in the same form as that derived by Young (37) and can be rewritten in the following form:

$$\frac{Q}{P} = \frac{\pi}{1 - P/P_{cr}} \frac{y_0}{L} \quad (C.3)$$

Eq. C.3 is solved and plotted in the upper graph in Fig. 24 for various ratios of  $y_0/L$ . As the ratio  $P/P_{cr}$  increases the ratio  $Q/P$  increases. The shear force increases at a more rapid rate than the axial load and when the ratio  $P/P_{cr}$  equals 1 the ratio  $Q/P$  is undefined.

The equation for the shear derived by Bleich (3) is similar to Eq. C.2 but does not have the same versatility because it does not contain an out-of-straightness term. Koenigsberger and Mohsin (20) show that Bleich's equation yields results similar to Young's for a fixed initial out-of-straightness.

To apply Eq. C.3 to the starred angle strut, values for the ratio of the initial out-of-straightness to the total length and the ratio of the axial load to the critical load must be determined. The curves of the shear to axial load ratio are plotted for three values of initial out-of-straightness in Fig. 24.

The ratio of  $P/P_{cr}$  in Eq. C.3 is not constant for the starred angle struts as is the case with the geometric properties. From Eq. 3.20 the critical load for the battened column is found. The maximum load that can be applied, however, is the Euler load about the V-V axis. Hence, the

Hence, the applied load,  $P$ , in the ratio  $P/P_{cr}$  shall be set equal to Eq. F.8. Dividing Eq. F.8 by Eq. 3.20 and reducing results in the following equation:

$$\frac{P}{P_{cr}} = \frac{I_v}{I_u} + \frac{\pi^2}{L^2} \frac{I_v}{I_u} \frac{d^2}{24} + \frac{\pi^2}{L^2} I \frac{db^2}{12I_{iu}} \quad (C.4)$$

The first term in Eq. C.4 can be rewritten as follows:

$$\frac{I_v}{2I_{u'} + Ab^2} \quad (C.5)$$

and further reduced to:

$$\frac{\frac{I_v}{I_{u'}}}{2 + \frac{Ab^2}{I_{u'}}} \quad (C.6)$$

Substituting  $I_v/I_{u'} = 7.68$ , based on the ratio  $r_v/r_{u'} = 1.96$ ;  $d = 0.85*L/3$ , where  $d$  is the center to center distance and 0.85 is a reduction factor (20); and Eq. C.6 into Eq. C.4 gives:

$$\frac{P}{P_{cr}} = \frac{3.84}{1 + \frac{b}{r_{u'}}^2} + 0.26 + 0.23 \frac{I_v}{I_{iu}} \frac{b}{L} \quad (C.7)$$

In the lower graph of Fig. 24 Eq. C.7 is a plot of the ratio of  $b/r_{u'}$  versus the ratio of  $P/P_{cr}$ . A family of

curves is plotted for the different values of the last term in Eq. C.7. For the test specimens with Type A interconnectors,  $I_v = 2.41 \text{ in.}^4$ ;  $b = 2.57 \text{ in.}$ ;  $I_{iu} = 0.25 \text{ in.}^4$ ; and  $L = 120 \text{ in.}$  The last term of Eq. C.7 is  $0.23 * 0.206$ ,  $b/r_{u'} = 5.25$ , and  $P/P_{cr} = 0.44$ .

From the lower graph on Fig. 24 for  $b/r_{u'} = 5.25$  and for the last term in Eq. C.7 =  $0.23 * 0.206$  a ratio of  $P/P_{cr} = 0.44$  is found. For  $P/P_{cr} = 0.44$  the upper graph, for a ratio of  $v_0/L = 0.001$ , yields  $Q/P = 0.6$  percent. This solution is drawn on Fig. 24.

As the axial load is divided equally between the two members the shear is also half of the total applied load and is used to calculate the forces acting on the interconnector (16,19,20,21).

The rest of this appendix uses the ratio of  $Q/P = 1.0$  percent for the calculation of the forces in the interconnector.

### C.3 DETERMINATION OF FORCES

Figs. 20(a) and 20(b) show two possible displaced shapes that the starred angle strut may take when there are no interconnectors. Fig. 20(a) demonstrates the case where the angles displace in opposite directions whereas Fig. 20(b) shows the angles displaced in the same direction.

There are six potential forces and moments at the ends of the interconnector which are shown in Fig. 21. The axial

force,  $F_v$ , and the two shears,  $F_u$  and  $F_z$ , could possibly exist because of the difference between the displaced shapes of each angle. The axial force,  $F_v$ , comes from the interconnector restraining the angles in the direction of the  $V$  axis and the shears,  $F_u$  and  $F_z$ , come from the restraint that the interconnector imposes in the direction of the  $U$  and  $Z$  axes, respectively.

Bending may occur as each angle is free to displace in any direction except at the points of interconnection where the individual angles are forced to displace together. The moment  $M_z$  comes from the restraint that the interconnector imposes on the rotation of the angles about the  $Z$  axes. The other two moments,  $M_v$  and  $M_u$ , are imposed on the interconnector due to the bending restraints of the angles about the  $V$  and  $U$  axes, respectively.

These six forces contribute to the stresses in the interconnector as follows:

$$\sigma_v = F_v/A_i + M_z/S_{iz} + M_u/S_{iu} \quad (C.8a)$$

$$\tau_{vu} = F_u/A_i \quad (C.8b)$$

$$\tau_{vz} = F_z/A_i + M_v/J_i \quad (C.8c)$$

where  $A_i$  = the area of the interconnector;  $S_i$  = the section modulus of the interconnector;  $\sigma_v$  = the normal stress;  $\tau_{vu}$  and  $\tau_{vz}$  = the shear stresses; and  $J_i$  = St. Venant's torsional constant of the interconnector. The subscripts  $u$ ,  $v$  and

z indicate the axis about which the geometric properties are taken and forces applied.

All the forces in Eq. C.8, shown in Fig. 21, are functions of the displaced shapes of the individual angles. When there are no interconnectors there is a total of 16 possible combinations of displaced shapes in the U-V plane. Each angle can potentially displace positively or negatively in the direction of the U and V axes. Of the 16 combinations of the displaced shapes half of them are duplicated in the opposite direction.

Based on the battened column theory the shear force,  $F_z$ , is a function of the shear, Q, in the main members. Q is a function of the axial load and for the specimens tested the nominal compressive resistance is 33.8 kips. One percent of this load is 338 lb. The shear in the interconnector,  $F_z$ , is:

$$F_z = \frac{Qd}{nb} \quad (C.9)$$

where n = the number of interconnectors.

For the starred angle member with two interconnectors  $F_z = 2240$  lb. The value for the spacing of the interconnectors, d, used to calculate  $F_z$  is the clear distance between interconnectors not the center-to-center distance (20).

The moment  $M_z$  is the twisting restraint that the interconnector imposes on the member angles and is due to torsional-flexural buckling of the members and initial

imperfections. Fig. 15 demonstrates that torsional-flexural buckling occurs when the length of the individual angles is less than 20.0 in., at a theoretical load of 204 kips (the load that causes yielding is 52.0 kips). For the case of the slender starred angle compression members having a length of 120 in. the Euler load is 44.5 kips therefore bending governs. Allowing the interconnectors to displace in the direction of the U axis the slope deflection equation can be applied as follows:

$$M_z = \frac{EI_{iz}}{b}(4\theta_1 + 2\theta_2) + \frac{6EI_{iz}}{b}(u_r - u_l) \quad (C.10)$$

where  $I_{iz}$  = the moment of inertia of the interconnector about the Z-Z axis in the Z-U plane.

Using the assumptions employed to derive Eqs. 3.2 and 3.3 and since the angles are longer than 20.0 in. the following assumptions are made:

a) the rotations of the individual angles are equal

$$\theta_l = \theta_r = \theta$$

b) because the rotations are very small let  $\theta = 0.0$ .

Fig. 25, a graph of the actual results for Load versus rotation for test 120A2.1, shows that the actual rotations are negligible, and

c) the lateral displacements are equal,  $u_l = u_r$ .

Based on these three assumptions Eq. C.10 gives  $M_z = 0.0$ .



The force  $F_U$  is a function of the difference in the displaced shapes of the individual angles in the direction of the U axis. If the lateral displacements are equal,  $u_l = u_r$ , then  $F_U = 0.0$ .

To calculate the moment  $M_U$  the battened column theory is applied and the following equation, from Ref. 16, is used:

$$M_U = \frac{Qd}{2n} \quad (C.11)$$

Substituting the value of Q previously calculated, a spacing of 34 in. and an n of 2 into Eq. C.11 results in  $M_U = 2870$  in.-lb.

$F_V$  is a function of the displaced shape of the member angles in the direction of the V axis. Battened column or spaced column theory assumes a zero axial force in the interconnector, see Fig. 22. The value of  $F_V$  is a function of the difference in the displacements in the direction of the V axis of the individual angles under the applied load. Because of the short length of the interconnectors there will be a very small difference in the displacements beyond the initial out-of-straightness. It is assumed that the effect of the axial force,  $F_V$ , is small compared to the effects of the shear,  $F_z$ , and the moment,  $M_U$  and therefore  $F_V = 0.0$ .

$M_V$  is a function of the bending about the V-V axis. With the assumption that  $\beta_l = \beta_r$  (Eq. 3.4)  $M_V = 0.0$ .

#### C.4 SUMMARY

From the foregoing the forces developed in the interconnectors are:

$$F_v = 0 \quad (C.12a)$$

$$F_u = 0 \quad (C.12b)$$

$$F_z = 2240 \text{ lb.} \quad (C.12c)$$

$$M_v = 0 \quad (C.12d)$$

$$M_u = 2870 \text{ in.-lb.} \quad (C.12e)$$

$$M_z = 0 \quad (C.12f)$$

These forces and moments result in a condition of plane stress. Substituting the geometric properties for a  $2 \times 3/8 \times 2$  in. interconnector, based on a 2 in.  $\times$  0.53 in. cross section as the interconnector is actually, in the X-Z plane,  $A_i = 1.06 \text{ in.}^2$ ;  $S_{iu} = 0.354 \text{ in.}^3$ ; and the results from Eq. C.12 into Eq. C.1 gives  $\sigma_v = 8100 \text{ psi}$  and  $\tau_{vz} = 2110 \text{ psi}$ . Using these values the principal stresses and maximum shear can be calculated as  $\sigma_1 = 8620 \text{ psi}$ ,  $\sigma_2 = -520 \text{ psi}$  and  $\tau_{12} = 4570 \text{ psi}$ .

These stresses are calculated for a specific type of interconnector and the stresses calculated are significantly less than the allowable stresses for G40.21 44W material.

Stresses in the  $3/16$  in. weld around the type A interconnector are 5808 psi which is below the allowable stresses for the E70XX Electrode.

Due to the number of variables involved in making the assumption that the force  $F_x$  and moment  $M_u$  could be reduced i.e., initial out-of-straightness of the angles or type of fastener, it is recommended that a value of  $Q/P = 1.0$  percent be used to calculate the shear force in starred angle compression members.

## Appendix D

### ANCILLARY TESTS

#### D.1 CALIBRATION

Several calibration tests were performed on the Tinius Olsen Testing machines, in the University of Windsor structures lab, which were then used to calibrate load cells and conduct tensile tests. The equipment used to calibrate the Tinius Olsen Machines 1, 2 and 3 was a Proving Ring, serial number 1916, manufactured by the Moore House Machine Company.

For the calibration of the Strainert 50 kip capacity flat load cell using the Tinius Olsen testing machine the Strain Indicator No. 5 having the serial number 017359 was used.

All the data was tabulated and analyzed statistically applying the method of least squares to calculate the appropriate slopes and intercepts of the curves. A linear relationship was assumed for the calibration curves and plots of the calibration data confirmed this assumption.

## D.2 MECHANICAL PROPERTIES

Four tension specimens were prepared according to ASTM A370-77 specifications for testing in the universal testing machine. The test specimens were cut at random from the end cuttings used to construct the starred angle tested specimens. Two strain gauges were then attached, one on each side of the specimen, to measure the elongation.

Loads were applied at two kip intervals to a load below the yield point and then released at five kip intervals. Both the load and the strains were recorded while the load was being increased and decreased. The tension specimens were then slowly reloaded to determine the yield stress, and the ultimate stress.

Results from the two strain gauges were averaged and the load divided by the cross-sectional area. With this stress and strain data, linear regression was applied to obtain Young's modulus. The average value of  $E = 29700$  ksi was attained. The average value of the yield stress,  $F_y$ , is 52.7 ksi with a standard deviation of 3.05, see Table 5.

## D.3 GEOMETRIC PROPERTIES

Four samples were taken from the end cuttings of the angles used to construct the starred angle specimens and were measured in detail using a micrometer and radii gauges. The measurements taken for each of the samples were:

- a) lengths of each of the legs,

- b) thickness of each of the legs,
- c) corner and fillet radii, and
- d) the included angle of the legs of the angle.

From this data the actual geometric properties of the angle were calculated neglecting the effects of the radii as is the practice in the CISC Handbook (7). The actual geometric properties are tabulated in Table 2 along with the nominal values of the geometric properties tabulated in the CISC Handbook (7).

#### D.4 END FIXTURES

Several tests were conducted using end connectors other than the standard Tee. These tests did not give any significant difference in load carrying capacity or buckled shape. The first such test was done with horizontal plates welded to the angles at each end, specimen 120A1.6P, shown in Fig 12(h), which is similar to the base plates on a column. The reason for conducting this test was to determine if the carrying capacity would be decreased due to the decreased length of the end stiffener.

Tests to prove that the knife edge assembly behaved as assumed were carried out using a single angle with a cap and base plate, having a length of 60 in. between centers of the knife edge assemblies. These were loaded to 50 percent of the Euler load and then unloaded. The specimen was then

rotated 90 degrees, maintaining the knife edge in the original orientation, and retested. The purpose of this test was to determine load-deflection curves for the angle when loaded in each of four orientations. These tests indicated that the behaviour of the knife edges was predictable, as only small variation was noted in the load-deflection curves. To ensure that the results from the four tests could be used to determine the acceptability of the knife edge assemblies the initial out-of-straightness was recorded prior to the specimen being tested or retested. Dial indicator readings were taken at the end of each test to check the out-of-straightness to establish that there were no residual deformations caused by the testing.

Lastly, on the first tests 120A1.1 and 120A1.2, dial indicators were placed on the lower platten, above the mechanical jack, to determine the amount of the rotation about the Z axis, if any, occurred. Readings indicated that there was some initial rotation, at low loads, which very quickly ceased. At higher loads, no significant changes were observed in the dial indicators measuring the rotation. This indicated that the end fixtures functioned as designed in preventing the knife edge assemblies from rotating about the Z axis.

**D.5 SUMMARY**

All ancillary tests were conducted to determine the properties of the specimens, calibrate the system and prove the individual elements of the test set-up. All the information was used to reduce the data obtained from tests and in the theoretical models.



## Appendix E

### NUMBER OF INTERCONNECTORS REQUIRED BY CSA STANDARDS S16 AND S16.1

During the course of the research it became apparent that only one interconnector is required for any pair of equal leg angles that form a cruciform by the requirements of the Canadian Standard. The reason that only one interconnector is required is that the geometric properties of the angles  $r_v / r_u \cong 2.0$ . This value was checked for all the equal leg angles listed in the CISC Handbook (7) and the average value is 1.96 with a standard deviation of 0.04.

With this geometric relationship it is simple to calculate the minimum number of interconnectors required by the Canadian Standards:

$$\frac{\frac{L}{r_v}}{\frac{d}{r_u}} = 1 \quad (E.1)$$

where  $d$  = the maximum spacing of the interconnectors.

Substituting  $r_v / r_u = 1.96$  and  $L/d = n+1$ , where  $n$  = the number of interconnectors into Eq. E.1 results in the following equation:

$$(n+1)/1.96 = 1$$

(E.2)

Solving Eq. E.2 for the number of interconnectors results in  $n = 0.96$  hence only one interconnector is required. This relationship is applicable to the North American Standards only. This relationship is also independent of the spacing of the angles  $b$  and therefore the ratio holds true for the box arrangement of double angles as well.

## Appendix F

### EFFECT OF END STIFFENERS ON BUCKLING LOAD

The work of Horne and Merchant (15) is used to prove that the end gusset plates have no significant effect on the strength of the member as a whole. Complete flexural rigidity over the length of the end stiffeners has been assumed by Horne and Merchant in the derivation of the modified stability function.

A single element is used and in applying the disturbances  $Q_a$  and  $Q_b$  (Fig. 26) the following matrix can be established:

$$\begin{bmatrix} \bar{S}k & \bar{S}\bar{C}k \\ \bar{S}\bar{C}k & \bar{S}k \end{bmatrix} \begin{bmatrix} Q_a \\ Q_b \end{bmatrix} = \begin{bmatrix} M_{ab} \\ M_{ba} \end{bmatrix} \quad (F.1)$$

where  $Q_a$  and  $Q_b$  = the applied disturbances at the ends of the column;  $M_{ab}$  and  $M_{ba}$  = the moments related to the disturbances  $Q_a$  and  $Q_b$ ;  $\bar{S}$ ,  $\bar{S}\bar{C}$ , and  $k$  = the stability functions (15).

Fig. 26 shows a simple column with end stiffeners in the initially straight and the deformed positions with the applied disturbances.

By evaluating the determinant of the 2 X 2 matrix and setting it equal to zero the load  $P$  at which the rotations

Q and Q are possible without the application of the end moments,  $M$  and  $M$ , are found thus:

$$\begin{vmatrix} \bar{S}k & \bar{S}\bar{C}k \\ \bar{S}\bar{C}k & \bar{S}k \end{vmatrix} = 0$$

$$(\bar{S}k)^2 - (\bar{S}\bar{C}k)^2 = 0 \quad (\text{F.2})$$

Dividing both sides by  $k^2$  gives:

$$\bar{S}^2 - \bar{S}^2\bar{C}^2 = 0 \quad (\text{F.3})$$

which can be written as:

$$(\bar{S} - \bar{S}\bar{C})(\bar{S} + \bar{S}\bar{C}) = 0 \quad (\text{F.4})$$

From Eq. F.4 there are two possible solutions:

$$\bar{S} - \bar{S}\bar{C} = 0 \quad (\text{F.5})$$

or

$$\bar{S} + \bar{S}\bar{C} = 0 \quad (\text{F.6})$$

Eqs. F.5 and F.6 have been checked and only Eq. F.5 will be elaborated on, as it produces the smallest force, P. Eq. F.6 produces an alternate mode of buckling which is of no interest in this work.

Substituting the stability functions for  $\bar{S}$  and  $\bar{S}\bar{C}$ , from Horne and Merchant (15) into Eq. F.5, and reducing gives:

$$s - sc - \mu_a P/k = 0 \quad (\text{F.7})$$

where  $\mu_a$  = the length of the end stiffener.

Solving Eq. F.7 with  $g_a = 0$ , gives  $\rho = 1$ ; where  $\rho = P/P_e$  hence,  $P = P_e$ . Where  $P$  = the applied load; and  $P_e$  = the Euler load as follows:

$$P_e = \frac{\pi^2 EI_v}{(KL)^2} \quad (F.8)$$

Using the nominal values of the geometric properties of the starred angles tested  $P_e = 44.5$  kips. With  $g_a = 6$  in.  $\rho = .81$  and, hence,  $P = 44.6$  kips.

The difference in load from  $g_a = 0$  in. to  $g_a = 6$  in. is less than one percent and negligible, hence the following two conclusions:

- a) that the effect of end stiffeners, having practical lengths, on the members is insignificant and can be neglected, and
- b) that the complete flexural rigidity of the short stiffeners has no effect on the load carrying capacity when the starred angles buckle about the V-V axis.

## Appendix G

### NOTATION

The following notation was used throughout this Thesis:

A	-area of the starred angle
$A_0$	-area of the angle
$C_f$	-factored axial load
E	-modulus of elasticity
F	-axial force in the element
$F_u, F_v, F_z$	-forces acting on the interconnector
$F_y$	-yield stress of material
G	-modulus of rigidity
$I_u, I_v, I_x, I_y$	-second moment of area for the starred angle
$I_u', I_v'$	-second moment of area for the angle
$I_i$	-second moment of area of the interconnector
$I_p$	-polar moment of inertia
$I_{uv}$	-product of inertia
J	-St. Venant torsional constant
K	-effective length factor
[K]	-stiffness matrices
$M_u, M_v, M_x$	-bending moments acting on the interconnector
P	-allowable load of the starred angle
$P_e$	-Euler buckling load
$P_{cr}$	-critical load of the starred angle
{P}	-load vector

Q	-shear in the starred angle
[T]	-transformation matrix
U	-displacement vector
U, V, Z	-axes of the starred angle
U', V', Z'	-axes of the angle
a	-back-to-back separation of angles
b	-spacing of angles between centroids
d	-spacing of interconnectors
$l_0$	-length of end stiffener
n	-number of interconnectors
$r_U, r_V$	-radii of gyration of the starred angle
$r_U', r_V'$	-radii of gyration of the individual angle
u, v, z	-linear degrees-of-freedom
$\alpha$	-inverse of the eigenvalue
$\beta$	-rotation about the V axis
$\theta$	-rotation about the Z axis
$\lambda$	-rotation about the U axis
$\phi$	-rotation of the Principle axes
$\Delta$	-used to indicate general displacement
$\Pi_p$	-total potential energy
$\psi$	-buckling constant in the German Specification

#### REFERENCES

1. AMERICAN INSTITUTE OF STEEL CONSTRUCTION, Structural Steel For Buildings, AISC-1969, Clause 1.13.2.4
2. AUSTRALIAN STANDARD, AS 1250-1975, Clause 6.7.5.
3. BLEICH , Buckling Strength Of Metal Structures, McGraw Hill, N.Y., N.Y., 1952
4. BRITISH STANDARDS, Specification for the Use of Structural Steel in Buildings, British Standard, BS 449-1970, Clauses 30, 36 and 37.
5. CANADIAN STANDARDS ASSOCIATION, Structural Steel for Buildings, Canadian Steel Specification, CSA Standard S16.1-1974, Clause 18.1.2 (a).
6. CANADIAN STANDARDS ASSOCIATION, Structural Steel for Buildings, Canadian Steel Specification, CSA Standard S16-1969. Clause 22.1.1.
7. CANADIAN INSTITUTE OF STEEL CONSTRUCTION Handbook of Steel Construction, Third Edition, CISC, Canada Limited, 1981
8. CONNER, J. J., LOGCHER, R.D. and CHAN, S.C., "Non Linear Analysis Of Elastic Framed Structures", ASCE Journal of the Structural Division, August 1963, pp 333-351.
9. FELIPPA, C.A., "Discussion of Incremental Finite Element Matrices", ASCE Journal of the Structural Division, Vol. 100, ST12, Dec. 1974, pp 2521-2523.
10. GALLAGHER, R. H., Finite Element Analysis Fundamental, Prentice Hall, Englewood Cliffs, New Jersey, 1975.
11. GAYLORD, E. H., and GAYLORD, C. N., Design of Steel Structures, McGraw Hill Book Company Inc., 1957
12. German Steel Specification, DIN 4114-1972, Clauses 8.2.13, 8.22 and 8.36.



13. HATHOUT, I.A., "Stability Analysis of Spaced Stayed Columns by Finite Element Method", Thesis presented to the University of Windsor, Windsor, Ontario, Canada in partial fulfillment of the requirements for the Degree of Masters of Applied Science, 1977
14. HETENYI, M., "An Analytical Study of Vierendeel Girders", Proceedings of the Fourth U.S. National Congress of Applied Mechanics, Volume 1, 1962, pp 627-633.
15. HORNE, M.R. and MERCHANT, W., The Stability of Frames, Pergamon Press Ltd., London, 1965.
16. JOHNSTON, B.G. (Editor Column Research Council), Guide To The Stability Design Criteria For Metal Structures, Third Edition, Wiley Interscience, John Wiley and Sons, New York, 1976.
17. JOHNSTON, B.G., "Spaced Steel Columns", ASCE Journal of the Structural Division, Volume 97, No. ST5, May 1971, pp 1465-1479
18. JOHNSTON, B.G., "Spaced Steel Columns" (closure and errata), ASCE Journal of the Structural Division, Volume 98 No. ST11, December 1972, page 2625.
19. JONES, B.D., "A Theory for Structures with Laced or Batten Bracing", The Structural Engineer, The Journal of the Institute of Structural Engineers, London England, Volume 30 No. 6, June 1952, pp 108-113.
20. KOENIGSBERGER, F. and MCHSIN, M. E., "Design of Load Carrying Capacity of Welded and Battened Struts", The Structural Engineer, The Journal of the Institute of Structural Engineers, London England, Vol 34 No. 6, June 1956, pp 183-203.
21. KOO, B., "Spaced Steel Columns" (Discussion), ASCE Journal of the Structural Division, Volume 98 No. ST2, February 1972, pp 513-515.
22. LIN, F.J., GLAUSER, E. C. and JOHNSTON, B.G., "Behaviour of Laced and Battened Structural Members", ASCE Journal of the Structural Division, Volume 96 No. ST7, July 1970, pp 1377-1401.
23. MALLET, R. H. and MARCAL, P.V., "Finite Element Analysis of Non Linear Structures", ASCE Journal of the Structural Division, Volume 94 No. ST9, September 1968, pp 2081-2105.

24. MALLET, R. H. and MARCAL, P. V., "Finite Element Analysis of Non Linear Structures" (closure and eratta), ASCE Journal of the Structural Division, Volume 96 No. ST1. January 1970, pp 132-133.
25. MARTIN, H. C., "On the Derivation of Stiffness Matrixes for the Analysis of Large Deflection and Stability Problems", AFFDL-TR-66-80, 1966, pp 697-716.
26. PAULS, G.C. and STRINGER, D.C., "Interconnection of Double Angle Structures An Experimental Investigation", Internal Report, Dominion Bridge Company Ltd., Corporate Engineering Department, Ottawa, Ontario, January 1978.
27. PIPPARD, A. J. S., "The Critical Load of a Battened Column", Philosophical Magazine, London, England, Volume 39, 1947, pp 58-66.
28. PIPPARD, A. J. S., NEBUCHIA, M., and DUORAK, F., "Design and Load Carrying Capacity of Welded Battened Struts", (Discussion), The Structural Engineer, The Journal of the Institute of Structural Engineers, London England, Vol 36 No. 2, Feb 1958, pp 74-77
29. RAJASEKARAN, S. and MURRAY, D.W., "Incremental Finite Element Matrixes", ASCE Journal of the Structural Division, Volume 99 No. ST12, December 1973, pp 2423-2437.
30. TEMPLE, M.C., "Buckling of Stayed Columns", ASCE Journal of the Structural Division, Volume 103 ST4, April 1977, pp 839-851.
31. TEMPLE, M.C. and SCHEPERS, J.A., "Interconnection of Starred Angle Compression Members", CSCE Annual Conference Proceedings, May 1980, pp S/22:1 to S/22:8
32. TIMOSHENKO, S. and MACCULLOUGH, G., Elements of Strength of Materials, Third Edition, D. VanNostrand Company Ltd., New York, 1949.
33. TIMOSHENKO, S. and GERE., Theory of Elastic Stability, Third Edition, McGraw-Hill Book Co., New York, 1961.
34. TOSSI, M., "On The Out of Plane Buckling of Battened Columns", International Journal of Mechanical Sciences, Pergamon Press, Great Britain, Volume 14, 1972, pp 511-521.

35. WONG, K. C., "Single Crossarm Stayed Column With Initial Imperfections", Thesis presented to the University of Windsor, Windsor, Ontario, Canada in partial fulfillment of the requirements for the Degree of Masters of Applied Science, 1980
36. YOUNG, D. H., "Rational Design For Steel Columns", ASCE Transactions, Paper No. 1931, Vol. 101, 1936, pp 422-500
37. YOUNG, D. H., "Shearing Stress in Steel Columns", Memoir, International Association of Bridge and Structural Engineers, Published by the General Secretariate in Zurich, Vol 2, 1933-34, pp 480-495

## VITAE AUCTORIS

The author was born in Montreal on November 7, 1953 and was raised in Windsor and Essex County. Public schools attended were: Hugh Beaton, in Windsor, and Maplewood, in Essex. He graduated from Essex District High School in 1972 and the same year entered the University of Windsor, obtaining a Bachelor of Applied Science in 1976.

Prior to joining the University full time in 1979, to carry out post graduate research, he was commissioned in the Naval Reserves and worked in construction and consulting on buildings and municipal projects.

In addition to University studies, courses on welding fundamental procedures and practices and engineered masonry construction were taken.